Efficacy of dianthin-based targeted toxins in a pancreatic carcinoma xenograft model

Inaugural-Dissertation to obtain the academic degree

Doctor rerum naturalium (Dr. rer. nat.)

Conducted at the

Institute of Laboratory Medicine, Clinical Chemistry and Pathobiochemistry Charité – Universitätsmedizin Berlin

and the

Institute of Pharmacy

Freie Universität Berlin

Submitted at the

Department of Biology, Chemistry, Pharmacy

Freie Universität Berlin

by

Cheenu Bhargava

Berlin, February 2017

First supervisor: Prof. Dr. Matthias F. Melzig

Second supervisor: Prof. Dr. Hendrik Fuchs

Disputation: 2nd May, 2017

Index

Abbreviations

ABC	:	ATP-Binding Cassette
ALAT	:	Alanine Transaminase
ASAT	:	Aspartate Transaminase
ATP	:	Adenosine Triphosphate
BCA	:	Bicinchoninic Acid
BSA	:	Bovine Serum Albumin
CAPSO	:	3-(Cyclohexylamino)-2-hydroxy-1-propanesulfonic acid
CBD	:	Chitin–Binding Domain
CTLs	:	Cytotoxic T Lymphocytes
DCs	:	Dendritic Cells
DE	:	Dianthin–EGF
DEAE	:	Diethyaminoethyl
DMEM	:	Dulbecco's Modified Eagle's Medium
DNA	:	Deoxyribonucleic Acid
DRC	:	Dose Response Curve
DT	:	Diphtheria Toxin
EDTA	:	Ethylenediaminetetraacetic Acid
EGF	:	Epidermal Growth Factor
EGFR	:	Epidermal Growth Factor Receptor
EPR	:	Enhanced Permeation and Retention
FBS	:	Fetal Bovine Serum
FPLC	:	Fast Protein Liquid Chromatography
GI	:	Gastrointestinal
HE	:	Hematoxylin and Eosin
HER	:	Human Epidermal Growth Factor Receptor
HPG	:	Hyperbranched Polyglycerols
HPLC	:	High Performance Liquid Chromatography
HRP	:	Horseradish Peroxidase
IHC	:	Immunohistochemistry
IMAC	:	Immobilized Metal–Affinity Chromatography
IPTG	:	Isopropyl β-D-1-thiogalactopyranoside
KRAS	:	Kirsten Rat Sarcoma
LB	:	Lysogeny Broth

MTD	:	Maximum Tolerated Dose
MTT	:	3-(4,5-Dimethylthiazol-2-yl)-2,5-diphenyltetrazolium bromide
NCI	:	Normalized Cell Index
NHS	:	N-Hydroxysuccinimide
NMWL	:	Nominal Molecular Weight Limit as defined by Merck Millipore
NOAEL	:	No Observed Adverse Effect Level
NTA	:	Nitrilotriacetic Acid
OATP	:	Organic Anion Transporting Polypeptide
PBS	:	Phosphate Buffered Saline
PC	:	Pancreatic Cancer
PEG	:	Polyethylene Glycol
pI	:	Isoelectric Point
PS	:	Penicillin Streptomycin
RIPs	:	Ribosome–inactivating Proteins
RNA	:	Ribonucleic Acid
RPMI	:	Roswell Park Memorial Institute medium
RT	:	Radiation Therapy
RTCA	:	Real–Time Cell Analysis
SDS-PAGE	:	Sodium Dodecyl Sulfate-Polyacrylamide Gel Electrophoresis
SLC	:	Solute Carrrier
SPDP	:	Succinimidyl 3-(2-pyridyldithio)propionate
TBE	:	Tris-Borate-EDTA
TFR	:	Transferrin Receptor
TGF-B	:	Transforming Growth Factor-Beta
TGR	:	Tumor Growth Rate
TLC	:	Thin Layer Chromatography
TP53	:	Tumor Protien p53
UV	:	Ultraviolet
VEGF	:	Vascular Endothelial Growth Factor

1. Introduction

1.1 Cancer

1.1.1 Cancer epidemiology

Cancer has an extensive brunt on society across the world. As per American Cancer Society, 1,685,210 new cancer cases and 595,690 cancer deaths were expected to occur in the United States in 2016 [1]. Out of which pancreatic cancer (PC) accounts for one of the tenth leading cause of occurrence and death in both sexes [1]. According to world cancer report 2014, an estimated 14.1 million new cases of cancer emerged in the world in 2012. Out of which 7.4 million were males and 6.7 million were females, bestowing a male: female ratio of 10:9. Lung cancer was discovered to be the most common cancer type in men whereas breast cancer in women. Prostate cancer was the second most common cancer diagnosed in males worldwide (15%). Colorectum, stomach and liver are the common cancer sites of the five most common cancers in males across the world, accounting for 10%, 9% and 7% of the male total, respectively [2]. All over the world, it is reckoned that there were 32.5 million men and women still alive in 2012, up to five years after their diagnosis. Most of these had been diagnosed with breast, bowel (including anus), or prostate cancer [3]. As the incidence and death rates are declining worldwide for 4 major cancer sites (breast, lung, prostate and colorectum), the cases of pancreatic cancer is accelerating. It is expected to over-take breast cancer to become the third leading cause of cancer-related death in United States as per the latest Cancer Statistics Report 2016 published by American Cancer Society [1]. It is anticipated that there will be 23.6 million new cancer cases worldwide each year by 2030. This is 68% more cases than in 2012, with slightly larger growth in low and medium human development index countries (66% more cases in 2030 than 2012) than in high and very high human development index countries (56% more cases in 2030 than 2012) [4].

1.1.2 Cancer and immunity

Cancer is a convoluted disease in which cells in a particular tissue are no longer plenarily responsive to the signals within the tissue regulating cellular differentiation, survival, proliferation and death. This in turn leads to accumulation of these cells within

the tissue, causing local damage and inflammation. The survival beyond its mundane life span and the ability to proliferate aberrantly are the prime characteristics possessed by a cancer cell [5]. In contrast, our immune system protects us from infectious and other foreign invaders, such as grafts and certain tumors. Immunology and oncology thus have a long connection within the biomedical sciences [6].

The formation of immunity to cancer is a cyclic system (Figure 1). It can be self-propagating, leading to amplification and broadening of T cell mediated responses. Nevertheless, inhibitory factors can also halt the development or limit immunity. The cancer-immunity cycle can be divided into a series of seven steps, originating with the release of antigens from the cancer cell as seen in figure 1 (step 1). The cycle ends at step 7 leading to cancer cell death [7].

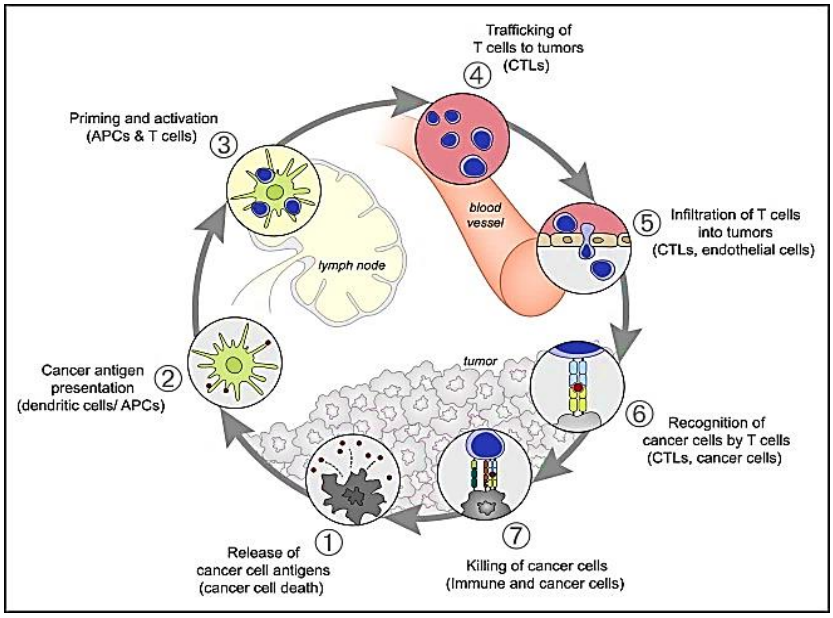

Figure 1. Cancer-immunity cycle. The cycle represents the release of neoantigens by cancer cells. The dendritic cells abduct the antigens and hand over them on MHCI and MHCII molecules to T cells. Determinately, the activated T cells infiltrate into tumor bed. The T cells bind to cancer cells by interacting with T cell receptor and antigen bound to MHCI. Finally, leading to cancer cell death as shown in step 7. APCs, antigen presenting cells; CTLs, cytotoxic T lymphocytes [8].

Each step of the cycle (Figure 1) requires the functioning of numerous factors, both stimulatory and inhibitory in nature. Stimulatory factors promote immunity, whereas inhibitors keeps the process in check and decrease immune activity and/or prevent autoimmunity. Immune checkpoint proteins, such as CTLA4, act at the level of T cell growth and inhibit the development of an active immune response (step 3). Immunostat

factors, such as PD-L1, performs inhibitory function that primarily acts to harmonize active immune responses in the tumor bed (step 7). Intratumoral T regulatory cells, macrophages, and myeloid-derived suppressor cells are key sources of many of these inhibitory factors (Figure 1).

In cancer patients, there is a disruption in the cancer-immunity cycle. Tumor antigens may not be encountered, dendritic cells and T cells may treat antigens as host rather than foreign entity. This leads to T regulatory cell responses rather than effector responses. It may also happen that T cells may not properly make their way to tumors and may be inhibited from infiltrating the tumor. It may also occur that tumor microenvironment might also suppress those effector cells that are produced as reviewed by Motz and Coukos [9].

Cancer therapies must therefore be carefully constructed to selectively target cancer cells that may provide anticancer activity but cause no damage to cancer cells and tissues.

1.1.3 Pancreatic cancer

Worldwide, over 200,000 people die of PC annually. In the United States, the American Cancer Society estimated about 53,070 people diagnosed and about 41,780 people dead of pancreatic cancer in 2016. It is the seventh most common cause of death from cancer including both sexes. Pancreatic cancer is accountable for 331,000 deaths per year worldwide [2]. The maximum number of cases and deaths (55%) occur in the more developed regions, with rates varying between 7 and 9 per 100,000 in men and 5 and 6.5 per 100,000 in women, with lower rates in less developed region [2]. The peak incidence of PC occurs in 65–75 year age group [10]. A median survival for locally advanced disease is 6–10 months whereas, for untreated metastatic PC is 3–5 months [11].

Environmental factors play a key role in the incidence of disease. Moreover, smoking is considered to be the most important factor leading to PC. A two fold increased risk of PC is observed in smokers compared to non-smokers [12]. A high caloric consumption and/or obesity can be a risk factor leading to PC [13, 14]. A causal tie

between diabetes mellitus and the subsequent development of pancreatic cancer has also been known since 1995 [15]. In order to plan a treatment, various tests and procedures are used to diagnose the stage of disease. Blood chemistry studies, tumor marker test, magnetic resonance imaging, computerized tomography scan, positron emission tomography scan, abdominal ultrasound, endoscopic ultrasound, endoscopic retrograde cholangiopancreatography, percutaneous transhepatic cholangiography, laparoscopy and biopsy are performed to examine pancreas.

1.1.4 Currents methods to treat cancer

Surgery, chemotherapy and radiation therapy are the most prevailing treatment strategies in case of cancer treatment. Surgery is one of the oldest and remains to be most effective method when the tumors are localized, however chemotherapy and radiation therapy are utilized to kill cancer cells or to prevent its dissemination to various other organs. Besides, several other treatment modalities are commonly used for cancer treatment as shown in figure 2.

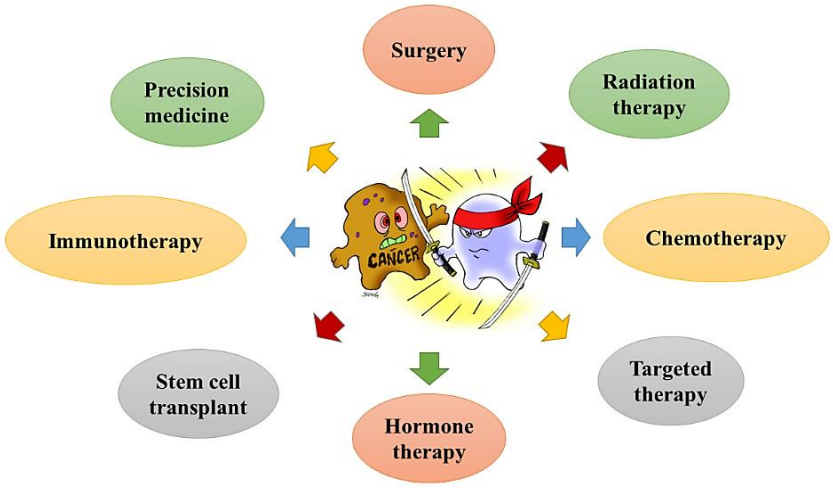

Figure 2. Major therapeutic modalities commonly used for the treatment of cancer.

1.2 Treatment options for pancreatic cancer

1.2.1 Surgery

The potentially curative (R0) and the palliative (R1/R2) are the two general types of surgery used for the treatment of pancreatic cancer. Surgical resection offers

significantly ameliorated prognosis with a median survival of 14–20 months and up to 25% 5-year survival rates [16-18]. Moreover, the median survival of 17 months was observed in patients with surgical resection alone as compared to 11 months in chemoradiation group of resectable PC [19]. Pancreaticoduodenectomy typically remains one of the surgical procedure in patients where the tumor is located in the head region of pancreas. However portal vein resections turns out to have better survival benefits and ability to reach R0 resection in contrast to multivisceral pancreatic head resections in patients with pancreatic ductal adenocarcinoma [20].

1.2.2 Radiation therapy

Radiation therapy (RT) induces cancer cell death by either directly causing DNA damage or creating free radicals within tumor cells that can, in turn, damage the host DNA. However, the survival benefit gained from adding RT in patients with locally advanced pancreatic ductal adenocarcinoma remains controversial, despite 5 randomized clinical trials published to date [21-24]. Nowadays, Carbon ion RT with simultaneous full dose gemcitabine turns out to be a well-tolerated and effective treatment strategy in patients with unresectable locally advanced PC [25, 26]. The major detriment of it is gastrointestinal ulcer (GI), however a GI dose constraint of $D_{2cm3} < 46$ Gy (relative biological effectiveness) decreases the risk of GI ulcer [27].

1.2.3 Chemotherapy

Adjuvant chemotherapy is given to patients after definitive therapy, most commonly surgery [28]. Neoadjuvant therapy refers to the administration of chemotherapy and/or chemoradiation to help facilitate a subsequent local therapy [29]. A multi-objective multi-drug optimization model for cancer chemotherapy treatment planning showed that this approach can identify the most promising low cost drug combinations, not achieved so far [30]. The final results of the European Study Group for Pancreatic Cancer 1 Trial showed that adjuvant chemotherapy has a significant survival benefit in patients with resected pancreatic cancer. The 21% five-year survival rate among patients who received chemotherapy and 8% among patients who did not receive chemotherapy (P=0.009) was seen [31].

A long-term 24-month survival in pancreatic anaplastic carcinoma (giant cell type) after S1 postoperative adjuvant chemotherapy (100 mg/day for four weeks) with no recurrence or metastasis has been revealed [32]. A combination of 5-FU/irinotecan/oxaliplatin (FOLFIRINOX) shows survival advantage but increased toxicity as compared to gemcitabine. However, FOLFIRINOX is an option for the treatment of patients with metastatic pancreatic cancer and has a good performance status [33]. A six month survival improvement was observed in gemcitabine-based cytotoxic combinations including gemcitabine-fluoropyrimidine analogues and gemcitabine-platinum analogues [34].

1.2.4 Immunotherapy

Immunotherapy is one of the most promising approaches in oncology, boosting the immune system. According to American Society of Clinical Oncology, immunotherapy, also called biologic therapy, "is a type of cancer treatment designed to boost the body's natural defenses to fight the cancer. It uses substances either made by the body or in a laboratory to improve or restore immune system function". Immunotherapy triggers the immune system to respond against tumor-associated antigens and attack tumor cells [35].

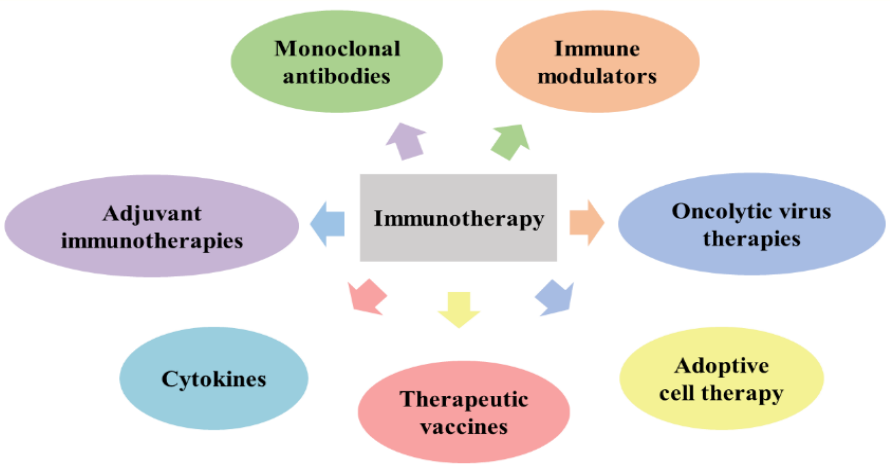

Figure 3. Seven main categories of immune-based therapeutic treatments in pancreatic cancer.

Immunotherapy can either stop or slow the growth of cancers cells. It can also stop cancer from spreading to other parts or help immune system to work better at destroying

neoplastic cells. Several types of immune-based treatments can be utilized as shown in figure 3.

So far, monoclonal antibodies have proven to be more beneficial to treat some cancers. Recombinant monoclonal antibodies target tumor-specific antigens. Tumor cells are killed either by direct lysis or through a delivery of a conjugated cytotoxic agent. Immune based-therapies pose a distinctive advantage over chemotherapy and radiotherapy due to several reasons. Firstly, in a way to act through a different mechanism by representing a non-cross-resistant treatment with an entirely different spectrum of toxicities. Secondly, the B cells and T cells of immune system are able to recognize a diverse array of tumor antigens. Moreover, both T and B cells can differentiate small antigenic differences between normal and transformed cells. This in turn provides specificity while minimizing toxicity. In pancreatic tumors, angiogenesis is regulated by platelet-derived endothelial-cell growth factor, fibroblast growth factor and VEGF family members. Monoclonal antibodies that target these signaling pathways have demonstrated efficacy in preclinical studies [36-38].

So far, monoclonal antibodies have been the most successful form of immunotherapy clinically. The specificity to target tumor cells while sparing normal tissue, ease of administration and low toxicity profile are the major advantages. However, the primary disadvantage being absence of T cell activation. This inhibits the T cell mediated cytotoxic killing and generation of memory immune responses [39].

1.3 Drug targeting strategies in pancreatic cancer

Targeted therapies act by blocking essential biochemical pathways or mutant proteins that are required for tumor cell growth and survival. Cell membranes are biological barriers that selectively inhibit the passage of drug molecules. Drugs may cross the cell membrane by passive diffusion, facilitated passive diffusion, active transport and pinocytosis.

Targeted anti-tumor toxins consists of a toxic functional moiety that is recombinantly fused or chemically linked to a cell-leading ligand. This kind of toxin is also utilized in the present research work. The toxic moiety kills cancer cells while the ligand directs the cell to the respective antigen present on the tumor cell [40]. To eradicate cancer

cells, a specific ligand that is solely expressed or overexpressed in cancer cells but not in normal cells is required. The passive and active targeting (Figure 4) are the two major types of drug targeting strategies as described below.

Passive targeting to tumors can be achieved through enhanced permeation and retention (EPR) effect as shown in figure 4 [41-43]. The nanomedicines cause passive accumulation of drug, enhancing therapeutic index while decreasing side effects [44-46].

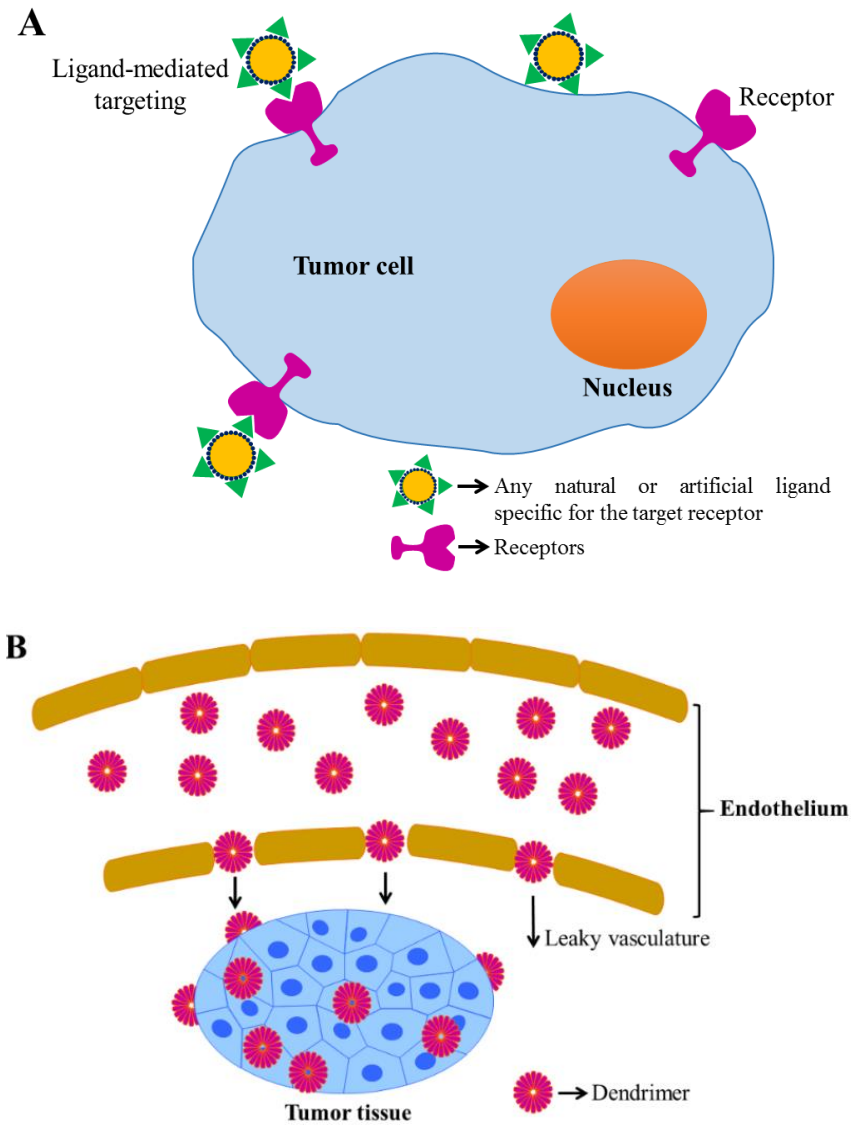

Figure 4. Active and passive targeting. (a) Active targeting is commonly based on ligand-attached or conjugated systems that explicitly bind to the target site leaving out non-target sites. (b) Passive targeting through leaky blood vessels. Passive targeting can be accomplished *via* a large molecule (e.g. polymer), which influences the enhanced permeation and retention (EPR) effect, leading to leakage that can result in targeting, such as in extremely vascularized and leaky blood vessels in solid tumors.

Active targeting utilizes biologically specific interactions between drug/drug carrier and target cells, usually through ligand receptor interaction or antigen antibody binding as depicted in figure 4. It can also be achieved by locally applied signals such as sonification or heating. Active targeting has several advantages which include:

- Specific interactions between targeting components with antigen available on target tissues. This leads to selective accumulation of the drug at the target site.
- Decrease in adverse effects, as drug accumulation takes place only on tumor sites allowing the drug uptake through endocytosis.
- It uses the characteristic features of tumor cells only. Cell surface tumor-specific antigens are overexpressed in tumors when compared to normal tissue.

A variety of alterations both on the tumor cell surface and signaling pathways play a pivotal role in the pathogenesis as well as in tumor therapy. The most common pathway aberrations involved in pancreatic cancer include KRAS, TGF-β, TP53, HEDGEHOG, NOTCH, WNT, MYC and EGFR-family. Oncogenic mutations of KRAS are present in over 70% cases of PC. Salirasib is one of the most potential KRAS inhibitors in pancreatic cancer as demonstrated in both preclinical and clinical sectors [47]. The TGF-β pathway is unique as it has tumor suppressor function in normal cells. Also, in early tumor cells it inhibits cell growth. However in later stage of tumorigenesis it causes an oncogenic effect. The preclinical efficacy of LY2109761 as a novel therapeutic approach to suppress pancreatic cancer metastasis by targeting TβRI/II kinase activity had also been studied [48].

Multiple alterations in HEDGEHOG signaling genes have been demonstrated in pancreatic tumor cell compartment [49]. Co-administration of gemcitabine with IPI-926 caused temporary control over tumor progression leading to an increase in overall survival time [50].

Furthermore, the EGFR family includes a group of cytoplasmic receptor tyrosine kinases mainly HER1 (EGFR), HER2, HER3 and HER4. Overexpression of HER2 receptor is present in certain pancreatic carcinoma cell lines [51]. Erlotinib, an EGFR tyrosine kinase inhibitor is one of the already approved drugs to be used in combination with gemcitabine for the treatment of PC [52].

1.3.1 Receptor mediated targeting of endocytotic pathway

The membrane associated proteins are termed as receptors. The ligands are considered to be the molecules that bind to these receptors. The interaction between ligand and receptor is essential to exert physiological functions. Receptor mediated endocytosis permits an accelerated means of ligand targeted internalization compared to that of untargeted complexes. Furthermore, the ligand-receptor complex is internalized either by clathrin-dependent or a clathrin-independent endocytotic process. The transferrin receptor (Tfr) [53, 54] and the epidermal growth fact receptor (EGFR) [55] are generally endocytosed *via* clathrin-coated vesicles as depicted in figure 5. The intracellular processing of drug molecules involves several compartments in the course of a multi-step transport sequence [56]. The compartments along the vesicular transport pathway consists of early endosome, late endosome, prelysosomes and lysosomes. The early endosome is the major sorting compartment of the endocytotic pathway. The acidification of endocytotic vesicles occur after their internalization at cell surface [57].

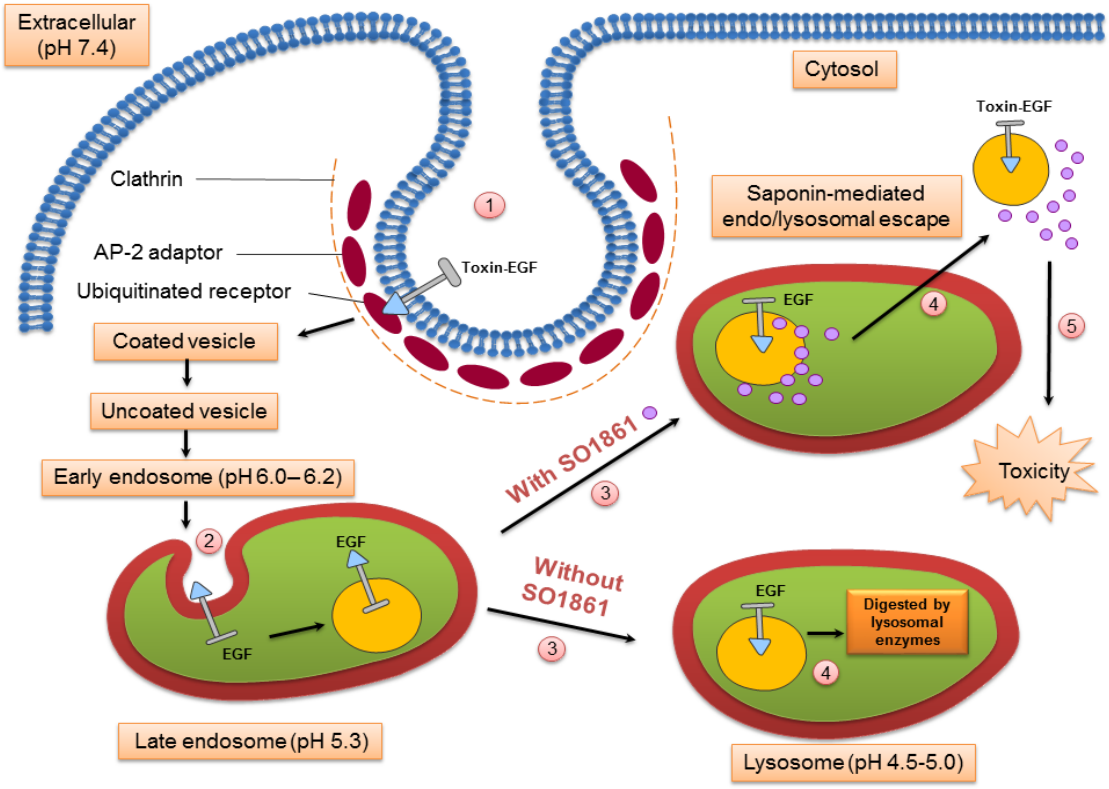

Figure 5. Endolysosomal escape pathway. The cancer-cell-specific ligands direct the internalization of the toxins *via* receptor-mediated endocytosis (1). Upon internalization the catalytic domain of the toxin is cleaved in the late endosome (2) and translocate to the cytosol leading to cell death in presence of SO1861 (3-5) or in its absence undergoes lysosomal degradation (3,4). EGF, epidermal growth factor.

The concept of endocytotic pathway basis itself on pH dependent action of distinct membrane compartments, which internalize molecules from the clathrin-coated pit at the plasma membrane and recycle them back to the surface. In general, pH ranges from 6.0-6.2 for early endosomes, 5.3 for late and prelysosomes and 4.5-5.0 for lysosomes [58]. The dissociated ligands under acidic conditions are further transported and degraded in lysosomes, while the receptors are recycled to the plasma membrane [59]. Thus, majority of selective targeting agents are chosen on their ability to be internalized *via* a clathrin-independent mechanism where the contents are not intended to undergo lysosomal degradative pathway. For targeted toxin to work as cytotoxic agent, the enzymatic fragment must translocate to cytosol. Once in the cytosol, targeted toxin turns out to be most potent killing agents.

Furthermore, cancer cells contain upregulated amounts of membrane receptors, typically epidermal growth factor (EGF) receptor, the proto-oncogene receptor HER2, the interleukin-2 receptor or cancer-associated carbohydrates [60, 61]. The overexpression of receptors in PC cells has led to the development of drug conjugates or targeted toxins with high affinity targeting agents to specifically aim cancer cells. Approximately 90% of pancreatic cancers, which have a 5-year survival rate of less than 5%, display overexpression of EGFR or its ligands [62, 63]. Mesothelin is a new target for anticancer therapy in PC [64].

Toxins of bacterial and plant origin have shown potent protein inhibitory action. Amongst toxins, plant ribosome inactivating proteins (RIPs) constitute as potent inhibitor of protein synthesis. Various RIPs are utilized for the construction of targeted toxins. The leading toxin components are ricin, saporin, dianthin, bouganin and gelonin. Specific targeting ligands can be coupled to these plant toxins leading to highly specific targeted toxins. Targeted toxins inactivate cytosolic protein synthesis and induce apoptosis in malignant cells. A heparin-binding epidermal growth factor fused to saporin showed increased specificity and cytotoxicity against EGFR overexpressing malignancies [65].

Besides RIPs, various well-known toxins inhibit protein synthesis at translation level, though *via* different mechanism: diphtheria toxin (DT) and *Pseudomonas* exotoxin A directly inactivate elongation factor 2 by ADP ribosylation, thereby inhibiting amino acid chain elongation and finally cell death [66, 67]. Denileukin diftitox was the first recombinant fusion formed by a truncated form of DT and human cytokine interleukin-

2 which was approved by the US Food and Drug Administration approved for the treatment of lymphomas [68].

Some targeted toxins have to be administered in high doses due to low cytosolic uptake. An ineffective uptake into the target cells and nonspecific cytotoxicity typically leads to vascular leak syndrome [69, 70] and hypersensitivity reactions [71]. A decrement in the side effects can be observed due to combined application of enhancers and targeted toxins. The combined administration of individually nontoxic concentrations of a targeted toxin and a saponin as an enhancer lead to a potent cytotoxic and tumor inhibitory tool in targeted tumor therapy [72-76].

1.3.2 Transporters as drug targets

Transporter proteins play a pivotal role in nutrient uptake and efflux of xenobiotics out of cells in order to maintain cell survival. The drug transporters influence drug absorption, distribution and elimination. In cancer cells many transporters are up-regulated compared to normal tissues [77, 78]. The differential expression of transporters on cancer cells provide a novel target to enhance drug delivery into the tumor cells. The solute carrier (SLC) transporters and ATP-binding cassette (ABC) transporters are considered to be two superfamilies of 'multispecific drug transporters'.

The SLC transporters are generally involved in the uptake of small molecules into cells [79-81]. Whereas, ABC drug transporters utilize ATP hydrolysis and function as efflux transporters [82, 83]. Numerous isoforms of SLC and ABC drug transporters are highly expressed in most epithelial cell barriers. These barriers separates almost all body fluid compartments regulating the movement of drugs in and out of various tissues and fluid compartments. Furthermore, knockout studies and some clinical phenotypes have further clarified the respective importance of particular transporters for a toxin or a drug [84-86].

Within the SLC superfamily, members of the SLCO (also known as OATPs), SLC22 and SLC47 family play a major key role in drug transport. Currently, a major focus of toxicological and pharmacological research is on SLCO transporters. OATPs are sodium-independent plasma membrane transporters. OATP expression is regulated by nuclear receptors, tissue factors and inflammatory cytokines. Particularly OATP

subfamily 1 is known to mediate the cellular uptake of anticancer drugs as shown in figure 6.

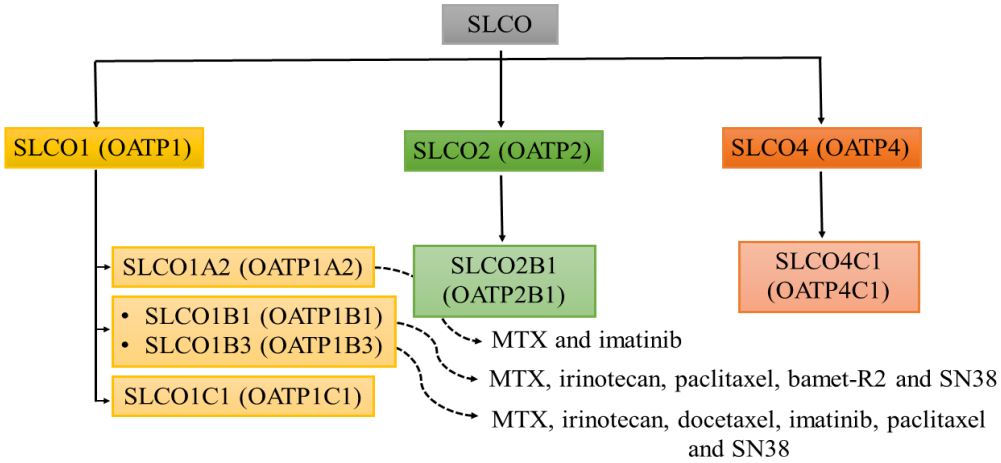

Figure 6. SLCO (solute carrier for organic anions) transporters implicated in xenobiotic and drug handling. Selected anticancer drug substrates acting on specific transporter are indicated with a dotted line. MTX, methotrexate; Bamet-R2, cis-Diamminechloro-cholylglycinate-platinum (II); OATP, organic-anion transporting polypeptide and SN38, an active metabolite of irinotecan.

OATP1B1/OATP1B3 are specifically expressed in normal liver and are regarded as 'liver-specific', whereas OATP4C1 is expressed in kidneys. An altered expression of OATPs is seen in different tumor entities. OATP1B1/OATP1B3 are highly expressed in cancers in gastrointestinal tract including pancreatic cancer. However they are downregulated in liver tumors. Thereby OATP1B1 and OATP1B3 serve as a unique target for OATP-targeted tumor therapy in pancreatic cancer [87]. In the era of targeted toxins, various microcystin analogues were optimized to target OATP-expressing metastatic cancers that are resistant to conventional chemotherapy [88].

Table 1. Selected anticancer drug as OATP1B1 inhibitors.

Inhibitors	IC_{50} (µM)	Reference
Irinotecan	-	-
Paclitaxel	0.03	[89]
SN-38	-	-
rTacrolimus	0.611[a]	[90]

a refers to K_i instead of IC_{50}.

Pazopanib and nilotinib are two small molecule tyrosine kinase inhibitors that showed *in vitro* inhibitory activity on OATP1B1 transporters [91]. An effort to target OATP1B1 pathway due to presence of organic anion polysulfate moiety is also performed in the present study.

1.4 Dianthin-30, a plant toxin for targeted tumor therapy

A wide range of plant toxins can be used to create anticancer drugs. Plant toxins cover a major part of ribosome inactivating proteins (RIPs). RIPs act predominantly on the ribosomal machinery *via* N-glycosidase enzymatic activity or polynucleotide adenosine glycosidase activity [92]. In general, RIPs, remove adenine from ribosomal RNA and depurinate the preserved α-sarcin loop of 28S ribosomal RNA from eukaryotic 80S ribosomes. This causes the inhibition of protein synthesis, furthermore induces apoptosis leading to cell death [93].

The plant RIPs are classified into 3 classes: type 1, 2 and in rare cases as type 3. RIPs can be single chain (type 1) or double chain (type 2). In contrast to type 2, type 1 RIPs lack galactose binding subunit. Type 1 RIPs thus have low aspecific toxicity for intact cells, are easier to handle and more stable than intact type 2 RIPs. All these features have attracted a lot of research groups to prepare cytotoxic conjugates with ligands and/or the combinatory use of endosomal escape enhancers [94-96].

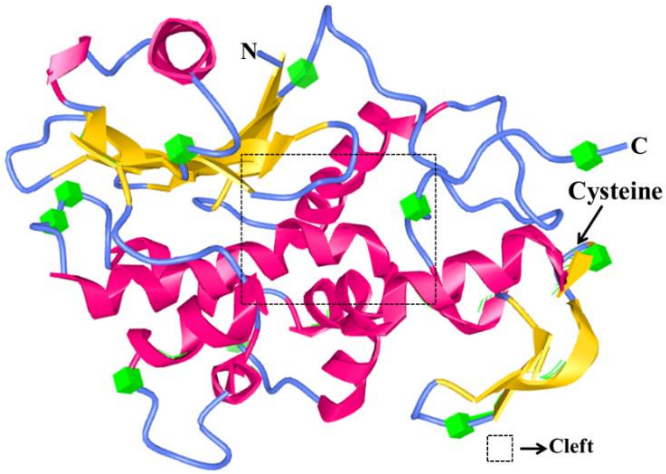

Figure 7. Structure of dianthin-30. Lysine residues and one cysteine as displayed by an arrow are highlighted with green. The protein structure (PDB 1RL0) was prepared from iCn3D software. N, N-terminal region; C, C-terminal region.

Dianthin-30 is a type 1 RIP isolated from the leaves of *Dianthus caryophyllus* L. plant [97, 98]. The molecular mass of dianthin-30 is 29,500 dalton [98]. Dianthin-30 is a basic glycoprotein having an isoelectric point (pI) 8.65 [97]. It also contains a glycosylation site and a C-terminal region (Figure 7) which may contain a vacuolar targeting signal [99].

The four catalytic residues (tyrosine 73, tyrosine 121, glutamic acid 177 and arginine 180) or the active site is located in a cleft between N- and C-terminal peptide chain (Figure 7). Interestingly, three strands (β7, β8 and β9) present in the C-terminal region are shorter in dianthin-30 in comparison to other RIPs. The reduced length of this loop located at one end of active pocket can bolster an easier accessibility to the substrate for protein [100]. This region also consists of three lysine residues (220, 226 and 234), which seem to be involved in molecular recognition of the ribosome.

In 1993 the first attempt to produce a recombinantly expressed biologically active dianthin-30 in *Escherichia coli* was performed [101]. Furthermore, recombinant dianthin-30 is easy to express, more stable and less immunogenic than other RIPs [102]. Dianthin-30 contains 1 cysteine, 4 methionine and 19 lysine residues. Therefore it is suitable for the preparation of tumor-targeting conjugates by coupling to different synthetic products, antibodies or other proteins.

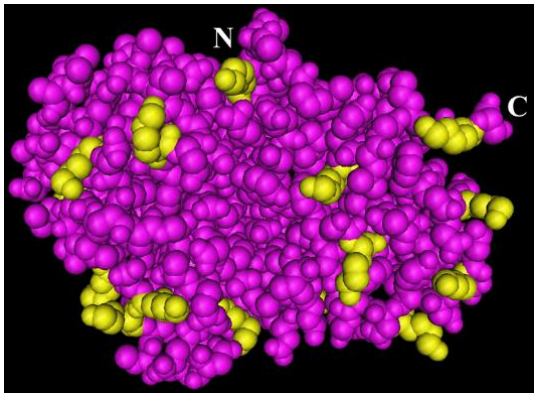

Figure 8. Space fill view of dianthin-30 showing exposed lysines on the surface. Lysine residues are highlighted in yellow. Structure was drawn with Cn3D 4.3 software.

The sulfur-containing amino acids (cysteine and methionine) are nonpolar and hydrophobic. In fact, methionine is one of the most hydrophobic amino acid and is

mostly oriented in the interior of the proteins. Cysteine however ionizes to yield thiolate ion but this is also buried inside dianthin-30 (Figure 8). The major reason can be that sulfur has low propensity to hydrogen bond, unlike oxygen which leads to H_2S gas under conditions that water is liquid. However conjugation with primary amines of lysine residues can lead to a cytotoxic agent in tumor therapy.

1.5 Construction of targeted toxin with dianthin-30

Paul Ehrlich postulated the concept of targeted toxins that antibodies fused to toxic moieties might serve as magic bullets [103]. Targeted toxins comprise a tumor specific ligand coupled to a polypeptide toxin. The lack of cell binding domain is a blessing in disguise for molecular biologists, and has assisted in the development of fusion proteins or synthetic analogs of type 1 RIPs together with ligands that are able to assist their cellular internalization. A targeted toxin with dianthin-30 can be prepared by synthetically introducing a thiol group for disulfide linkage. A recombinant fusion protein can also be produced to act as targeted toxin. Targeted toxin territory mainly includes the use of growth factors, cytokines, antibodies or small peptides. Toxins when transformed to targeted toxins provide high selectivity and specificity towards target antigens overexpressed in tumor cells.

1.5.1 Targeted toxin with dendritic polyglycerol sulfates (dPGS)

Kim and Webster introduced the term ‘hyperbranched polymers’ to describe dendritic macromolecules. Dendritic polyglycerol sulfates (dPGS; Figure 9) possess tree-like, hyperbranched architecture presenting anionic sulfate groups. The highly negative charge of dPGS makes the targeted toxin (dianthin-dPGS conjugate) to selectively interact with positively charged amino acids of the ligand binding pockets overexpressed in tumor cells [104].

The excellent biocompatibility [105-107] of polyglycerols (PGs) *in vitro* [107] and *in vivo* [108] has led to great significance in biomedical applications including bioconjugation with peptides. Hyperbranched PGs improve the solubility and plasma half-life of drug [109]. The prime advantage of polymeric carriers is to facilitate the passive targeting of drug conjugates to solid tumors [41]. This leads to selective

accumulation of targeted toxin in tumor tissue, also called EPR effect. *In vitro* cellular uptake studies of dye labeled with dPGS revealed rapid internalization inside the cytosol in contrast to neutral dPG [110]. Therefore, dPGS represent a promising candidate in drug delivery of dianthin-dPGS conjugates to tumor cells where it bypasses the endosomal escape mechanism of type 1 RIPs, leading to the desired toxic effect in the cytosol.

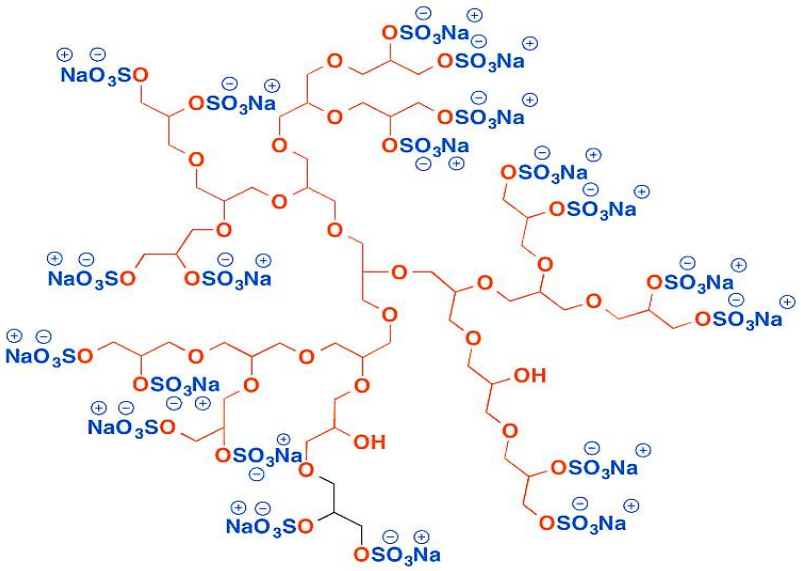

Figure 9. Chemical structure of polyglycerol sulfates (PGs) [104].

1.5.2 Epidermal growth factor as a ligand to targeted toxin

EGFR ligands are of special importance in tissues as they regulate cell proliferation, migration, adhesion, and inflammatory processes. EGFR is highly expressed in most of the cancers including pancreatic cancer [63, 111]. Natural ligands like growth factors or cytokines are utilized as cell binding domain thus rendering potent cytotoxic effect [112]. Specific cell binding ligands can be genetically fused to plant toxins. In 2012, dianthin-30 fused to human epidermal growth factor was cloned by Weng *et al.* [113]. A small decrease in enzymatic activity is generally observed when RIPs are transformed to targeted toxins. Studies also revealed that small structural differences in a number of amino acids can also effect the protein expression [114]. The increased protein yield of the fusion protein compared to the unfused toxin can be attributed to the fact of being less toxic to its host [114]. Immunogenicity is a major limitation in

toxin linked tumor-targeted therapies. *In vivo* studies of bispecific targeted toxins comprising toxin, EGF and interleukin-4 proved to 90% less immunogenic to native drug [115].

1.6 Saponin as efficacy enhancer

Various chemical, viral, bacterial and eukaryotic substances are employed to augment the efficacy of targeted toxins by endosomal escape mechanism. A scant cytosolic uptake of the toxin components is a major concern in tumor targeted therapies. The logic behind it is poor internalization, recycling to cell surface and lysosomal degradation. It is thus understandable that efficacy enhancers are valuable gadgets to boost up endosomal escape route. To achieve this, saponin, a plant glycoside is utilized in combination with targeted toxins [76]. Saponins consist of a triterpenoid, steroid or steroid alkaloid aglycone part along with one or more sugar chains linked by glycosidic bonds. An interesting property of saponins is cell cycle arrest leading to apoptosis in cancer cells. The use of saponins has also broadened the therapeutic window by making it possible to use a low dose of targeted toxins with more than 1000 fold increment in cytotoxicity when used in combination [72-74, 116-118]. This effect of saponins makes it a magnificent tool in combinatorial approach to treat tumors.

1.7 Objectives

The major objective of this thesis was to create a highly purified targeted toxin utilizing two disparate ligands in both cases together with dianthin being a common plant toxin. Lately a comparative therapeutic efficacy of two targeted toxins on pancreatic carcinoma xenograft model will be determined in presence of an endosomal escape enhancer (SO1861). Also in this way the therapeutic efficacy of receptor- as well as transporter - mediated pathway will be explored. In order to accomplish the aforementioned goal, the following subgoals were defined.

Targeted toxins consist of a targeting polypeptide covalently linked to a peptide toxin. The targeted toxins are hybrid protein therapeutics consisting of ligands that bind to the surface of neoplastic cells and deliver toxin, inhibiting protein synthesis and cause cancer cell death. The tumor-selective feature of a targeted toxin has thus made it an

utmost magnificent tool to be utilized in targeted cancer therapies. Nevertheless many targets were abandoned prior to *in vivo* or clinical testing. These targets lack the crucial property of permitting the entry of the toxin from endosomes into the cytosol after their receptor - mediated internalization. Moreover a major challenge in the designing of targeted toxins is to identify adequately specific ligands and to inhibit the nonspecific binding of toxic moiety to normal cells.

Firstly, a targeted toxin comprising dianthin and dendritic polyglycerol sulfates (dPGS) will be chemically constructed in a highly purified state. Simultaneously another targeted toxin consisting of dianthin coupled to epidermal growth factor (EGF) will be recombinantly expressed and purified. The enzymatic activity of both targeted toxins will be further analyzed and evaluated.

Secondly, dianthin-based targeted toxins will be characterized *in vitro* and their cytotoxicity will be compared on antigen/receptor overexpressing cell lines in combination with endosomal escape enhancer (SO1861) or not.

Thirdly, an acute toxicity study in order to determine the no observed adverse effect level (NOAEL) of drugs in BALB/c mice will be performed. Special attention will be given on the after-effect of toxicity treatments on different organs. For this all organs will be isolated and analyzed immunohistochemically. Also a maximum tolerated dose (MTD) will be determined. Thereafter, a dose will be selected for further dose response curves (DRC).

Fourthly, a pancreatic cancer xenograft model that has been described in the literature will be established. Furthermore, the therapeutic efficacy of dianthin-based targeted toxins on CD-1 nu/nu mice were examined in contrast to placebo. Subsequently, one of the two dianthin-based targeted toxins will be deduced as more efficacious and potent for future developments.

Finally, *ex vivo* hematological parameters will be studied in case of dianthin-EGF (DE) treated animals. In contrast, liver enzymes with especial preference to transaminase level test will be given to dianthin-dPGS treated animals. *Ex vivo* analyses will be done to take into consideration the side-effect or adverse effect of therapy cycles along with its efficacy.

2. Materials and methods

2.1 Materials

2.1.1 Instruments and devices

2.1.1.1 Electrophoresis

- Dual Vertical Mini-Gel Unit MGV-202-U (CBS Scientific Company, San Diego, CA, USA)
- E835 power supply (Consort, Turnhout, Belgium)
- Mini Sub Cell GT System (Bio-Rad, Hercules, CA, USA)

2.1.1.2 Western blot

- Optimax X-Ray Film Processor (Protec Medizintechnik, Oberstenfeld, Germany)
- Siemens 13 × 18 Cassette (Siemens, München, Germany)
- Trans-Blot Cell (Bio-Rad, Hercules, CA, USA)

2.1.1.3 Spectrophotometers

- Nanodrop ND-1000 Spectrophotometer (Peqlab, Erlangen, Germany)
- Ultrospec 3000 UV/visible spectrophotometer (Pharmacia Biotech, Piscataway, USA)
- SpectraMax 340PC Absorbance Microplate Reader (Molecular Devices, Sunnyvale, CA, USA)
- Infinite M200 microplate reader (Tecan Trading AG, Männedorf, Switzerland)

2.1.1.4 Cell culture

- CO_2-Incubator Modell 311 (Forma Scientific/Thermo Scientific, Waltham, MA, USA)
- Nicool LM 10 freezing unit (Air Liquide, Düsseldorf, Germany)
- HERA cell incubator (Heraeus, Waltham, MA, USA)
- Heraeus HERAsafe Safety Cabinet (Heraeus/Thermo Scientific, Waltham, MA, USA)

- Neubauer chamber (Labor Optik, Bad Homburg, Germany)
- Luna fl dual fluorescence cell counter (Logos Biosystems, Villeneuve-d'Ascq, France)
- xCELLigence System RTCA (Roche Applied Science, Mannheim, Germany)

2.1.1.5 Centrifuges

- Megafuge 2.0 R (Heraeus/Thermo Scientific, Waltham, MA, USA)
- Microcentrifuge 5424 R (Eppendorf, Hamburg, Germany)
- Microcentrifuge 5417 R (Eppendorf, Hamburg, Germany)
- Varifuge 3.0 (Haraeus Sepatech, Hanau, Germany)
- Spectrafuge Mini (Labnet International Inc., Edison, USA)
- Sorvall RC 5B refrigerated superspeed Centrifuge (Thermoscientific, Waltham, MA, USA)
- Sorvall RC 3B plus (Thermoscientific, Waltham, MA, USA)

2.1.1.6 Devices for animal experiment

- Surgical scissor (Fine Science Tools, Heidelberg, Germany)
- Tissue forcep (Fine Science Tools, Heidelberg, Germany)
- Narrow pattern forcep (Fine Science Tools, Heidelberg, Germany)
- Inhalation anesthesia apparatus Sulla 808; Isoflorane vapor 19.3 (Drägerwerk AG, Lübeck, Germany)
- Ohmeda Isotec 5 Vaporiser (Siemens, Munich, Germany)

2.1.1.7 Other devices

- Äkta FPLC (Amersham Biosciences Europe GmbH, Freiburg, Germany)
- Certomat BS-1 shaker (Sartorius AG, Göttingen, Germany)
- Thermomixer comfort 1.5 mL (Eppendorf AG, Hamburg, Germany)
- Heidolph REAX 2 overhead shaker (VWR International GmbH, Darmstadt, Germany)
- CK30 culture microscope (Olympus optical Co., Hamburg, Germany)
- Branson Sonifier 250 (G. Heinemann, Schwäbisch Gmünd, Germany)
- Systec VB-150 autoclave (Systec GmbH, Linden, Germany)

- BIO RAD Gel Dryer Model 583 (Bio-Rad Laboratories GmbH, Munich, Germany)
- Diaphragm Vacuum Pump (Vacuubrand GmbH + Co., Wertheim, Germany)
- C25KC Incubator shaker (New Brunswick scientific, Enfield, USA)
- MS 1 minishaker (Ika, Sigma Aldrich, Munich, Germany)
- Waterbath 1086; (GFL Gesellschaft für Labortechnik GmbH, Burgwedel, Germany)
- Agilent 6210 ESI-TOF-MS (Agilent, Santa Clara, USA)
- CAMAG TLC 4 Scanner (CAMAG, Berlin, Germany)

2.1.2 Consumables

2.1.2.1 Western blot

- Nitrocellulose membrane Hybond-C Extra (GE Healthcare, Uppsala, Sweden)
- Photographic paper Amersham Hyperfilm ECL (GE Healthcare, Uppsala, Sweden)
- Whatman filter paper (Whatman GmbH, Dassel, Germany)

2.1.2.2 Chromatography

- Econo-Pac chromatography columns (Bio-Rad, Hercules, CA, USA)
- Ni-nitrilotriacetic acid (NTA) agarose (Protino Ni-NTA agarose, Macherey-Nagel, Düren, Germany)
- Chitin resin (New England BioLabs, Ipswich, England)
- HiTrap DEAE FF 1mL column (GE Healthcare Europe GmbH, Freiburg, Germany)

2.1.2.3 Biochemical assays

- Ethylendiamintetraaceticacid (EDTA) (Carl Roth, Karlsruhe, Germany)
- Herring sperm-DNA (Thermo Scientific, Waltham, MA, USA)
- Microplate Maxi Sorb U16 Module (Thermo Scientific, Waltham, MA, USA)

2.1.2.4 Cell culture

- 96-well E-plate (Roche Applied Science, Mannheim, Germany)

- CellTrics 0.22 µm filter device (Partec, Görlitz, Germany)
- Injekt Luer 10 ml syringe (B. Braun Melsungen AG, Melsungen, Germany)
- Rotilabo syringe filters 0.22 µm sterile (Carl Roth GmbH, Karlsruhe, Germany)

2.1.2.5 Materials for animal experiments and histology

- Myjector U-100 Insulin 1ml sterile syringe (Terumo Corporation, Tokyo, Japan)
- BD microlance 3 25G 1″ - Nr.18 needle (Becton Dickinson, Dublin, Ireland)
- Forene, Isoflurane 100% (Abott GmbH, Wiesbaden, Germany)

2.1.2.6 Materials for complete blood count analysis

- S-Monovette 1.2 ml K3E (Sarstedt AG & Co., Nümbrecht, Germany)
- Sterican 24G X 1″ - Nr.20 needle (B. Braun Melsungen AG, Melsungen, Germany)
- BD microlance 3 27G 3/4″ Nr-20 needle (Becton Dickinson, Dublin, Ireland)
- Omnifix-F Tuberculin 1 ml/Luer solo sterile syringe (B. Braun Melsungen AG, Melsungen, Germany)
- Leukoplast surgical tape (BSN medical, Hamburg, Germany)

2.1.2.7 Other consumables

- Amicon Ultra-15, 10,000 nominal molecular weight limit (NMWL) (Merck Millipore, Carrigtwohill, Ireland)
- ZelluTrans/Roth dialysis membrane T4, 12,000-14,000 MWCO (Carl Roth, Karlsruhe, Germany).

2.1.3 Chemicals

2.1.3.1 Plasmids

- 6× his-tagged-dianthin-30-epidermal growth factor (DE)-pET11d [113]
- 6× his-tagged-dianthin-30-pET11d [119]

2.1.3.2 Vector

- pET11d for Protein expression in *E. coli* (Invitrogen GmbH, Karlsruhe, Germany)

2.1.3.3 Antibodies

- Anti-His-tag monoclonal antibody (Clontech laboratories, Inc., France).
- Anti-EGFR pharmDx Monoclonal Mouse IgG1 Antibody (DAKO, Hamburg, Germany)

2.1.3.4 Other proteins

- Bovine serum albumin (BSA) (Albumin Standard, Thermo Scientific, Waltham, MA, USA)

2.1.3.5 Saponin

- SO1861 from *Saponaria officinalis* L. was isolated from the roots of the plant (Galke, Gittelde, Germany) by HPLC by Dr. Alexander Weng [120]

2.1.3.6 Cell culture

- 0.25% Trypsin-ethylenediaminetetraacetic acid (EDTA) (Gibco/Invitrogen, Karlsruhe, Germany)
- Dulbecco's modified Eagle's medium (DMEM) (PAA Laboratories, Pasching, Austria)
- Dulbecco's phosphate buffered saline (PBS) without Ca^{2+} and Mg^{2+} (PAA Laboratories, Pasching, Austria)
- Dulbecco's phosphate buffered saline (PBS) with Ca^{2+} and Mg^{2+} (PAA Laboratories, Pasching, Austria)
- Fetal bovine serum (FBS) (BioChrom KG, Berlin, Germany)
- Penicillin/Streptomycin (PS) (Gibco/Invitrogen, Karlsruhe, Germany)
- RPMI-1640 medium (PAA Laboratories, Pasching, Austria)

2.1.3.7 Electrophoresis reagents

- Acrylamide 4K - Solution (30%) - Mix 37.5:1 Acrylamide : Bisacrylamide (AppliChem, Darmstadt, Germany)
- Bromophenol blue Na-salt (Serva Electrophoresis, Heidelberg, Germany)
- Coomassie Brillant blue R-250 (AppliChem, Darmstadt, Germany)

2.1.3.8 Marker

- Unstained Protein Molecular weight marker (Thermo Scientific, Waltham, MA, USA)
- PageRuler prestained marker (Thermo Scientific, Waltham, MA, USA)

2.1.3.9 Buffer and medium

The following are recipes for a number of common biological buffer and medium used for various methods. Special buffers needed for individual methods are presented separately under the relevant methods.

The buffers were prepared with ultrapure water (MilliQ water).

Table 2. List of buffers and mediums

Buffer/Medium	Reagents
PBS buffer	150 mM sodium chloride, 8.33 mM disodium hydrogen phosphate, 1.67 mM calcium dehydrogenate, pH 7.4
LB-Medium	10 g/L peptone, 5 g/L yeast extract, 10g/L sodium chloride, pH 7.0
$LB_{AMP.}$	LB-Medium with 50 µg/mL Ampicillin-sodium salt
Buffer A	CAPSO buffer, pH 9.5
Buffer B	CAPSO Buffer + 2 mM NaCl, pH 9.5

2.1.3.10 Kits

- Pierce BCA Protein Assay (Pierce/Thermo Scientific, Waltham, MA, USA)
- Zyppy Plasmid Miniprep Kit (Zymo Research, Irvine, CA, USA)
- EGFR pharmDx™ Kit (DAKO, Hamburg, Germany)

2.1.3.11 Other reagents

- Adenine (Sigma-Aldrich, Steinheim, Germany)
- Nickel sulfate (Sigma-Aldrich, Steinheim, Germany)

- 3-(4,5-Dimethylthiazol-2-yl)-2,5-diphenyltetrazolium bromide (MTT) (Calbiochem, Darmstadt, Germany)
- Ampicillin sodium salt (Carl Roth, Karlsruhe, Germany)
- Heparin-Natrium 500 (Ratiopharm GmbH, Ulm)
- Protease inhibitor Complete (Roche Applied Science, Mannheim, Germany)
- Triton X-100 (Sigma-Aldrich, Steinheim, Germany)
- Tween-20 (Bio-Rad Laboratories GmbH, Munich, Germany)
- Formalin solution, neutral buffered, 10% (Sigma Aldrich, Steinheim, Germany)
- Counterstain: Dako's Automation Hematoxylin (code S3301; DAKO, Hamburg, Germany)
- Proteinase K (Thermo Scientific, Waltham, MA, USA)

2.1.4 Bacterial strains

- *Escherichia coli* Library Efficiency DH5α Competent Cells (Life Technologies, Carlsbad, CA, USA)
- *Escherichia coli* NiCo21(DE3) Competent Cells (New England BioLABS, Frankfurt, Germany)

2.1.5 Cell lines

Table 3. List of cell lines along with their origin and company obtained.

Cell Line	Origin
NIH3T3	Mouse embryonic fibroblast
MIA PaCa-2	Human pancreatic ductal adenocarcinoma
BxPC-3	Human pancreatic ductal adenocarcinoma
QGP-1	Human pancreatic islet cell carcinoma
Ca Ski	Human cervical carcinoma

2.1.6 Type and origin of mouse strains

- BALB/c immunocompetent albino mice, male; Charles River
- CD1 nu/nu athymic nude mice, male; Charles River

2.1.7 Computer softwares

- GraphPad Prism 6 (GraphPad Software, La Jolla, CA, USA)
- RTCA Software 2.1.1002 (Roche Applied Science, Mannheim, Germany)
- Magellan™ V 6.4 (Tecan, Data Analysis Software, Männedorf, Switzerland**)**
- SoftMax Pro (Molecular Devices Corporation, Sunnyvale, California)
- iCn3D (NCBI, USA)
- Cn3D 4.3 (NCBI, USA)

2.2 Saponin isolation and characterization

SO1861 was isolated from *Saponaria officinalis* L. The dried roots were finely ground and extracted by 90% methanol. The methanol was evaporated by vacuum distillation and cold acetone was added to the remaining aqueous extract. The resulting suspension was centrifuged and the pellet was dissolved in 20% methanol at 20 mg/mL. SO1861 was isolated by semi-preparative HPLC using an UltraSep ES PHARM RP18E (7 µm, 250 × 8 mm) column from SepServ (Berlin, Germany) and an methanol/water (0.01% TFA) gradient starting with 20% methanol to 80% methanol over 80 min. Flow rate was 1.5 mL/min. Fraction of SO1861 was freeze dried and analyzed by ESI-MS. Purity of SO1861 was assessed by densitometry using the CAMAG TLC 4 Scanner (CAMAG, Berlin Germany).

2.3 Protein chemistry methods

2.3.1 Transformation of expression vectors

Plasmids (6×his-tagged-dianthin-30-epidermal growth factor (DE)-pET11d and 6×his-tagged-dianthin-30-pET11d) were transformed either into *Escherichia coli* Library Efficiency DH5α Competent Cells (Life Technologies) for replication or into

Escherichia coli NiCo21 (DE3) competent Cells (Novagen) to recombinantly express the encoded protein. Firstly, a tube of NiCo21 (DE3) competent *E. coli* cells were thawed on ice for 10 min. Thereafter, the plasmid DNA [100 ng (1 µL)] was added to 20 µL of competent cell mixture. The mixture was then standstill on ice for 30 min. Heat shock at 42 °C for 90 s and 2 min on ice was then executed. Thereafter, the bacteria were supplemented with 300 µL Lysogeny broth (LB) (10 g/L peptone, 5 g/L yeast extract, 10 g/L NaCl, pH 7.0) medium without antibiotic. The suspension was incubated (1 h, 37 °C) under vigorous shaking (200 rpm). A prewarmed LB medium-agar plate with 50 µg/mL ampicillin was inoculated with 20 µL bacterial suspension. The plate was then incubated overnight at 37 °C for colony formation.

2.3.2 Plasmid preparation

To replicate the plasmid DNA, transformation was done into *Escherichia coli* Library Efficiency DH5α competent cells as described in section 2.3.1. To produce a starter culture, a colony of the bacteria transformed by the plasmid was picked and resuspended in 5 mL LB-medium with 50 µg/mL ampicillin. The starter culture was incubated overnight (37 °C, 200 rpm, 14 h). On the next day, 4 mL of the 5 mL starter culture was centrifuged at 5,000g for 5 min. The supernatant was removed and the pellet was re-suspended in 600 µL MiliQ water. Then, the plasmid was extracted with the Zyppy Plasmid Miniprep Kit (Zymo Research). After following the protocol indicated by the manufacturer (Zymo Research), the DNA concentration was determined by the NanoDrop ND-1000 Spectrophotometer and the plasmid DNA was stored at –20 °C.

2.3.3 Protein expression in *Escherichia coli*

The plasmid coding for dianthin-30-epidermal growth factor (DE) (6×his-tagged-DE-pET11d) and dianthin (6×his-tagged-Dianthin-30-pET11d) were transformed into NiCo21 (DE3) Competent *Escherichia coli* cells. LB-medium (3 mL) supplemented with 50 µg/mL ampicillin was inoculated with a colony from the transformed agar-plate. The bacterial suspension was incubated (6 h, 37 °C and 200 rpm) in order to get a starter culture. Thereafter, the starter culture (50 µL) was added to 500 mL LB-medium with 50 µg/mL ampicillin and was allowed to grown overnight (37 °C and 200

rpm). Subsequently, the volume of bacterial suspension was scaled-up to a culture of 2 L until an optical density (A_{600}) of 0.9 was reached (Photometer 1101 M, Eppendorf). Thenceforth, isopropyl β-D-1-thiogalactopyranoside (IPTG) at a final concentration of 1 mM was added to induce protein expression. The induction was carried out for 3 h (37 °C and 200 rpm). Finally, the bacterial suspension was centrifuged (5,000g, 4 °C, 5 min). The supernatant was discarded and the bacterial pellets were re-suspended in 20 mL phosphate buffered saline (PBS; 137 mM NaCl, 2.7 mM KCl, 8.1 mM Na_2HPO_4 and 1.47 mM KH_2PO_4 according to Dulbecco's). The resuspended pellets were stored at –20 °C until further required for purification step.

2.3.4 Protein purification

2.3.4.1 Immobilized metal-affinity chromatography

After expression the bacterial suspensions were thawed on water bath. The bacterial lysis were performed by an ultrasound device (Branson Sonifier 250, G. Heinemann). The lysates were centrifuged (16,100g, 4 °C and 30 min) and the supernatant was pooled together. Imidazole was added at a final concentration of 20 mM to the pooled supernatant. Immobilized metal-affinity chromatography (IMAC) was utilized to purify his-tagged protein. The supernatant containing his-tagged protein was purified by Ni-nitrilotriacetic acid (NTA) agarose affinity chromatography (Protino Ni-NTA agarose). The Ni-NTA agarose was washed three times with 10 mL ddH_2O. The agarose was recharged with $NiSO_4$ (3 mL, 100 mM) followed by three times washing with 10 mL wash buffer (50 mM NaH_2PO_4, 300 mM NaCl, 20 mM imidazole, pH 8.0). The supernatants were incubated with 3 mL Ni-NTA agarose under continuous shaking (1 h at 4 °C) in inverting device (Heidolph REAX 2). Subsequently, the material was poured into a 20-mL - column (Econo-Pac chromatography columns, Bio-Rad). The column was washed three times with 10 mL wash buffer followed by further elution of protein by increasing concentrations of imidazole in wash buffer (125 and 250 mM, see table 4). Proteins were eluted by 30 mL of each imidazole concentration. Eluates were collected and analyzed by sodium dodecyl sulfate-polyacrylamide gel electrophoresis (SDS-PAGE) [12% (w/v) gel depending on the molecular mass of the protein, see section 2.3.5], and dialyzed overnight (4 °C) against 1 L CBD Buffer (see section 2.3.6, table 5).

Table 4. Buffers used in Ni-NTA affinity chromatography.

Reagents	Wash Buffer	125 mM Imidazole buffer	250 mM Imidazole buffer
$NaH_2PO_4 \cdot 2H_2O$	7.80 g	7.80 g	7.80 g
NaCl	17.54 g	17.54 g	17.54 g
Imidazole	1.36 g	8.5 g	17 g
Milli-Q water	ad 1 L	ad 1 L	ad 1 L

pH adjusted to 8.00 with 5 M NaOH.

Table 5. Reagents for CBD buffer preparation.

Reagents	Amount per L	Amount per 5 L
NaCl	29.22 g	146.10 g
Tris(hydroxymethyl)-aminomethane·HCl	3.152 g	15.76 g
EDTA·2 H_2O (disodium salt)	0.372 g	1.86 g
Tween-20	1 mL	5 mL
Elix water	ad 1 L	ad 5 L

pH adjusted to 8.00 with 5 M NaOH.

2.3.4.2 Chitin column affinity chromatography

Further purification by chitin column affinity chromatography served to isolate target protein by removing bacterial proteins fused to an intein-chitin binding domain fusion. The chitin slurry (20 mL) was poured into a 20-mL - column (Econo-Pac chromatography columns, Bio-Rad) and equilibrated with 100 mL CBD buffer. Thereafter, the dialyzed fraction containing dianthin-EGF (DE) and dianthin (30 mL, 125mM) were incubated with equilibrated chitin resin under continuous shaking (1 h at 4 °C) in inverting device (Heidolph REAX 2). Subsequently, the material was poured into a 20-mL - column (Econo-Pac chromatography columns, Bio-Rad) until a bed volume of 20 mL was established. The protein solution was passed through the column and collected as flow through. The flow through was allowed to pass again through the chitin slurry column. Furthermore CBD buffer (20 mL) was passed through the column and collected into the same fraction. The column was washed two times with 20 mL CBD buffer. After elution with CBD buffer, the fractions were analyzed by SDS-PAGE [12% (w/v) gel depending on the molecular mass of the protein, see section 2.3.5]. Fractions containing target proteins (DE and dianthin) were dialyzed overnight (4 °C)

against 2 L PBS (see table 1). The next day, the desalted his-tagged proteins were concentrated by an Amicon Ultra-15, 10,000 NMWL. The protein concentration was determined by a bicinchoninic acid (BCA) assay (see section 2.3.7) and the proteins were stored at –4 °C.

2.3.5 SDS-PAGE analysis

Proteins were analyzed by sodium dodecyl sulfate-polyacrylamide gel electrophoresis (SDS-PAGE). SDS-PAGE (12% w/v) gel was prepared as per table 7 using various reagents as shown in table 6. Electrophoresis was performed (200 V, 60 mA, 45 min) for each gel (E835 power supply from Consort) in a Dual Vertical MiniGel Unit MGV-202-U (CBS Scientific Company). Unstained Protein Molecular Weight Marker (14.4–116 kDa; Thermo Scientific) was used in the analysis of low molecular mass proteins. The PageRuler Prestained Protein Marker (10–170 kDa) (Thermo Scientific) was used for proteins that were further characterized by Western blot (see section 2.3.8).

Table 6. Reagents for sodium dodecyl sulfate-polyacrylamide gel electrophoresis (SDS-PAGE) analysis.

Reagents	Composition
Loading Buffer	192 mM Glycine, 20 mM Tris, 0.1%(w/v) SDS
4 × Sample Buffer	0.25 mM Tris, 40% (v/v) Glycerol, 8% (w/v) SDS, 8% (v/v) 2-Mercaptoethanol, 0.004% (w/v) Bromophenol blue, pH 6.8
Separating gel Buffer	1.5 M Tris, pH 8.8, 0.4% (w/v) SDS
Stacking gel Buffer	0.5 M Tris, pH 6.8, 0.4% (w/v) SDS
Acrylamide mixture	30% Acrylamide, 0.8% Bisacrylamide
Marker	Unstained Protein Molecular Weight Marker (14.4 – 116 kDa)

Furthermore, SDS-PAGE was performed under reducing conditions. A solution of 0.1% (w/v) coomassie blue R-250 (AppliChem) in 40% (v/v) methanol and 10% (v/v) acetic acid was used as a staining solution for gels. Thereafter the gels were destained

(45 min) in a solution of 20% (v/v) ethanol and 10% (v/v) acetic acid. The gels were then placed in a continuous shaking device in a chamber filled with ddH_2O for 15 minutes. In order to dry, the gels were placed for 2 h in a BIO RAD Gel Dryer (Model 583) attached to Diaphragm Vacuum Pump (Vacuubrand GmbH + Co., Wertheim, Germany) which further served to dehydrate the gels.

Table 7. Preparation of SDS-PAGE gels.

Reagents	**Separating gel (12% w/v)**	**Stacking gel (4.5% w/v)**
MilliQ water	3.5 mL	1800 µL
Separating gel Buffer	2.5 mL	—
Stacking gel Buffer	—	750 µL
30% Acrylamide	4.5 mL	450 µL
10% APS	50 µL	10 µL
TEMED	5 µL	3 µL

2.3.6 Dialysis and concentration of protein solution

The fractions that contained a single purified band of DE and dianthin at 36 kDa and 30 kDa respectively (previously purified by chitin column affinity chromatography and analyzed by SDS-PAGE) were dialyzed overnight (4 °C) against 2 L PBS. To achieve a concentrated protein solution, the desalted protein was concentrated by repeated centrifugation steps (5 min and 4,000g) with the Amicon Ultra-15, 10,000 NMWL until a volume of 10 mL was achieved.

2.3.7 Determination of protein concentration by BCA assay

Protein concentration was determined by the bicinchoninic acid assay (Pierce BCA Protein Assay, Pierce/Thermo Scientific). A standard curve of bovine serum albumin (BSA; Albumin Standard, Thermo Scientific) was created following the indications of

the manufacturer (Pierce/Thermo Scientific) for various concentrations (0.03, 0.06, 0.12, 0.25, 0.50 and 1.00 mg/mL) deducting it from the blank (PBS). The absorbance (562 nm) was measured by the SpectraMax 340PC Absorbance Microplate Reader.

2.3.8 Western Blot

Proteins (DE and dianthin) were separated by SDS-PAGE [12% (w/v) gel] and then blotted (50 V, 15 °C, 1 h) to a nitrocellulose membrane (Hybond-C Extra). The membrane was blocked for 30 min with blocking buffer (table 8) and incubated with an anti-his-tag monoclonal antibody conjugated to HRP (1:10,000 diluted; Clontech laboratories, Inc.) for further 60 min.

Table 8. Reagents for Western Blot analysis

Reagents	Composition
Blot Buffer	191.8 mM Glycine, 25 mM Tris, 10% Ethanol
4 × Sample Buffer	0.25 mM Tris, 40% (v/v) Glycerol, 8% (w/v) SDS, 8% (v/v)
	2-Mercaptoethanol, 0.004% (w/v) Bromophenol blue, pH 6.8
Separating gel Buffer	1.5 M Tris, pH 8.8, 0.4% (w/v) SDS
Stacking gel Buffer	0.5 M Tris, pH 6.8, 0.4% (w/v) SDS
Acrylamide mixture	30% Acrylamide, 0.8% Bisacrylamide
Wash Buffer	150 mM NaCl, 8.3mM Disodiumhydrogen-phosphate, 1.7mM Pottassiumdihydrogen-phosphate, (pH 7.4), 0.2% (w/v) Brij
Blocking Buffer	PBS with 5% (w/v) skim milk powder
ECL Reagent	Reagent A: 100 mM Tris HCl, Luminol; Reagent B: P-Coumaric acid, DMSO; Reagent C: 30% H_2O_2
Marker	PageRuler prestained marker (10 – 170 kDa)

The membrane was washed 4 times with wash buffer [PBS with 0.2% (w/v) Brij58, pH 7.4] at an interval of 10 min each. Thereafter, it was treated with polyclonal goat anti-

rabbit immunoglobulins/HRP (1:10,000 diluted) (Dako Cytomation) for 30 min. The membrane was washed again for 4 times with $PBSB_{0.2}$. The binding of the secondary antibody was detected by enhanced chemiluminescence reaction. After exposure, the photographic paper (Amersham Hyperfilm ECL, GE Healthcare) was developed by an Optimax X-Ray Film Processor (Protec Medizintechnik).

2.3.9 Determination of N-glycosidase activity

N-glycosidase activity of proteins was determined by the cleavage and release of adenine residues from herring sperm DNA. First, an adenine standard curve was prepared by measuring the absorbance at 260 nm (reference at 300 nm) for various concentrations (1.87, 3.75, 7.50, 15.00, 30.00 and 60.00 µM). The NanoDrop ND-1000 Spectrophotometer (Peqlab) was used to measure absorbance. To determine the N-glycosidase activity of a targeted toxin, herring sperm DNA (10 µL, 100 µg; Invitrogen) stock solution was prepared in acetate buffer. Stock solution was heated at 100 °C (5 min) and thereafter at 50 °C (10 min). 100 µg herring sperm DNA (Invitrogen) was added to protein/toxin (see table 9) and acetate buffer (50 mM CH_3COONa, 100 mM KCl, pH 5.0) up to 100 µL. The mixture was incubated under continuous shaking (50 °C, 1 h). Subsequently, the mixture was transferred to a filtration device (3,000 MWCO; Millipore) and centrifuged (4 °C, 20 min and 5,000g). Absorbance of the filtrate was measured at 260 nm (reference at 300 nm).

Table 9. Reagents for N-glycosidase activity assay

Reagents	Toxin	Adenine (Positive control)	BSA (Negative control)	Blank
Herring sperm DNA	10 µL (100 µg)	—	10 µL (100 µg)	10 µL (100 µg)
Toxin/Adenine	600 nM	60 µM	600 nM	—
Acetate buffer	ad 100 µL	ad 100 µL	ad 100 µL	ad 100 µL

2.3.10 Synthesis and coupling of dPGS to dianthin

The dendritic polyglycerol sulfate (dPGS) is a hyperbranched dendrimer based on polyglycerol. The synthesis is accomplished by a synergistic built-up of the dendrimer starting from pentaerythritol (PE) using methods described by Paulus et al. 2014.

To incorporate a linker for conjugation to dianthin, PE-triallyl was synthetically modified with an azidohexyl residue. Subsequently, the dendrimer was built up by an alternating stepwise dihydroxylation (potassium osmate) and allylation (sodium hydride, allylbromide), giving azidohexyl dendron of generation 1 (6 hydroxy groups), generation 2 (12 hydroxy groups), generation 3 (24 hydroxy groups), and finally generation 4 (48 hydroxy groups). In the next step, the dendrimer with 48 hydroxy groups was sulfated using sulfur trioxide pyridinium, followed by reduction of the azido group to the amine using tris(2-carboxyethyl)phosphine (TCEP).

Finally, the heterobifunctional linker NHS-PEG(8)-SPDP was coupled to the amino group of the sulfated dPGS moiety. All intermediates were purified by silica chromatography, the sulfated intermediates and the final product dendron(48)-PEG(8)-SPDP (dPGS) was purified by RP C-18 HPLC. The scale of this 12-step synthesis was in the range of 50 mg final product. The synthesis of dPGS was performed by the group of Dr. Kai Licha at Freie Universtity, Berlin.

To couple dPGS to dianthin, protein solution (1 mg/mL) was first centrifuged (10 min, 4° C 21130 rcf) in order to remove any particulates. Traut's reagent (2-iminothiolane) was added to the protein solution in a molar ratio of 1:1 to create sulfhydryl groups. Thereafter the mixture was kept in a thermomixer at 500 rpm (25° C; 1 h). Subsequently, 30 fold molar excess solution of formerly synthesized dPGS was added and mixed for 5 min. Thereby dianthin-dPGS conjugate mixture was created and further purified by FPLC.

2.3.11 Purification by FPLC

The isoelectric point of dianthin is 8.65 as reported in former studies [97]. To purify dianthin-dPGS from solution, anion exchange chromatographic technique using HiTrap DEAE FF 1 mL column was selected. After elution with 20 mM 3-(Cyclohexylamino)-2-hydroxy-1-propanesulfonic acid (CAPSO) buffer (pH 9.5) and 2 M NaCl (50% Buffer B), the eluted fractions were analyzed with SDS-PAGE (12% w/v) and native

gel (8% w/v) as shown in figure 13. The his-tagged protein-dPGS was eluted in NaCl concentration. However, remaining protein was eluted with 100% buffer B followed by 20% ethanol during cleaning step.

2.3.12 TBE-polyacrylamide gel electrophoresis

Dianthin-dPGS conjugate was analyzed by native gel electrophoresis. Tris-borate-EDTA (TBE) polyacrylamide (8% w/v) gel was prepared as per table 11. Electrophoresis was performed (70 V, 30 mA and 2 h 30 min) for each gel (E835 power supply from Consort) in a Dual Vertical MiniGel Unit MGV-202-U (CBS Scientific Company). Furthermore, TBE gel electrophoresis using TBE buffer (see table 10) was performed under reducing conditions. A solution of 0.1% (w/v) coomassie blue R-250 (AppliChem) in 40% (v/v) methanol and 10% (v/v) acetic acid and alcian blue staining solution (pH 2.5) in 3% (v/v) acetic acid was used as a staining solution for reverse and normal TBE gel, respectively. The principle behind using this technique is that alcian blue is a large planar pthalocyanine molecule with a copper atom in the center. The molecule also contains four basic isothiouronium, groups which carry a positive charge. The positive charge imparted by these groups results in the attraction of the alcian blue dye molecules to the highly anionic sites (sulfate groups) present in the conjugate.

Thereafter the gels were destained (45 min) in a solution of 20% (v/v) ethanol and 10% (v/v) acetic acid. The gels were then placed in a continuous shaking device in a chamber filled with ddH_2O for 15 minutes. In order to dry, the gels were placed for 2 h in a BIO RAD Gel Dryer (Model 583) attached to Diaphragm Vacuum Pump (Vacuubrand GmbH + Co., Wertheim, Germany) which further served to dehydrate the gels.

Table 10. TBE buffer (5 ×) preparation

Reagents	Amount per L	Final concentration (M)
Tris base	60.55 g	0.5
Boric acid	30.9 g	0.5
EDTA·2 H_2O (disodium salt)	7.4 g	0.02
Elix water	ad 1 L	

Table 11. Preparation of TBE-polyacrylamide gels

Reagents	2 × TBE-Polyacrylamide gel (8% w/v)
MilliQ water	5.23 mL
5 × TBE	2.0 mL
30% Acrylamide	2.66 mL
10% APS	100 µL
TEMED	10 µL

2.4 Cell biology methods

2.4.1 Cell culture

The cell lines were cultured in respective growth medium (table 12) supplemented with 10% fetal bovine serum (FBS) (BioChrom KG) and with/without 1% Penicillin/Streptomycin (PS) (Gibco/Invitrogen). Cells were allowed to proliferate at 37 °C in a humidified 5% CO_2 incubator. Dulbecco's PBS without Ca^{2+} and Mg^{2+} (PAA Laboratories) was used in the washing steps and 0.25% Trypsin-EDTA (Gibco/Invitrogen) for cell detachment.

Table 12. Growth medium for cell lines

Cell Line	Growth medium
NIH3T3; MIA PaCa-2 and Ca Ski	Dulbecco's Modified Eagle's medium (DMEM) + 10% FCS + 1% Penicillin/Streptomycin
BxPC-3 and QGP-1	RPMI 1640 + 10% FCS

2.4.2 Determination of cytotoxicity by MTT-assay

An initial amount 100 µL/well of growth medium as shown in table 10 containing 4000 cells was pipetted in a 96-well plate. The cell number count was calculated with a Luna fl dual fluorescence cell counter. Cells were allowed to proliferate at 37 °C and 5% CO_2 for 24 h. Then, 100 µL of fresh medium supplemented with targeted toxins was added to the wells. Cells were allowed to proliferate further 72 h under the same conditions as mentioned earlier.

The 3-(4,5-dimethylthiazol-2-yl)-2,5-diphenyltetrazolium bromide (MTT) assay was utilized to determine the degree of cell growth. A stock solution of MTT (5 mg/mL) was prepared. The solution was filtered through a 0.22 µm filter. The solution (30 µL/well) was pipetted directly to the media. The 96-well plate was incubated at 37 °C for 2 h. Thereafter, the media containing MTT was removed. Formazan solubilizer (50 µL/well, see table 13) was added to the plate. The plate was then kept on plate shaker for 10 min. The absorbance was measured at a wavelength of 570 nm (reference at 630 nm). Thereafter, the percentages of cell viability were calculated referring to untreated cells

To determine the safely tolerated concentration of SO1861 on cells after 72 h the cells were seeded in 96-well transparent round bottom plates (4000 cells/well) and grown for 24 h. Cells were then treated with culture medium either supplemented with SO1861 or not. Thereafter viability of DE (final concentration 10 pM to 1 µM) and dianthin-dPGS (final concentration 1 nM to 300 nM) either supplemented with SO1861 or not after 48 h/72 h was determined. Controls were treated only with culture medium or SO1861.

Table 13. Reagents used for MTT assay

Reagents	Composition
MTT	3-(4,5-Dimethyltiazol-2-yl)-2,5-diphenhyltrazoliumbromide
Formazan Solubilizer	205 mL Isopropanol, 25 mL 10% SDS, 20 mL 1 M HCl

2.4.3 Real-time monitoring of cytotoxicity

Real-time monitoring of the cell growth after treatment with SO1861 in combination with DE was carried out using the xCELLigence real-time cell analyzer (Roche, Basel, Switzerland). With this device cell proliferation can be recorded continuously during the experiment by measuring the impedance of the cells that are attached on the surface of cell culture plates with interdigitated gold microelectrodes (e-plates).

NIH-3T3, MIA PaCa-2, BxPC-3, QGP-1 and Ca Ski cells were trypsinized by using trypsin/EDTA (0.25%). Meanwhile the blank measurement (50 µL DMEM, or RPMI-1640 for BxPC-3 and QGP-1) was done on 96-well e-plates (16-well for BxPC-3) in the xCELLigence device. Thereafter, 4000 cells/100 µL were seeded per well. After 24 h when the impedance-based cell index reached between 0.5 to 1, DE and dianthin-dPGS with and without SO1861 was added in triplicates (in duplicates for BxPC-3 and QGP-1) in different concentrations (100 pM to 1 µM for single DE treatment, 10 pM to 100 nM in case of combination treatment of DE with SO1861, 30 nM to 300 nM for single dianthin-dPGS treatment and 1 pM to 100 pM for combination treatment of dianthin-dPGS treatment with SO1861). Prior to combination treatment a dose-dependent real time cell monitoring was observed for SO1861 concentrations (0.2 to 10 µg/mL final concentration) on one cell line (BxPC-3). After 120 h of real time measurement, cytotoxicity was evaluated using the xCELLigence software (RTCA 2.0).

All the *in vitro* experiments, unless otherwise mentioned in the legend were performed in quadruplicates in three independent experiments and the values are reported as their mean.

2.5 Organ analyses

2.5.1 Hematological analysis

The organ analyses were carried out from 7 months old male CD1 nude xenografted mice. Approximately 1.2 mL blood was collected by cardiac puncture on the 25th day of the experiment in isoflurane anaesthetized mice. Blood was collected in S-Monovette® 1.2 mL, K3 EDTA sterile tubes and were sent to Labor 28 GmbH, Berlin, Germany for complete blood count (CBC) analysis, including red and white blood cell

counts, platelets, hemoglobin, hematocrit, mean corpuscular volume, mean corpuscular hemoglobin and mean corpuscular hemoglobin concentration.

2.5.2 Immunohistochemical analysis

The animals were sacrificed on the 25th day of the experiment after isoflurane inhalation by cervical dislocation. The tumors were collected along with the adjoining skin. In case no tumor was macroscopically seen, the skin from the site of tumor cell injection was prepared. In addition, the spleen, liver, lung, heart, intestine and kidneys were also collected. The specimens were then preserved in 10% (v/v) neutral buffered formalin solution (Sigma Aldrich). The specimens were then embedded in paraffin as described in the next section.

2.5.2.1 Specimen preparation

Specimens were blocked into a thickness of 3 – 4 mm and fixed for a certain time period. The tissues were then dehydrated and cleared in a series of alcohols and xylene. The fluid replacement was followed by molten paraffin wax. It was taken into account that the paraffin temperature should not exceed 60°C. Tissue specimens were then cut into sections of 3 – 5 µm. After sectioning, tissues were mounted on slides and placed in drying racks. The slide racks were pounded on an absorbent towel to remove water trapped under paraffin and on glass and then dried at room temperature for one hour. The rack of slides were then placed in a 56–60°C incubator for one hour. Any excess water remaining on slides after removal from the incubator were removed by pounding slides on towels and drying for one additional hour in the incubator. After removal from the incubator, slides were held at room temperature until cool and paraffin was hardened. The specimen preparation and staining procedures were done by the working group of Dr. Horst Dürkop at Pathodiagnostik Berlin.

2.5.2.2 Deparaffinization and rehydration

Prior to staining, all tissue slides were deparaffinized to remove embedding medium and rehydrated. Slides were placed in a xylene bath and incubated for 5 minutes. Baths

were changed and repeated again. Slides were tapped off to remove excess liquid and placed in absolute ethanol for 3 minutes. Baths were changed and the same step was repeated again. Thereafter, the slides were placed in 95% ethanol for 3 minutes and subsequently in reagent-quality water for 5 minutes.

2.5.2.3 Staining

The excess reagent-quality water was tapped off. A lintless tissue was used to carefully wipe around specimen to remove any remaining liquid and to keep reagents within the prescribed area. Proteinase K solution (20 mg/mL, 100 µL) was applied to cover specimen and incubated for 5 minutes. The slides were gently rinsed with reagent-quality water from a wash bottle and placed in a fresh reagent-quality water bath (5 min). Excess water was tapped off and the slides were wiped as before. Peroxidase block solution (H_2O_2, 100 µL) was applied to cover the tissue specimen and incubated for 5 minutes.

Subsequently, the specimens were rinsed gently with wash buffer (Tris buffered saline solution containing Tween 20, pH 7.6; EGFR pharmDx™ Kit). The slide was placed in a fresh wash buffer bath (5 min). The slides were then placed in a humid chamber during the primary antibody/negative control reagent and labeled polymer incubations to avoid drying of tissues. Excess buffer was tapped off and the slides were wiped as before. Thereafter, 100 µL of primary antibody (EGFR pharmDx Monoclonal Mouse IgG1 Antibody; EGFR pharmDx™ Kit) was applied to cover the specimen. Slide was incubated (30 min) in a humid chamber.

The slide was rinsed again with wash buffer and excess buffer was tapped off. Subsequently, 100 µL of horseradish peroxidase labelled polymer (Labelled Polymer, HRP; EGFR pharmDx™ Kit) was applied to cover the tissue specimen and incubated (30 min) in a humid chamber. Slides were again rinsed with wash buffer and excess buffer was tapped off. The slides were then wiped as before.

Thereafter, 100 µL of DAB^+ Substrate Chromogen solution (Substrate buffer solution, pH 7.5; EGFR pharmDx™ Kit, DAKO, Hamburg, Germany) was applied to cover the tissue specimen, incubated for 10 minutes and rinsed the slide gently with deionized water. The DAB^+ substrate-chromogen solution waste was collected in a hazardous

materials container for proper disposal. Then, the slide was placed in deionized water bath for 5 minutes.

2.5.2.4 Counterstaining

The colored end-product of the staining reaction is alcohol and water insoluble. The slides were immersed in a bath of hematoxylin and incubate for 5 minutes, depending on the strength of hematoxylin used. Rinsed the slide gently in a deionized water bath. To ensure that all residual hematoxylin had been cleared, the slides were rinsed gently in deionized water bath for 5 minutes. The tissues were then examined for any histopathological alterations.

2.6 *In vivo* methods

2.6.1 Toxicity study in BALB/c mice

The target of the toxicity study was to determine the maximum tolerated dose (MTD). This is the dose at which no severe side effects occur. The no observed adverse effect level (NOAEL) denotes the level of exposure of an organism, found by observation, at which there is no biologically or statistically significant increase in the frequency or severity of any adverse effects in the exposed population when compared to its appropriate control. NOAEL is of fundamental importance because it determines the upper limit of the potential therapeutic window. The NOAEL is below the MTD.

For DE, the acute toxicity study was performed on 7 months old male BALB/c mice weighing 30–35 g. The study comprised of 4 groups each containing 3 mice. Doses of 40.0 µg, 4.0 µg and 0.4 µg DE in 100 µL PBS were given per mouse in groups A, B and C, respectively, and group D was control group (placebo). Doses were administered intraperitoneally once. Thereafter the mice were observed every 1 h on the first day for 9 hours and then twice every 24 h for their body weight and behavioral changes for 1 week. Animals were then sacrificed and organs were collected and prepared for histopathological analysis.

Table 14. Definition of adverse effect symptoms in toxicity studies. Category A: negligible effects; category B: weak effects and category T: toxic (adverse effects). Body condition scores (BCS), Body condition (BC) 1: Mouse is emaciated (skeletal structure extremely prominent); Body condition (BC) 2: Mouse is under-conditioned (segmentation of vertebral column evident).

Treatment specific symptoms	**Category**
Skin irritation or small area of hair loss (< 1 cm2)	A
Large area hair loss (> 1 cm2)	T
Local inflammation at the injection site	B
Slightly shallow breathing	B
Tingling or apathy or significantly shallow breathing	T
Weight and body condition scoring (BCS)	
Body weight loss < 15% but tendency of the past 24 h increasing	A
Body weight loss < 15% and tendency of the past 24 h decreasing	B
Body weight loss ≥ 15% or BC 1 or BC 2	T
Other symptoms	
Shaggy fur or scratches	A
Retarded motion	A
Decreased food intake	A
Separation of the animal	A
Dehydration	B
Temporary squatting or trembling	B
Sunken or dull eyes or lividness at eyes, ear or skin	T
Motor abnormalities such as paralysis	T
Superficial injuries (e.g. bite wounds)	T
Automutilation of limbs	T
Blood on body openings or bloody feces	T
Systemic infections	T
Constant squatting or trembling or abnormal posture	T
Paralysis	T
Rectal prolapse	T
Dark discoloration of the abdomen	T
Moribund	T

In case of dianthin and dianthin-dPGS conjugate, OECD guidelines 425 were utilized for the determination of acute toxicity study in mice. The advantage of this method is that it requires fewer animals than the classical toxicity test. In this method individual animals were successively tested. 10 µg was set as the starting dose. Further dose increment or decrement (3.16 fold) were done in accordance to the fulfillment of main

criteria of study. 300 µg was set as the maximum administrated dose. Due to the experimental design of OECD guideline, the maximum dose is achieved only if the substance is not toxic. The experiment is terminated if either there occurs 5 reversals in 6 mice, 3 mice are administered with highest dose consecutively, a total of 15 mice are used or a probability index is reached according to OECD 425 guideline. In the present study, the process was terminated until 5 reversals of up and down doses were observed in 6 mice. The main test method is applied after dose reversal principle. Symptoms of adverse effect were noted according to table 14 approved by animal welfare authorities.

2.6.2 Development of a xenograft model in nu/nu mice

To develop a tumor growth rate curve 1.25×10^6 BxPC-3 cells/100 µL in PBS/mouse were injected subcutaneously into the right flank of six 7 months old male CD-1 nu/nu mice (28–35 g; Charles Rivers, Germany). Animals were observed daily for their body weight shifts and tumor development. After 13 days a small palpable tumor was observed, although not measurable using vernier caliper. Two days later, tumor size was measured by caliper and the process was followed, twice weekly for 4 weeks. Animals were then sacrificed and tumor growth rate curve was established. The EGFR expression level was determined histologically for the grown tumors.

2.6.3 Tumor therapy in a pancreatic carcinoma xenograft model

The *in vivo* efficacy experiments were carried out in 7-months-old CD-1 nu/nu mice, comprising of five (single DE treatment and combination treatment with SO1861) and eight (dianthin-dPGS treatment) animals per group. The mice were housed in individually ventilated cages under a constant day and night cycle (12 h each) and had free access to animal feed (Ssniff, Soest, Germany) and water. All animals were monitored daily for health and well-being during the entire experiment. In order to slightly elevate tumor growth, the tumor was inducted by a subcutaneous injection of 1.3×10^6 BxPC-3 cells (instead of 1.25×10^6 as tested before, see 2.6.2) at the right flank of each animal with sufficient distance to the vertebral column. The cells were diluted in 100 µL PBS and injected with a 29-gauge needle.

Based on our previous toxicological experiments by Thakur *et al*., 2013 [118], the dosage of SO1861 was fixed at 30 µg/treatment diluted in 100 µL Dulbecco's PBS without Ca^{2+} and Mg^{2+}, which was applied subcutaneously into the neck. A total of 60 minutes later, 0.35 µg DE (subcutaneously in the back, in the vicinity of the tumor) again in 100 µL PBS was injected. The control group was treated with PBS alone administered in the neck and in the back. In some individuals of all groups, the tumor developed slightly shifted from the right flank to the back so that injection in the vicinity of the tumor also includes a position at the back near the tumor.

Dianthin-dPGS (15 µg in 100 µL PBS) was administered intraperitoneally similar to the route of administration selected for acute toxicity study. The therapy was started after randomly assigning the animals to three different groups of five (DE, DE + SO1861 and placebo) or eight (dianthin-dPGS and placebo) animals each on day 7 for the former and day 10 for the latter when a palpable tumor of approximately 2 mm was formed at the site of injection of tumor cells in all the animals. In total there were 6 therapy cycles per mouse carried out on days 7, 10, 13, 16, 19 and 22 after tumor cell injection in case of DE. A total of 8 therapy cycles per mouse were carried out on 10, 13, 16, 19, 22, 25, 28 and 31 after tumor cell injection in case of dianthin-dPGS. The growth of the tumor was monitored and all the tumor size measurements were determined with the help of digital vernier caliper. Finally, tumor volume was calculated using the formula, tumor volume = $(L \times W^2)/2$, where L is tumor length and W is tumor width.

3. Results

3.1 Purification of proteins and determination of enzymatic activity

To investigate the efficacy of dianthin-based targeted toxins, it is first required to synthesize the conjugates. While the protein ligand was linked to dianthin in form of a fusion protein, the dendrimer was coupled chemically. Aim of the first experiments was therefore to express and purify dianthin-based targeted toxins. The Ni-NTA chromatography and chitin column chromatography were utilized to purify dianthin and DE.

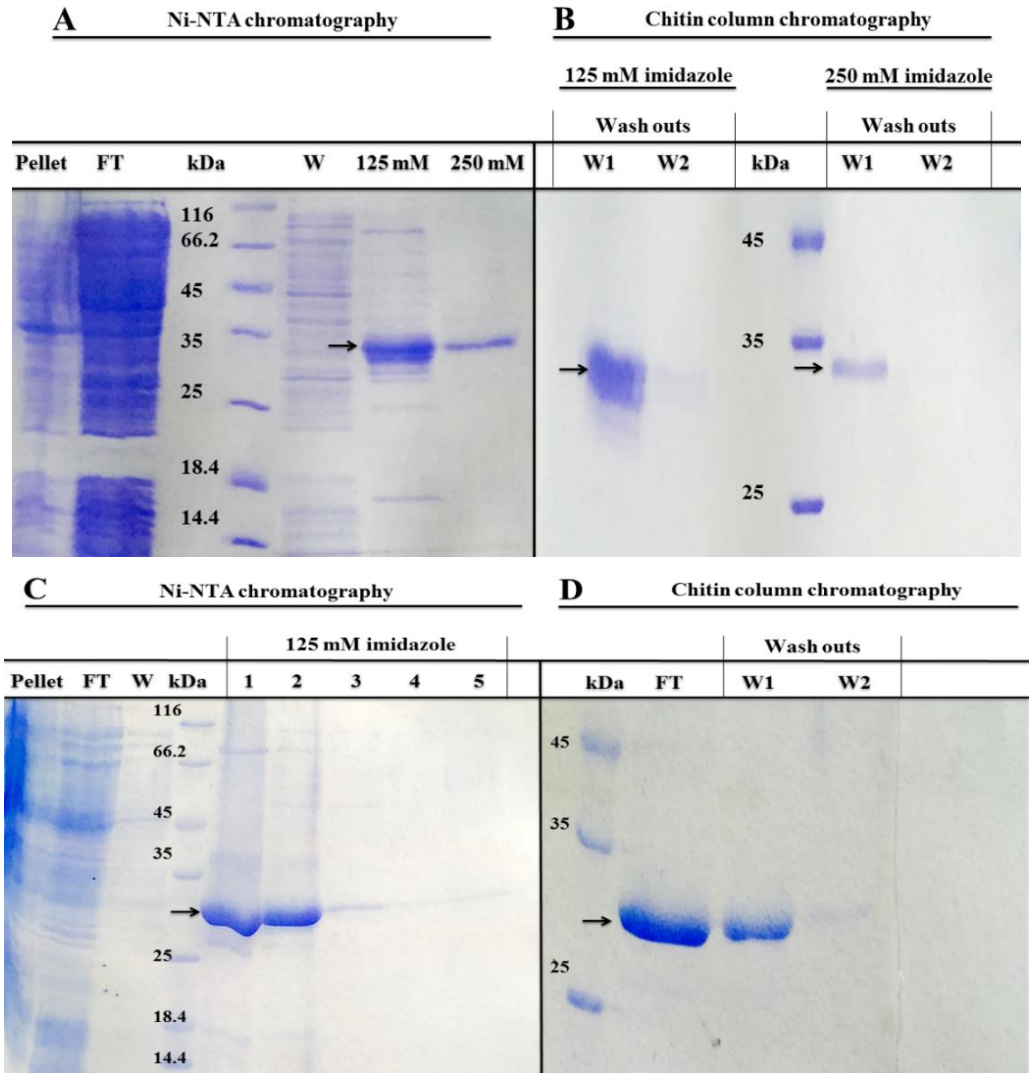

Figure 10. SDS-PAGE (12%) of pellet obtained after ultrasonication and purified fractions of proteins (A, B) DE and (C, D) dianthin obtained after (A, C) Ni-NTA chromatography and (B, D) chitin column affinity chromatography as shown by arrows. FT, flow through; W, W1 and W2, washouts obtained after different elution concentrations. Concentrations (125 mM, 250 mM) indicate imidazole eluates. In (C) 1, 2, 3, 4 and 5 refer to 125 mM imidazole concentration eluates.

As can be seen in figure 10, the recombinantly expressed DE and dianthin was purified by Ni-NTA chromatography. Obtained fractions were analyzed by SDS-PAGE (A and C; Figure 10). No substantial amounts of DE (approximately 35 kDa) and dianthin (30 kDa) were found in the pellet obtained after ultrasonication, the flow through of the column and the washout. However other bacterial proteins were present in the former specified elutions. At approximately 35 kDa (A and B; Figure 10) and 30 kDa (C and D; Figure 10) a clear band of DE and dianthin respectively was detected in the 125-mM-imidazole eluate, but slight contaminations of bacterial proteins were also observed. Since the 250-mM-imidazole eluate of DE also contained some DE, both fractions were dialyzed and then applied to a chitin column chromatography to remove contaminating proteins. SDS-PAGE revealed highly purified DE and dianthin with no contaminants visible in the coomassie stain (B and D; Figure 10). The total yield for DE and dianthin from 2 L of bacterial suspension was around 8.0 mg and 5.8 mg, respectively. In an enzymatic activity assay for ribosome-inactivating proteins, recombinant DE released 42 pmol adenine/pmol toxin/h compared to 67 pmol adenine/pmol toxin/h for ligand-free dianthin, indicating 37% loss in catalytic activity due to fusion to EGF. Thereafter the protein identity was further verified using western blot.

3.2 Protein identity authentication

The identity of DE and dianthin was authenticated by Western blot. Western blot analysis with a monoclonal antibody for the his-tag (Figure 11) confirmed that the his-tagged protein at ~35 kDa band corresponds to the recombinant fusion protein, DE, and the band at 30 kDa corresponded to dianthin.

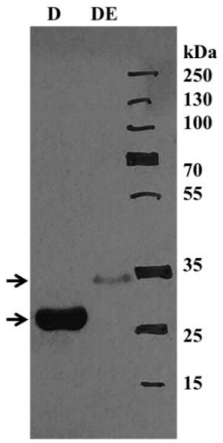

Figure 11. Western blot of DE (arrow at ~35 kDa) and dianthin (arrow at 30 kDa) after final purification. The protein was detected with an anti-His-tag monoclonal antibody conjugated to HRP. D, his-tagged dianthin; DE, his-tagged dianthin-EGF

As seen in the blot in figure 11, DE and dianthin were observed as a single band at ~35 kDa and 30 kDa as expected. Therefore the identity of DE and dianthin was confirmed.

3.3 Chemical coupling

3.3.1 Coupling, isolation and purification of dianthin-dPGS conjugate

In order to couple dianthin to dPGS moiety, a sulfhydryl group was introduced in dianthin *via* chemical reaction between 2-iminothiolane and primary amine of lysine residues. To incorporate a linker for conjugation to modified dianthin, the heterobifunctional linker NHS-PEG(8)-SPDP was coupled to amino group of the sulfated (48) dendron (D48) moiety. Finally, the HPLC purified D48-PEG(8)-SPDP was coupled to the modified dianthin, leading to formation of the dianthin-dPGS conjugate. No turbidity was observed during and after conjugation

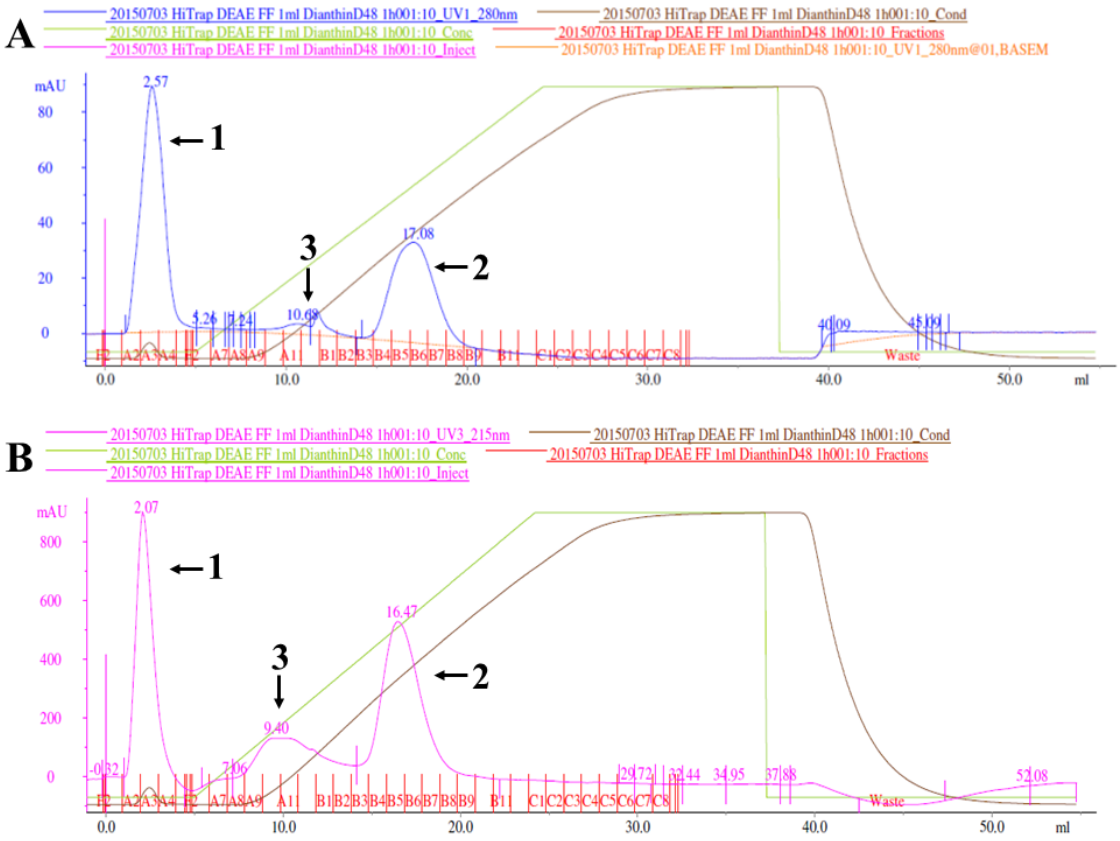

Figure 12. ÄKTA-FPLC chromatogram of the protein conjugate mixture. The mixture was applied to FPLC HiTrap DEAE fast flow weak anion-exchange column (1 mL) and the bound proteins were obtained in different fractions represented by peaks (1 and 2) as shown by arrows. The UV absorbance was measured at a wavelength of (A) 280 nm and (B) 215 nm. The fractions were then analyzed for furthermore identity on SDS-PAGE and native gel. The green color line, salt concentration; brown, conductivity; red, fractions; blue, UV absorbance at 280 nm; UV absorbance at 215 nm

Nevertheless, the conjugate mixture was centrifuged before loading the sample into FPLC. As seen in FPLC chromatogram in figure 12 conjugated dianthin (peak 2) was separated from the unconjugated dianthin (peak 1) using ion exchange chromatography. Three peaks (1, 2 and 3; Figure 12) were observed in the chromatograms (A and B; Figure 12).

Peak 1 in chromatogram A and B is unbound free diathin eluted with buffer A without salt. Peak 1 at 2.57 mL in chromatogram A and 2.07 ml in chromatogram B resulted in peak areas of 130.49 mAU*mL and 1137.95 mAU*mL. As the salt concentration was increased gradually, a broad peak starting from 7.06 mL up to 9.40 mL (Figure 12B) was observed due to change in buffer conditions. Peak 2 at 17.08 mL (area = 100.20 mAU*mL) in chromatogram A and 16.47 mL (area = 1355.08 mAU*ml) in chromatogram B is purified dianthin-dPGS conjugate eluted with 50% buffer B (CAPSO buffer + 2 M NaCl). According to the peak area 43.43% of conjugated dianthin (peak 2) was isolated from the whole mixture. Peak 1 and peak 2 area in total was considered as 100%. Finally, the peak 1 and peak 2 containing fractions were pooled and analyzed *via* gel electrophoresis to further confirm the purity.

3.3.2 Validation of conjugate identity

As seen in figure 12, peak 1 and peak 2 contained protein and were therefore analyzed by SDS-PAGE (Figure 13A). Unconjugated dianthin served as a positive control. In case of conjugated dianthin (dianthin-dPGS; C), a band at about 30 kDa confirmed the presence of protein after coupling. Peak 1 and Peak 2 (Figure 13A) apparently showed the presence of dianthin. In fractions A11, A12 and B1 (peak 3) no protein bands were visible.

In addition to this, reverse native gel (8%; Figure 13B) electrophoresis was performed to assess the purity of the conjugate. Dianthin was used as a positive control. The conjugation batch (C, Figure 13B) before FPLC purification, apparently still showed the presence of dianthin. However, in peak 1 the band was observed at the same height to unconjugated dianthin. This in turn confirmed that Peak 1 was unconjugated pure dianthin. This further confirmed the fruitful isolation of free dianthin from the conjugated mixture.

In case of peak 2 (Figure 13B), no visible bands were seen. A net negative charge of the highly sulfated conjugated protein in peak 2 prevents the conjugated protein from migrating into the reverse native gel. This further confirms the presence of highly purified protein conjugate in peak 2 since the SDS gel gave evidence that dianthin is contained in this fraction. Fractions A11, A12 and B1 comprising peak 3 showed no protein bands, furthermore confirming that the broadening of this peak was rather due to increment in salt concentration gradient in the buffer than protein content.

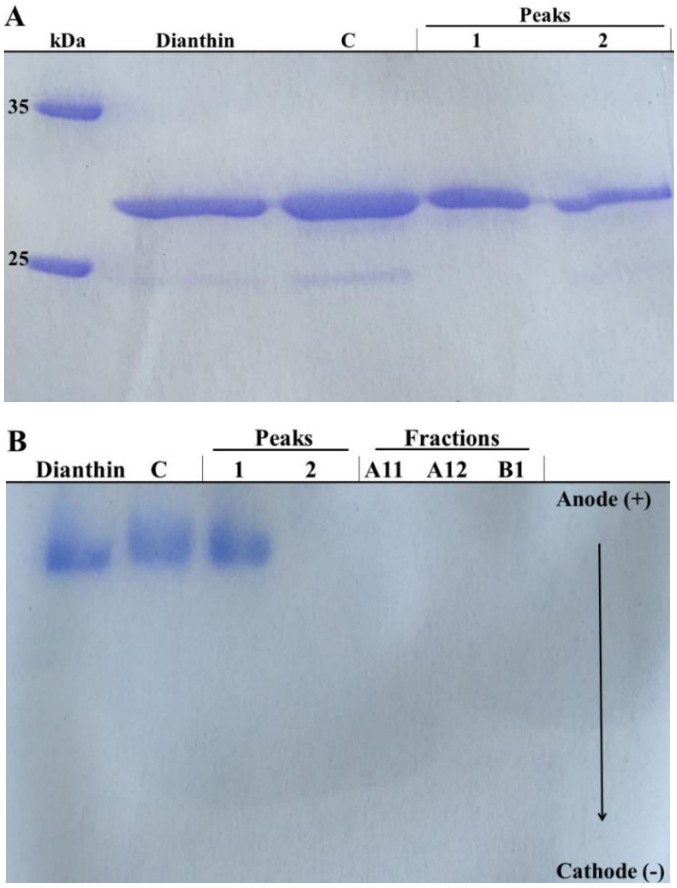

Figure 13. SDS-PAGE (12%) and reverse TBE-polyacrylamide gel (8%) electrophoresis. Lane C, dianthin-dPGS conjugate mixture obtained before separation by FPLC; A11, A12 and B1, fractions obtained after FPLC purification (see Figure 12).

3.3.3 Confirmation and quantification of dianthin-dPGS conjugate

The aim was to confirm the presence of highly polysulfated groups in the conjugation batch (C; Figure 14, Lane C) as well as in peak 2, after the confirmation of protein alone (dianthin) in peak A and targeted toxin (dianthin-dPGS) in peak 2. Therefore, an alcian blue staining technique of the native gel was performed.

In case of unconjugated dianthin and peak 1 (Figure 14) no bands were observed. This however confirmed that peak 1 was free dianthin isolated by FPLC. The blue bands (represented in Figure 14 with black arrows) in the conjugate (C; Figure 14) and peak 2 signified the presence of highly polysulfated groups in both samples. No bands in other fractions (A11, A12 and B1) indicate the absence of polysulfated groups.

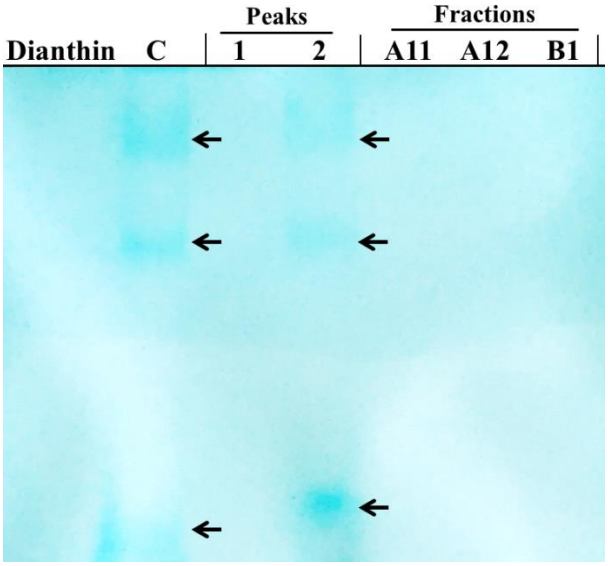

Figure 14. Polysulfates group validation by alcian blue staining in TBE-polyacrylamide gel (8%). Lane C, dianthin-dPGS conjugate mixture obtained before separation by FPLC; 1 and 2, peaks obtained after FPLC purification; A11, A12 and B1, fractions obtained after FPLC purification (see Figure 12). For better reproduction, the image was highlighted by 20%.

Thereby, a highly pure targeted toxin was procured in peak 2. The amount of concentrated protein was quantified by BCA assay. The total yield of the targeted toxin (dianthin-dPGS) obtained after purification was 2.7 mg. To engineer the targeted toxin, 4.1 mg of dianthin was utilized in the beginning. Thus, 1.4 mg of unconjugated dianthin was lost during the conjugation procedure.

Thereafter, the enzymatic activity of the targeted toxin was further determined by N-glycosidase enzymatic activity.

3.3.4 N-glycosidase activity of targeted toxins

The N-glycosidase activity of the targeted toxin was determined by an adenine release assay. The amount of adenine release mediated by the targeted toxin (dianthin-dPGS)

was measured and compared to the unconjugated recombinantly expressed toxin (dianthin) (Figure 15). This was done to investigate whether there was an influence of the chemical coupling on enzymatic activity of the toxin moiety. The enzymatic activity of dianthin was assessed as positive control. The enzymatic activity of bovine serum albumin (BSA) was considered as negative control.

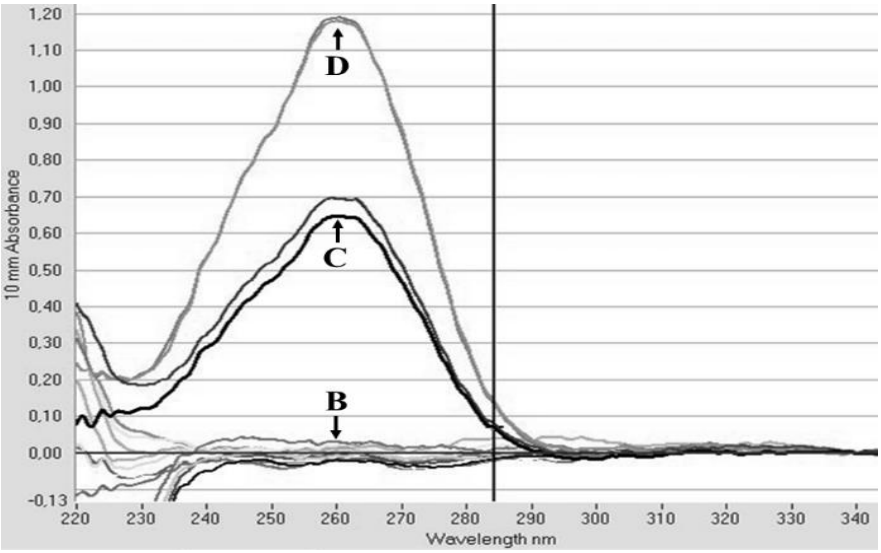

Figure 15. Plot of adenine release. The release of adenine from herring sperm DNA was recorded by nanoDrop spectrometer. BSA was used as a negative control. The curves represent two independent sample meausurements. D, dianthin; C, dianthin-dPGS; B, bovine serum albumin (BSA).

Table 15. N-glycosidase activity of protein/targeted toxin.

Protein/Targeted toxin	**Adenine release (pmol adenine/pmol toxin/h)**	**Adenine release (%)**
Dianthin	101.53 ± 0.6	100.00
Dianthin-dPGS	56.02 ± 1.9	55.07
BSA	0.02 ± 0.3	2.00

A 45% decrease in adenine release occurred after coupling. The unconjugated dianthin released 101.5 ± 0.6 pmol adenine/pmol toxin/h. Dianthin-dPGS conjugate released

56.0 ± 1.9 pmol adenine/pmol toxin/h. The different percentages of released adenine are shown in table 11. Although the activity decreased to 55.1% (table 15), nevertheless the enzymatic activity was sufficient enough to cause toxicity as compared to BSA.

Thereafter, the cytotoxicity of targeted toxin/toxin was further analyzed on carcinoma cell lines.

3.4 Cytotoxicity of targeted toxins

3.4.1 Cytotoxicity of targeted toxins by MTT assays

To first characterize efficacy and selectivity of dianthin-based targeted toxins on pancreatic cell lines and the enhancer effect of SO1861, cytotoxicity of DE in the absence and presence of SO1861 were determined. Cytotoxicity was analyzed on the EGFR overexpressing pancreatic carcinoma cell lines BxPC-3 and MIA PaCa-2 as well as on non-target NIH-3T3 cells. Likewise cytotoxicity of dianthin-dPGS were determined on the OATP overexpressing QGP-1 and Ca Ski cells.

For the combination treatment with SO1861, a safe concentration of the enhancer alone was determined first by a concentration variation in the range from 0.12–4.0 µg/mL (Figure 16).

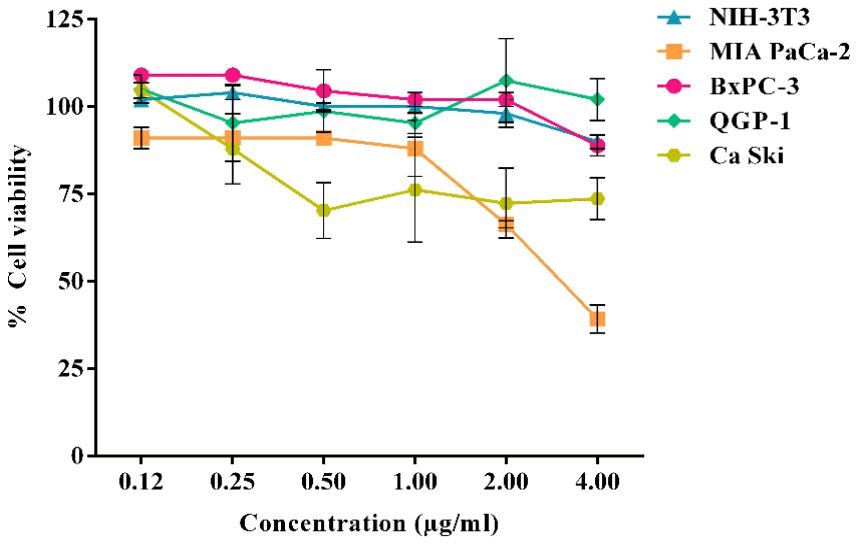

Figure 16. Determination of a safe SO1861 concentration. (a) BxPC-3, (b) MIA PaCa-2 (c) QGP-1, (d) Ca Ski and (e) NIH-3T3 cells were seeded in 96-well plates and grown for 24 h. Cells were then treated with SO1861 (0.12 to 4 µg/mL final concentration) or not (used as reference value). Cells were further incubated for 72 h. Viability was determined by an MTT assay.

The highest concentration of 4 µg/mL resulted in at least 88.9% cell viability in BxPC-3, QGP-1 and NIH-3T3 cell lines. In case of Ca Ski 73.6% cell viability was observed at 4 µg/mL. In case of MIA PaCa-2 39.2% cell viability was observed. As shown in a graph (Figure 16), 0.5 µg/mL SO1861 resulted in 91% and 100% cell viability in MIA PaCa-2 and NIH-3T3 cells whereas 1.0 µg/mL SO1861 resulted in 102%, 95.3% and 76.2% cell viability in BxPC-3, QGP-1 and Ca Ski cells respectively. As a result, 0.5 µg/mL was applied in all further experiments for MIA PaCa-2 and NIH-3T3 cells whereas 1.0 µg/mL was used for BxPC-3, QGP-1 and Ca Ski cells.

The IC_{50} of DE was found to be 1.0×10^{-7} M for BxPC-3 (Figure 17A) and 3.0×10^{-8} M for MIA PaCa-2 (Figure 17B) cells after 48 h. Similarly, NIH-3T3 cells revealed an IC_{50} of 7.3×10^{-8} M (Figure 17C) indicating no relevant difference between target and non-target cells. The IC_{50} of dianthin-dPGS was found to be 2.7×10^{-8} M for QGP-1 (Figure 17D) and 1.83×10^{-7} M for Ca Ski (Figure 17E) cells after 72 h.

In the presence of SO1861, a clear enhancement of the DE related toxicity within 48 h was observed on target cells i.e. EGFR overexpressing cells, as compared to the non-target cell line (IC_{50} of 1.7×10^{-10} M for BxPC-3, 5.3×10^{-9} M for MIA PaCa-2 and 1.1×10^{-7} M for NIH-3T3 cells, Figure 17A, B and C). This clearly indicated a cytotoxic synergism between DE and SO1861 on pancreatic tumor cell lines.

Moreover, in case of dianthin-dPGS tremendous enhancement of toxicity was observed in OATP overexpressing cells within 48 h. A 41.9 ± 3.8% cell viability at lowest concentration (1×10^{-14} M, Figure 17D) was observed in QGP-1 cells. However, Ca Ski cells showed cytotoxic effect (IC_{50} of 2.8×10^{-11} M for Ca Ski cells, Figure 17E) similar to DE-based treatment on BxPC-3 cells. Notably, the synergistic effect is target-cell specific suggesting that both targeted toxins are also internalized successfully in the absence of SO1861 but are ineffective due to insufficient endosomal escape, which is then triggered by SO1861 in the combined treatment.

As a result, a tremendous enhancement in cytotoxicity was observed in OATP expressing cells. QGP-1 and Ca Ski cells showed more than 2,700,000 and 6535 fold enhancement in cytotoxicity respectively.

Thereafter the cytotoxicity of targeted toxins alone and in combination with SO1861 was determined in real time *via* real time cytotoxicity analysis (RTCA) device.

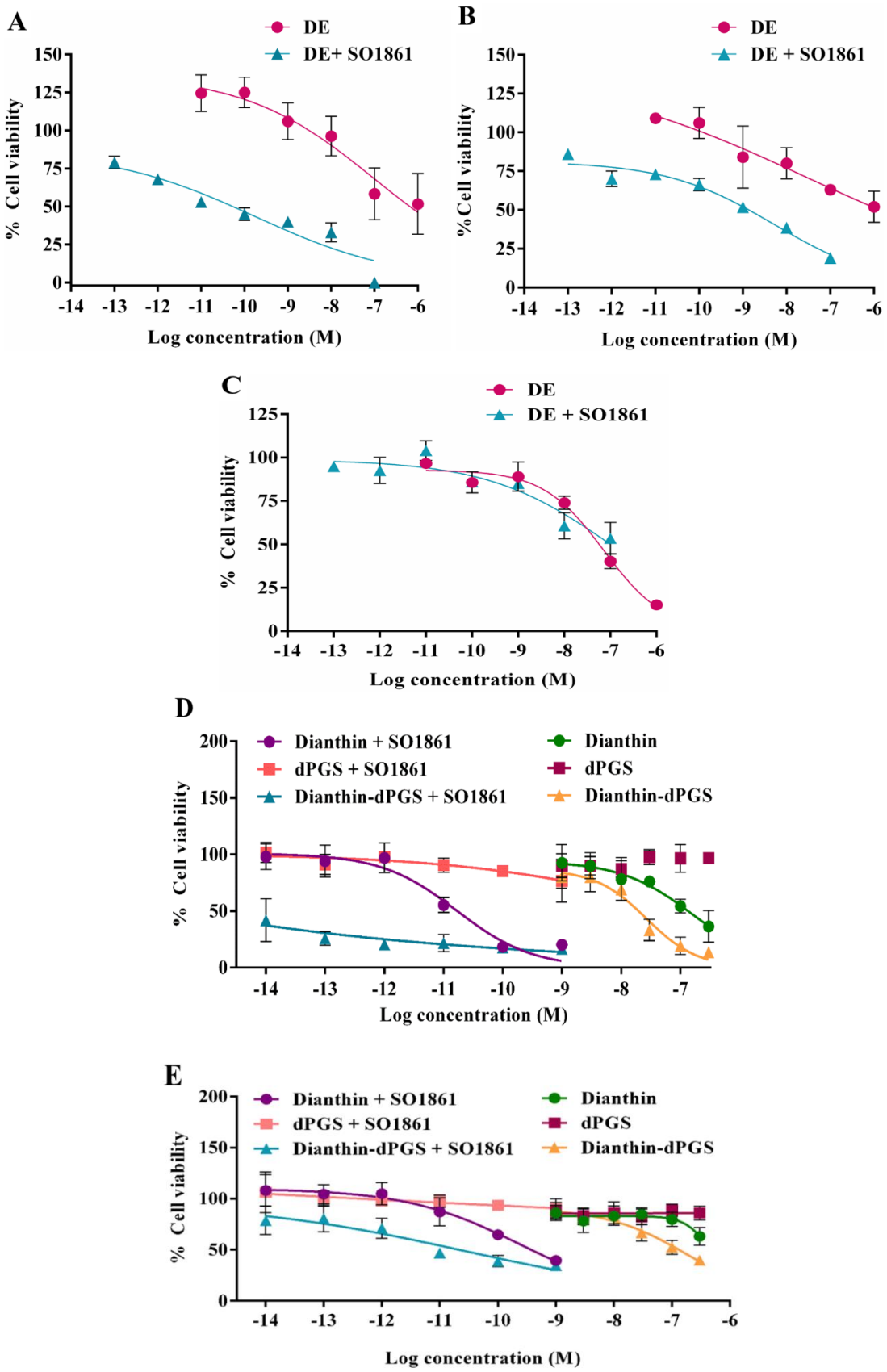

Figure 17. SO1861-mediated augmentation of dianthin-EGF (DE) and dianthin-dPGS. (A) BxPC-3, (B) MIA PaCa-2, (C) NIH-3T3 cells, (D) QGP-1 and (E) Ca Ski cells were seeded in 96-well plates and grown for 24 h. Cells were then treated with dianthin-EGF, dianthin-dPGS, dianthin and dPGS in medium either supplemented with SO1861 (0.5 µg/mL final concentration for MIA PaCa-2 and NIH-3T3 cells and 1 µg/mL for BxPC-3, QGP-1 and Ca Ski cells) or not. Each value represents the mean of

three independent experiments performed in triplicates. A statistical significant effect between single and combination treatments was observed in MIA PaCa-2 ($p < 0.05$) and BxPC-3 ($p < 0.01$) cell lines. A statistical significant effect in single dianthin-dPGS treatment was observed for QGP-1 cells ($p < 0.01$ for dianthin-dPGS versus dPGS, $p < 0.05$ for dianthin versus dPGS). Moreover, a statistical significant effect was observed in combination treatment in QGP-1 ($p < 0.001$ for dianthin-dPGS versus dPGS, $p < 0.05$ for dianthin versus dianthin-dPGS) and Ca Ski cell lines ($p < 0.01$ for dianthin-dPGS versus dPGS). Student t-test was used to determine statistical significance.

3.4.2 Cytotoxicity of dianthin-based targeted toxins recorded in real time

The kinetics of DE cytotoxicity was evaluated in real time in BxPC-3, MIA PaCa-2 and NIH-3T3 cell lines (Figure 19). Dianthin-dPGS related cytotoxicity was evaluated in the OATP overexpressing QGP-1 cell line. A gradual increase in the impedance signal (i.e. cell growth) compared to the normalized cell index (NCI) was observed when cells were treated with the targeted toxin in the absence of SO1861 at 100 pM, 10 nM and 1 µM except for BxPC-3 (1 µM DE) and QGP-1 cells (300 nM dianthin and dianthin-dPGS) where a cytostatic effect was observed (Figure 19A-D). Cell growth was reduced beginning 30 h and 46 h after toxin incubation for BxPC-3 (1 µM DE) and QGP-1 (300 nM dianthin and dianthin-dPGS) cells, respectively. The reduction was dose-dependent and continued until the end of the experiment (92 h after induction) but cell proliferation was still seen at any time except for BxPC-3 cells at 1 µM and QGP cells at 300 nM.

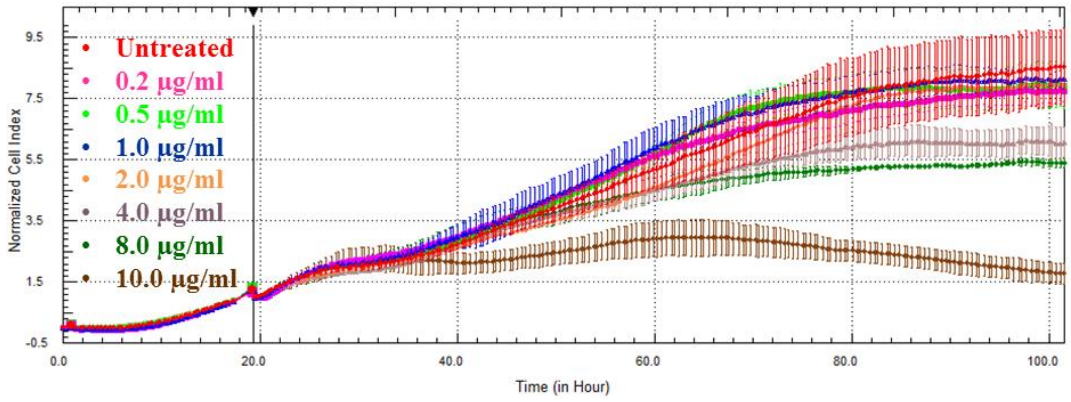

Figure 18. Real time cell analysis showing the dose-dependent increase in cytotoxicity in BxPC-3 cells with SO1861 (0.2 to 10 µg/mL final concentration). The y-axis shows the impedance-based cell index that was normalized after 19 h just before treatment started. The normalized cell index can be assumed to be proportional to the number of living cells.

Furthermore, a prior dose-dependent cytotoxic behavior of SO1861 (0.2 to 10.0 µg/mL final concentration, Figure 18) was confirmed for the pancreatic carcinoma cell line

BxPC-3. A gradual dose-dependent increase in cell growth was observed. A similar growth pattern of cells was observed for SO1861 in a concentration range of 0.2 to 2.0 µg/mL. A cytostatic behavior in the beginning of 78 h was observed for 4.0 and 8.0 µg/mL SO1861 concentrations. A further toxic effect at 10.0 µg/mL was visible with a decline in cell growth at the begining of 70 h after SO1861 addition at 19.5 h.

In contrast, a dose-dependent decrease in NCI (i.e. cell death) was observed with the combined application of SO1861 and targeted toxins (Figure 19E-H), finally leading to complete cell death for MIA PaCa-2 cells 72–92 h after beginning of the treatment for concentrations of 100 nM, 10 nM and 100 pM of the targeted toxin (DE) while off-target NIH-3T3 cells only show a decreasing signal at 100 nM (Figure 19F). BxPC-3 cells do not reach complete cell death in the observed time period, however, the signal was still decreasing at the end of the experiment. It must be taken into consideration that untreated BxPC-3 cells proliferate much faster than MIA PaCa-2 and QGP-1 cells. The lowest concentration of 10 pM DE resulted only in a cytostatic effect 20 h after start of the incubation for MIA PaCa-2 cells and in no effect for BxPC-3 cells. Whereas 10 pM dianthin-dPGS resulted in a cytotoxic effect 14 h after start of incubation for QGP-1 cells. The lowest concentration of 1 pM dianthin-dPGS resulted in a cytotostatic effect for 54 h after incubation, thereafter slight cell growth was observed (16% cell proliferation compared to untreated) at the end. A clear target specific effect of dianthin-dPGS was observed at 10 pM in contrast to ligand free toxin (dianthin).The kinetics of the first observable effect was faster in the combination therapy (14–24 h after treatment start for concentrations down to 100 pM) compared to the monotherapy (30 h, except for BxPC-3 cells at 1 µM).

The enhancer effect of SO1861 is target cell-specific since cell growth of NIH-3T3 cells was not substantially more reduced than with the monotherapy (Figure 19B and F) and cell proliferation was observed for all concentrations except for the highest concentration of 100 nM that resulted in cytostatic behavior.

Thereafter, the adverse effect levels of dianthin, dianthin-dPGS and DE were evaluated by acute toxicity studies in BALB/c mice.

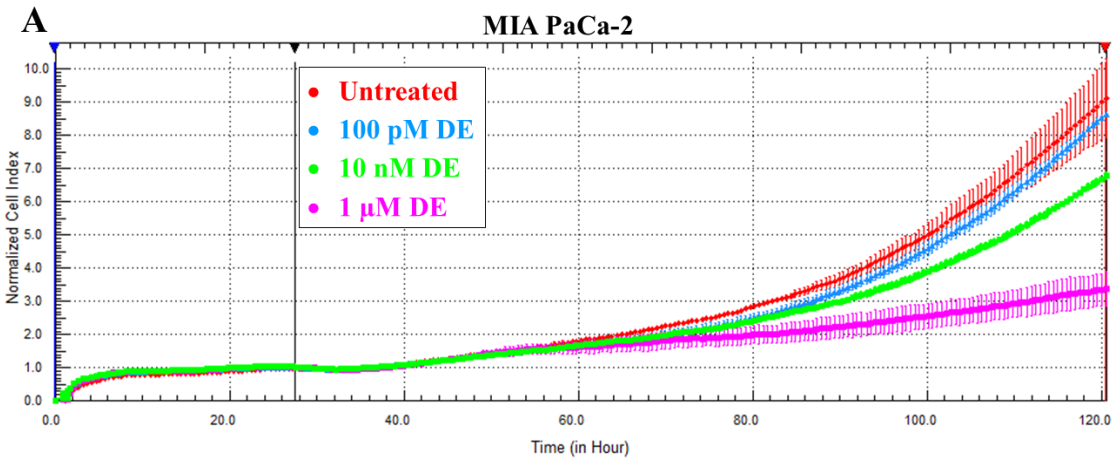
A
MIA PaCa-2
Untreated
100 pM DE
10 nM DE
1 µM DE
Normalized Cell Index
Time (in Hour)

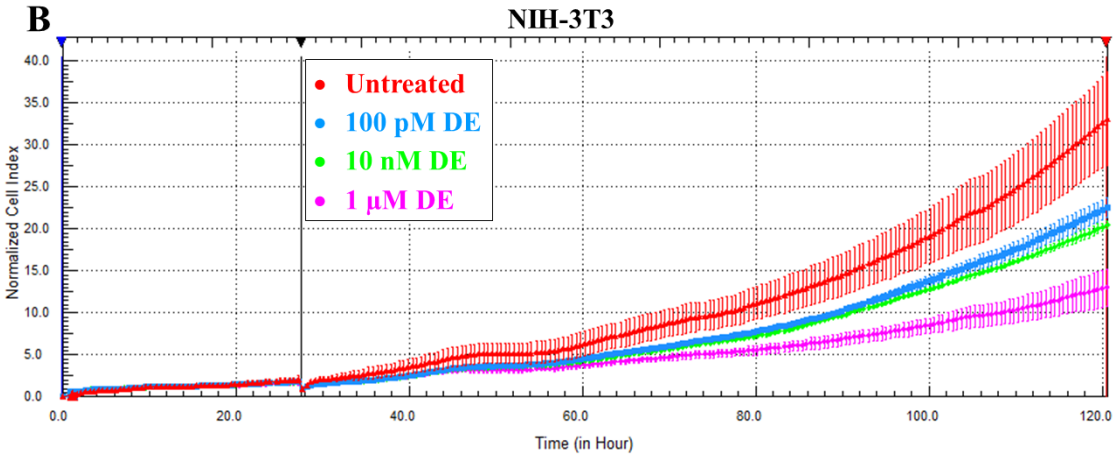
B
NIH-3T3
Untreated
100 pM DE
10 nM DE
1 µM DE
Normalized Cell Index
Time (in Hour)

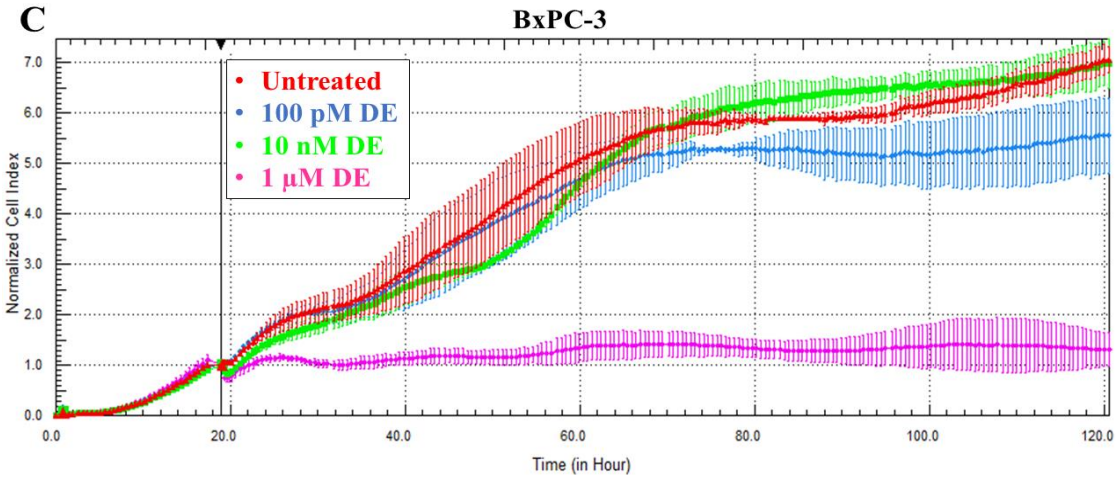
C
BxPC-3
Untreated
100 pM DE
10 nM DE
1 µM DE
Normalized Cell Index
Time (in Hour)

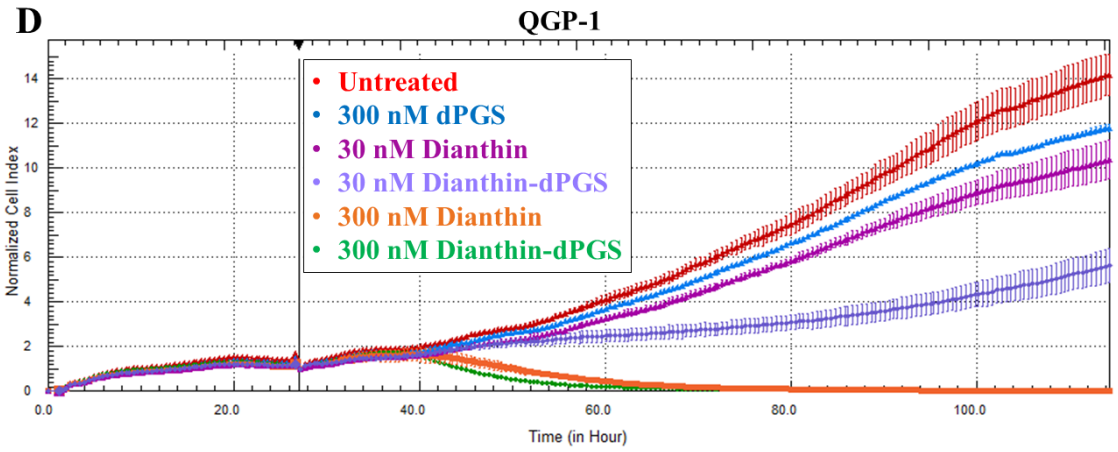
D
QGP-1
Untreated
300 nM dPGS
30 nM Dianthin
30 nM Dianthin-dPGS
300 nM Dianthin
300 nM Dianthin-dPGS
Normalized Cell Index
Time (in Hour)

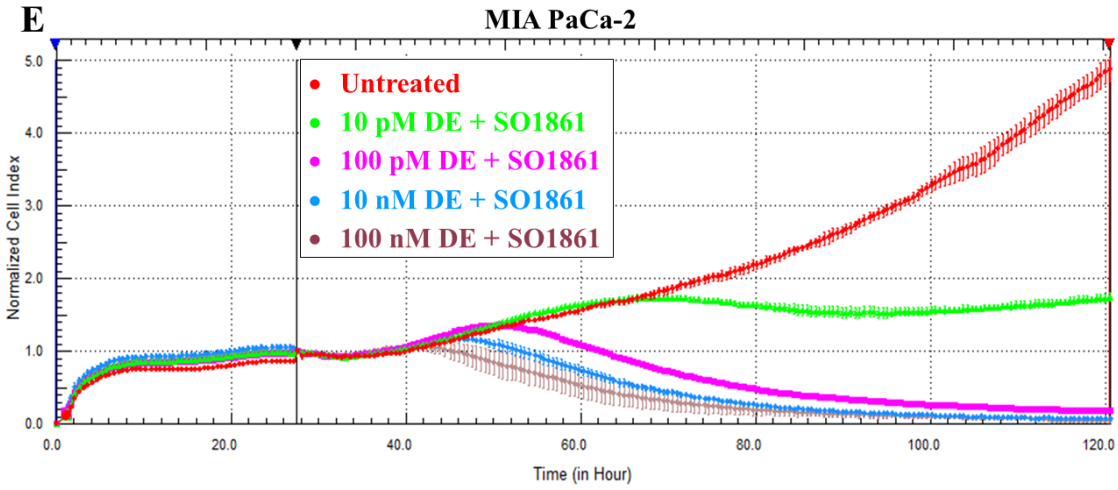
E
MIA PaCa-2
Untreated
10 pM DE + SO1861
100 pM DE + SO1861
10 nM DE + SO1861
100 nM DE + SO1861
Normalized Cell Index
Time (in Hour)

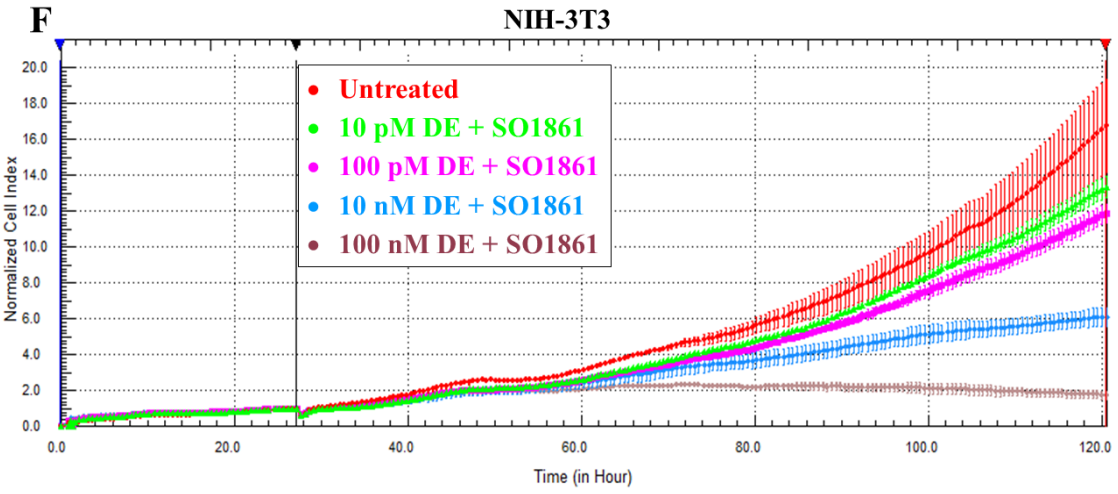
F
NIH-3T3
Untreated
10 pM DE + SO1861
100 pM DE + SO1861
10 nM DE + SO1861
100 nM DE + SO1861
Normalized Cell Index
Time (in Hour)

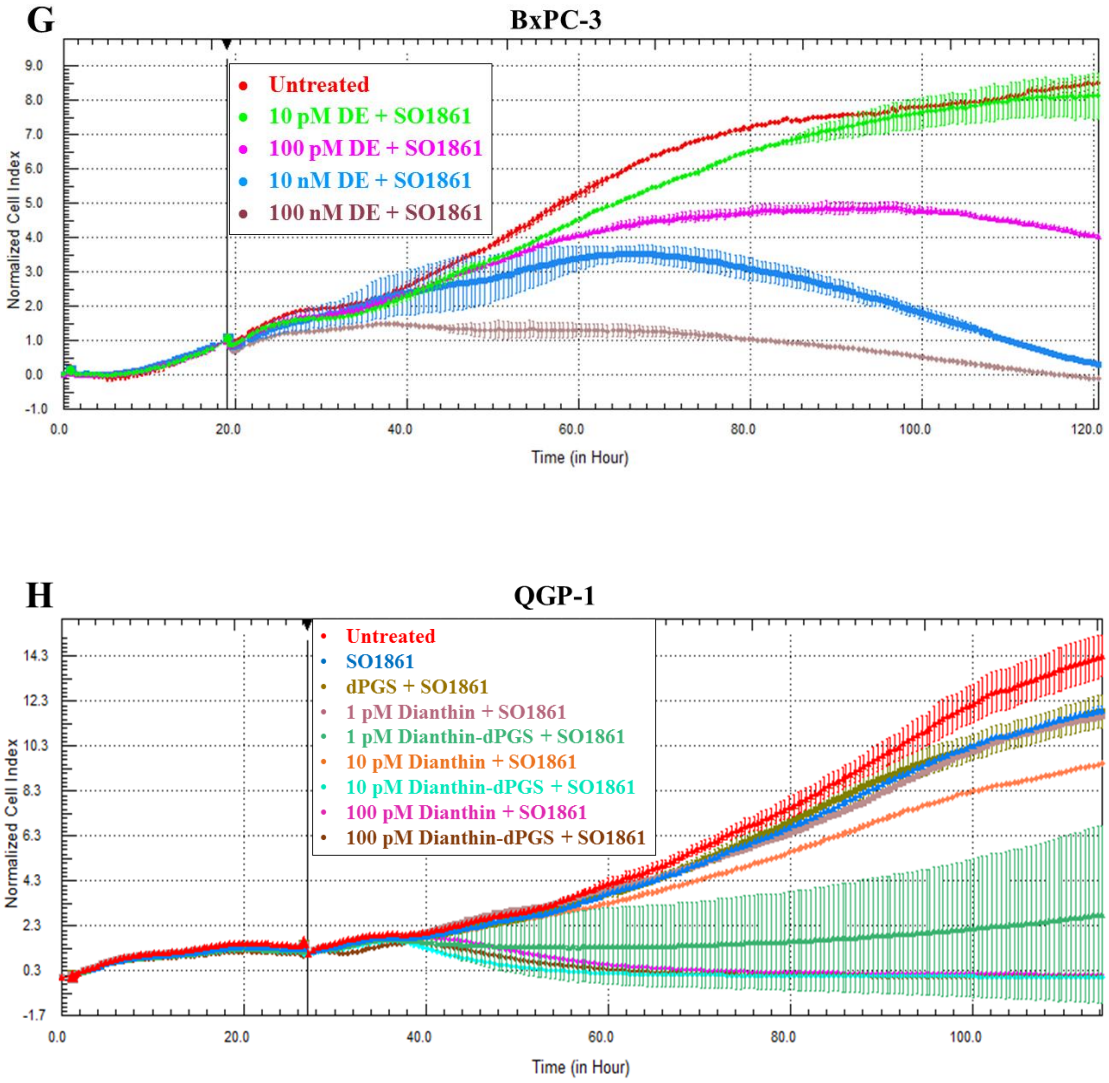

Figure 19. Real time cell analysis showing the dose-dependent increase in cytotoxicity in monotherapy with DE (A–C), dianthin-dPGS (D) and in combination therapy together with SO1861 (E–H). Cytotoxic effect was observed in EGFR overexpressing MIA PaCa-2 (A, E), BxPC-3 (C, G) as compared to NIH-3T3 cells (B, F), which is a non-target cell line. Cytotoxicity of dianthin-dPGS was determined in OATP overexpressin QGP-1 cells (D, H). The y-axis shows the impedance-based cell index that was normalized to 1.0 after 19 h (C, G) or 27 h (A, B, D-F and H) just before treatment started. The cell index can be assumed to be proportional to the number of living cells.

3.5 Evaluation of effect levels by acute toxicity studies

For dianthin alone (Figure 20A), 10.0 µg/mouse was found to be a safe dose. This dose was defined as no observed adverse effect level (NOAEL) as no adverse effect symptoms (shown in table 14) as per animal welfare authorities were observed in this group although a significant decrease in body weight was observed at this dose. A higher dose of 30.0 µg led to a greater than 15% body weight loss on day 7 with no other symptoms as described in table 14. Furthermore, on day 4, 100.0 µg dianthin caused more than 15% body weight loss with white ocular discharge and moribundity.

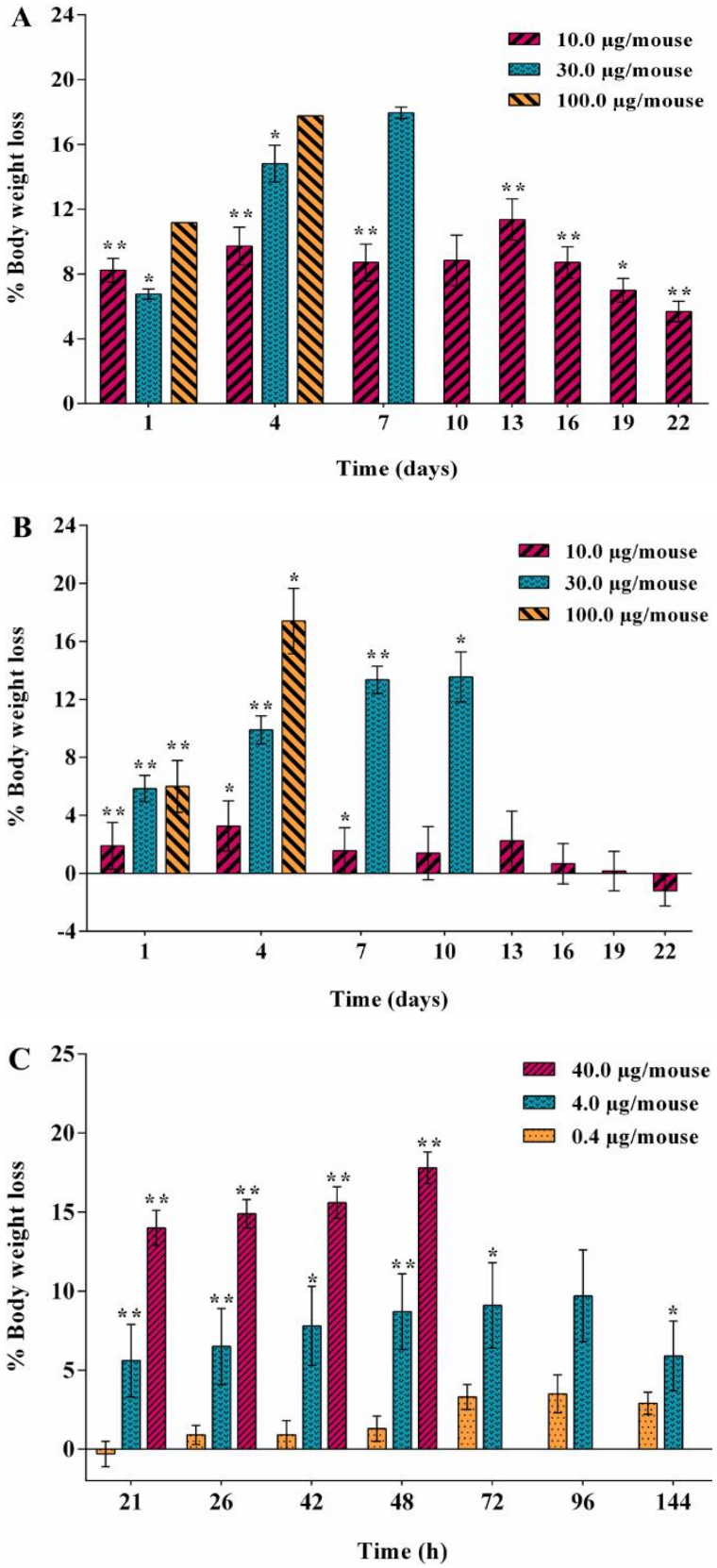

Figure 20. No observed adverse effect level (NOAEL) evaluation. Body weight loss observed after several applications of different doses of (A) dianthin, (B) dianthin-dPGS conjugate and (C) DE. The values refer to the body weight just before treatment. Significance in body weight changes is indicated by * ($p < 0.05$) and ** ($p < 0.01$).

Thus, 100.0 µg dianthin was highly toxic when given intraperitoneally in mice. The animals were sacrificed on day 4, day 7 and day 22 for 100.0 µg, 30.0 µg and 10.0 µg doses, respectively.

For dianthin-dPGS conjugate alone (Figure 20B), 10.0 µg dose was found to be non-toxic and construed as the no observed effect level (NOAEL). The body weight remained constant throughout 22 days consisting of 8 applications. However, a significant descrease in body weight was observed in 30 µg treated animals at day 10. A white ocular discharge in one eye of 100% population was noticed. Animals in this group also possessed a squatted posture (an adverse effect, see table 12). Furthermore, 100 µg dose (Figure 20B) caused a significant body weight loss (> 15%) on day 4 accompanied with white ocular discharge (Figure 21A), sqatted posture (Figure 21A) and moribundity. Animals treated with 100.0 µg, 30.0 µg and 10.0 µg dose were sacrificed on day 4, 10 and 22 respectively.

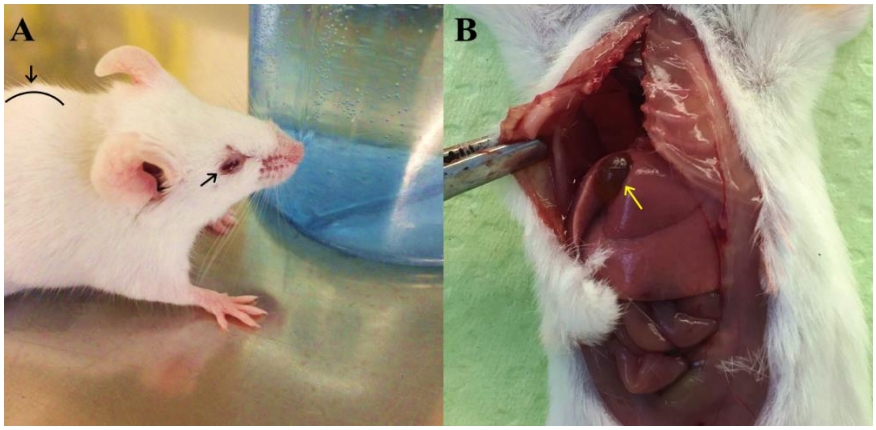

Figure 21. Images displaying detrimental effects on mice injected with highest (100 µg/mouse) dose of dianthin-dPGS along with (A) squatted posture and ocular discharge as depicted by arrows. Administration of highest dose also caused (B) increase in gall bladder size as depicted by yellow arrow.

For DE alone (Figure 20C), 0.4 µg/mouse was found to be non-toxic. It was defined as NOAEL since the body weight remained constant throughout the week after single dose administration. A significant decrease in body weight was observed with no adverse observational effects (NOAEL as defined in table 14) for 4.0 µg/mouse. However, 40 µg dose caused moribundity accompanied with white ocular discharge (Figure 22) in 100% population. Furthermore, more than 10% body weight loss within 48 h was also observed (Figure 20C). The animals administered with 40.0 µg DE were sacrificed

before 48 h whereas the animals treated with 0.4 µg and 4.0 µg doses were sacrified after 1 week. The organs of all the mice after sacrificing were preserved for further toxicological analyses by immunohistochemistry.

As a result, 0.35 µg DE and 15.0 µg dianthin-dPGS dose is considered to be a safe dose for dose response curves. Thereafter efficacy of DE and dianthin-dPGS was further determined in CD-1 nu/nu mice.

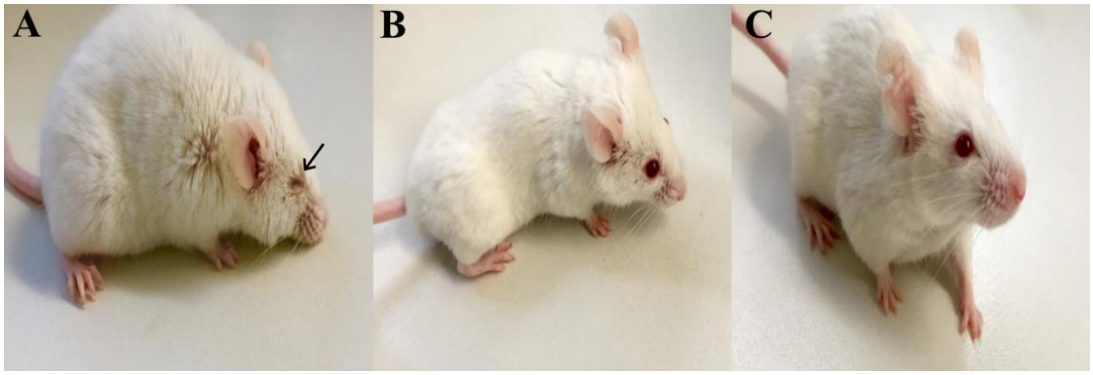

Figure 22. Images displaying dose dependent discernible physical traits of mice injected with (A) 40.0 µg/mouse with white ocular discharge as depicted by arrow, (B) 4.0 µg/mouse and (C) 0.4 µg/mouse.

3.6 Efficacy of dianthin-dPGS against DE in a pancreatic carcinoma xenograft model

3.6.1 Tumor growth rate (TGR) curve

A subcutaneous injection of 1.25×10^6 cells/mouse on day 0 at the right flank showed a tremendous increase in tumor volume (up to 295.83 mm^3) at the end 40^{th} day. On day 13 past injection of tumor cells, a visibly small, palpable though unmeasurable tumor was observed at the injection site of each mouse. On day 15, an average tumor volume of 9.8 mm^3 was measured. On day 40 a 295 mm^3 tumor volume leading to skin lesion on the surface was observed. Thereafter, animals were sacrificed. To determine the EGFR expression level immunohistochemically, tumors were isolated and preserved. The TGR curve led to the important finding that further experiments for efficacy studies can be performed up to 36 days (163.2 mm^3) to prevent skin lesions and great stress to animals. As shown in figure 23, 1.2×10^6 cells/mouse was found as optimal cell number to be injected in mice for further efficacy studies.

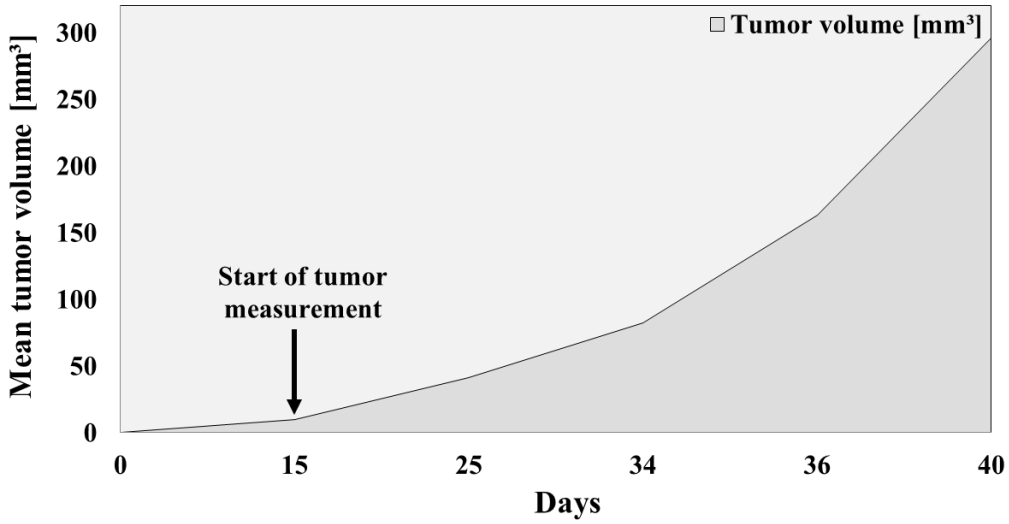

Figure 23. Tumor growth rate (TGR) curve showing increase in tumor volume up to 40 days.

3.6.2 Efficacy of targeted toxins

The therapeutic effect of the targeted therapy with DE in tumor bearing nude mice was determined for a period of 25 days comprising six treatment cycles. There was a 96.5% average reduction in the tumor volume for the group treated with the combination of DE and SO1861 compared to the placebo (tumor volume 84.5 mm^3 ± 51.9 for placebo and 3.0 mm^3 ± 3.3 for combination) and 4 out of 5 mice showed complete regression (Figure 24A).

The monotherapy with DE also caused a decrease in tumor volume (40.8 mm^3 ± 61.3), which was a 51.7% average reduction when compared to placebo, however, treatment together with SO1861 resulted in a more than 13-fold better efficacy (Figure 24A). As a non-severe side effect, SO1861-induced skin hardening was observed at the back of the neck after 2 therapy cycles. No complete regressions were observed in the DE monotherapy, 2 mice had continuous tumor growth and 3 had retarded tumor growth. The experiment was concluded after six therapy cycles and mice curatively treated with the combination therapy did not show any skin lesions neither at the injection nor at the tumor site (Figure 25B, C).

In case of the targeted toxin dianthin-dPGS, the therapeutic effect in tumor bearing mice was determined for a period of 34 days. The therapy comprised eight treatment cycles (Figure 24B). There was an 80.8% average reduction in tumor volume compared to placebo (tumor volume 79 mm^3 ± 35.1 for placebo and 15.2 mm^3 ± 23.1 for dianthin-dPGS) and two out of eight mice showed complete regression. Two mice exhibited

continuous tumor growth. Four out of eight mice had a slow tumor growth rate until day 25. Thereafter, tumor started developing further on. The experiment was concluded after eight treatment cycles. No skin lesions were observed at the injection site of mice (Figure 25E).

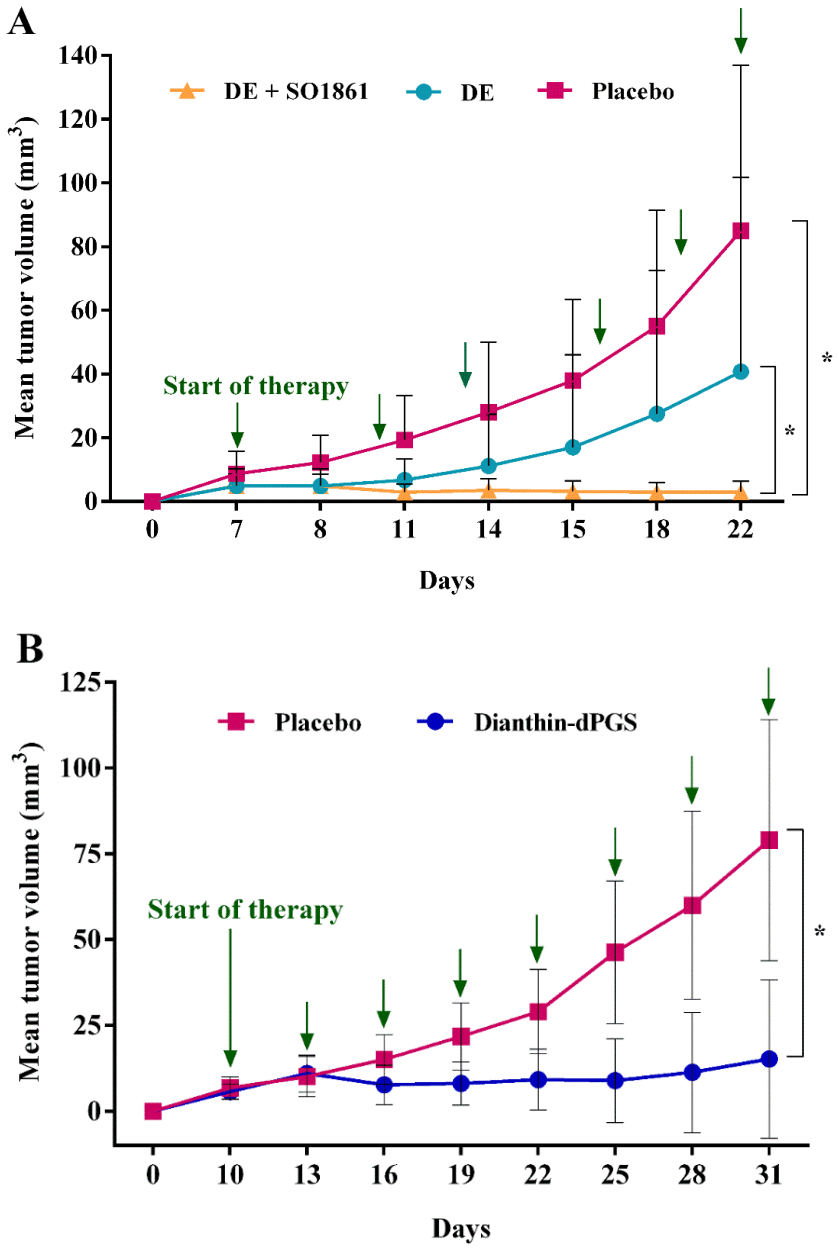

Figure 24. Xenograft tumor volume evaluated by use of a digital vernier caliper. (A) Placebo (PBS only), single (DE; 0.35 µg/treatment) and combination (DE; 0.35 µg/treatment + SO1861; 30 µg/treatment) therapy. (B) Tumor volume evaluation for placebo (PBS only) and dianthin-dPGS conjugate (15 µg/treatment). A statistical significant decrease in the tumor volume was observed in the combination treatment for the curves as a whole ($p < 0.05$ versus single therapy versus placebo) and dianthin-dPGS treatment versus placebo ($p < 0.05$). Green arrows represent treatment days. dPGS, dendritic polyglycerol sulfate.

In order to compare the treatment efficacy of targeted toxins the average percentage reduction of the tumor volume (table 16) was calculated. The average tumor volume in placebo group was found to be 81.75 mm^3 ± 37.5. Thereafter, organ analyses were further performed to determine the after-effect of therapy on tumor and other organs.

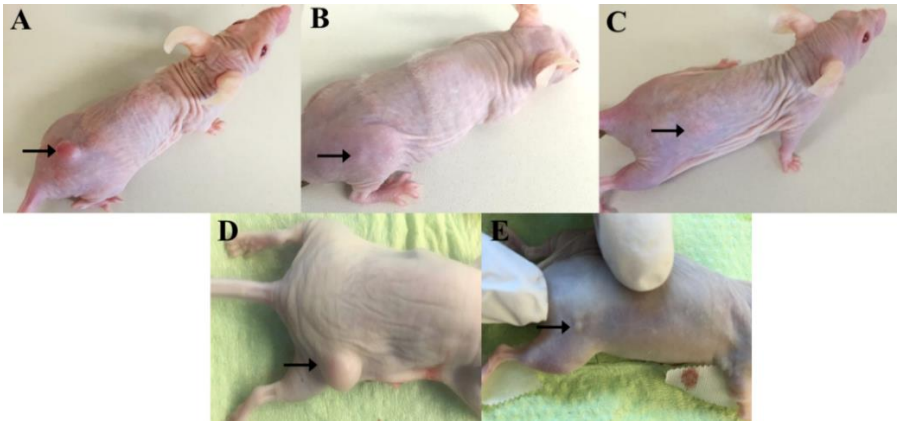

Figure 25. Images depicting tumor volumes and lesion-free skin after 6 (A-C) and 8 (D and E) therapy cycles of (A,D) placebo, (B) DE, (C) DE in combination with SO1861 and (e) dianthin-dPGS. The pictures show one representative animal of each group comprising 5 mice in case of A, B and C while 8 mice in case of D and E.

Table 16. Average tumor volume reduction at the end of treatment therapies.

Targeted toxin therapy	Dose/treatment	Tumor volume (mm^3)	Average reduction (%)
Dianthin-EGF	0.35 µg	40.8 mm^3 ± 61.3	50.1
Dianthin-dPGS	15.00 µg	15.2 mm^3 ± 23.1	81.4
Dianthin-EGF + SO1861	0.35 µg + 30.00 µg SO1861	3.0 mm^3 ± 3.3	96.3

3.7 Histopathological outcome of organs

3.7.1 Consequence of acute toxicity study treatments

To evaluate the acute toxicity, histopathological analyses of isolated organs by hematoxylin and eosin (HE) stains were performed. Most of the organs did not reveal any alterations and were labeled as regular. Especially, no alteration was seen in

stomach, heart, kidney and intestine of any mice as shown in tables 17, 18 and 19. However, mild to moderate alterations with single cell/group of necrotic cells (Figure 26) were observed in liver tissue of mice. In case of toxin (dianthin) alone (table 17), the mice in which the highest dose (100 µg/mouse) was administered showed groups of necrotic hepatocytes. Nevertheless, no severe damage was observed. Activation of spleen was observed in all cases due to immunogenic reactions of the toxin *in vivo* as BALB/c mice used in acute toxicity studies are immunocompetent in comparison to CD-1 nu/nu mice used in efficacy studies.

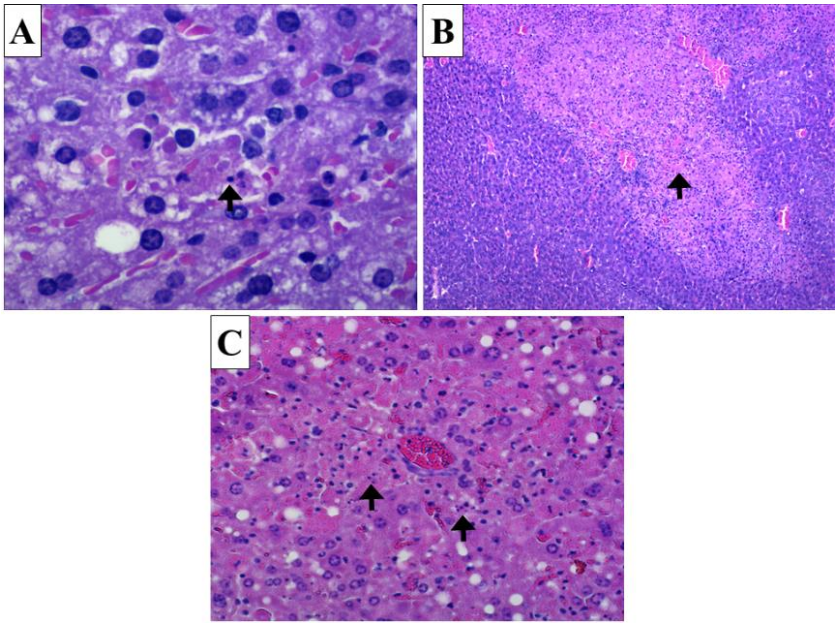

Figure 26. Immunohistochemical evaluation of liver samples. Hematoxylin and eosin staining showed mild alterations (A) in liver tissues isolated from mice administered with low doses of dianthin and dianthin-dPGS (10 µg and 30 µg) conjugate. The mild alteration is referred to single cell necrosis as depicted by an arrow. Moderate alterations were observed with (B) the highest doses of dianthin and dianthin-dPGS (100 µg). The necrosis of groups of hepatocytes as shown by an arrow is a clear information of expanded inflammation in the liver due to a high dose of dianthin and dianthin-dPGS. (C) Necrosis of small groups of hepatocytes, i.e. moderate alterations in liver tissues isolated from mice administered with the highest single dose of DE (40 µg). dPGS, dendritic polyglycerol sulfate.

In case of dianthin-dPGS (table 18), a little activation of spleen was observed along with an acute damage to liver. One out of three mice with the highest dose (100 µg/mouse) showed group of necrotic hepatocytes followed by focal fibrosis when liver was examined microscopically. In case of DE (table 19) the liver showed mild to moderate alterations leading to acute and fibrotic damage. Lungs were diagnosed with mild focal emphysema due to inhalation of isoflurane to a higher extent while

sacrificing the mice. Mild activation in spleen might be due to immunogenic reactions of the toxin on spleenocytes. Nevertheless no severe damage was observed

Table 17. Histological evaluation of organs isolated from the monotherapy with dianthin.

Dose	Liver*	Kidney	Stomach	Spleen	Heart	Pancreas	Lung	Intestine
10 µg	1-0	regular	regular	little activation	regular	regular	regular	regular
	1-0	regular	regular	little activation	regular	regular	regular	regular
	1-0	regular	regular	little activation	regular	regular	regular	regular
	1-0	regular	regular	little activation	regular	regular	regular	regular
30 µg	1-0	regular	regular	activation	regular	regular	regular	regular
	1-0	regular	regular	little activation	regular	regular	regular	regular
	2-1	regular	regular	little activation	regular	regular	regular	regular
100 µg	2-0	regular	regular	activation	regular	regular	regular	regular

*** Liver damage index:** First number = acute damage, 0 = none, 1 = single cells, 2 = groups of cells, 3 = large areas; Second number = fibrotic damage, 0 = none, 1 = focal fibrosis

Table 18. Histological evaluation of organs isolated from the dianthin-dPGS treatment.

Dose	Liver*	Kidney	Stomach	Spleen	Heart	Pancreas	Lung	Intestine
10 µg	1-0	regular	regular	little activation	regular	regular	regular	regular
	1-0	regular	regular	moderate activation	regular	regular	regular	regular
	1-0	regular	regular	little activation	regular	regular	regular	regular
30 µg	1-0	regular	regular	little activation	regular	regular	regular	regular
	1-0	regular	regular	little activation	regular	regular	regular	regular
	1-0	regular	regular	moderate activation	regular	regular	regular	regular
	2-0	regular	regular	little activation	regular	regular	regular	regular
100 µg	1-0	regular	regular	activation	regular	regular	regular	regular
	1-0	regular	regular	little activation	regular	regular	regular	regular
	2-1	regular	regular	little activation	regular	regular	regular	regular

*** Liver damage index:** First number = acute damage, 0 = none, 1 = single cells, 2 = groups of cells, 3 = large areas; Second number = fibrotic damage, 0 = none, 1 = focal fibrosis

Table 19. Histological evaluation of organs isolated from dianthin-EGF treatment.

Dose	Liver*	Kidney	Stomach	Spleen	Heart	Pancreas	Lung	Intestine
0.4 µg	1-0	regular	regular	mild activation	regular	regular	regular	regular

	1-0	regular	regular	mild activation	regular	regular	mild focal emphys-ema	regular
	2-1	regular	regular	mild activation	regular	regular	mild focal emphys-ema	regular
4.0 µg	2-1	mild lympho-cytic inflamm-ation	regular	mild activation	regular	regular	mild focal emphys-ema	regular
	1-0	regular	regular	moderate activation	regular	regular	mild focal emphys-ema	regular
	1-0	regular	regular	moderate activation	regular	regular	mild focal emphys-ema	regular
40.0 µg	2-1	regular	regular	mild activation	regular	regular	mild focal emphys-ema	regular
	2-1	regular	regular	mild activation	regular	regular	mild focal emphys-ema	regular
	1-0	regular	regular	mild activation	regular	regular	mild focal emphys-ema	regular

*** Liver damage index:** First number = acute damage, 0 = none, 1 = single cells, 2 = groups of cells, 3 = large areas; Second number = fibrotic damage, 0 = none, 1 = focal fibrosis

3.7.2 After-effect of targeted therapies on organs

To evaluate after-effects of different dianthin-based targeted therapies, histological analyses of the organs were performed. Most of the organs did not reveal any alterations and were labeled as regular. Especially, no alteration was seen in stomach, heart, kidney and intestine of any mice as shown in tables 20-23. Effects were observed in hepatocytes and spleenocytes.

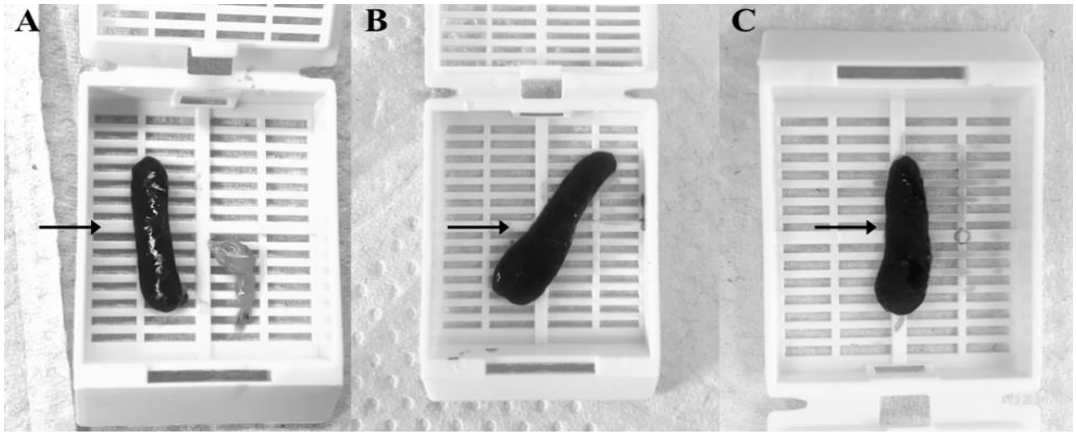

Figure 27. Images of spleens with visible effect of targeted toxin therapy on spleen size. An increase in spleen size as compared to (A) dianthin-dPGS was observed in mice administered with (B) DE treatments alone and (C) DE in combination treatment with SO1861.

Acute damage to liver with mild alterations consisting of single cell necrotic cells were observed in liver tissue of mice (all treatment groups). Nevertheless, no fibrotic damage in liver due to toxin/targeted toxin was observed at the therapeutic dose used for dose response curves. No severe damage was observed. Activation of spleen was observed histologically as well as visually in all groups (Figure 27). Mild activation in spleen might be due to immunogenic reactions of the toxin on spleenocytes. Nevertheless, no severe damage was observed. Lungs were diagnosed with mild focal emphysema due to inhalation of isoflurane to a higher extent while sacrificing the mice.

Table 20. Histological examination of organs isolated from efficacy study performed in 7 – 8 weeks old CD-1 nu/nu mice. In the placebo group animals were injected with PBS (100 µL/treatment).

Liver*	Kidney	Stomach	Spleen	Heart	Pancreas	Lung	Intestine
1-0	regular	regular	little activation	regular	regular	regular	regular
1-0	regular	regular	moderate activation	regular	regular	atelectasis	regular
1-0	regular	regular	little activation	regular	regular	atelectasis	regular
1-0	regular	regular	moderate activation	regular	regular	atelectasis	regular
1-0	regular	regular	moderate activation	regular	regular	regular	regular
1-0	regular	regular	little activation	regular	regular	regular	regular

*The liver damage index 1-0 means single cell necrosis and no fibrotic damage.

Table 21. Histological examination of organs isolated from animals administered with Dianthin-dPGS (15 µg/treatment).

Liver*	Kidney	Stomach	Spleen	Heart	Pancreas	Lung	Intestine
1-0	regular	regular	little activation	regular	regular	atelectasis	regular
1-0	regular	regular	moderate activation	regular	regular	bronchopneumonia	regular
1-0	regular	regular	little activation	regular	regular	atelectasis	regular
1-0	regular	regular	little activation	regular	regular	regular	regular
1-0	regular	regular	moderate activation	regular	regular	regular	regular
1-0	regular	regular	little activation	regular	regular	regular	regular

*The liver damage index 1-0 means single cell necrosis and no fibrotic damage.

Table 22. Histological examination of organs isolated from animals administered with DE (0.35 µg/treatment) alone.

Liver*	Kidney	Spleen	Heart	Pancreas	Lung	Intestine
1-0	regular	mild activation; small hematopoiesis	regular	regular	mild focal emphysema	regular
1-0	regular	mild activation; small hematopoiesis	regular	regular	mild focal emphysema	regular
1-0	regular	mild activation; small hematopoiesis	regular	regular	mild focal emphysema	regular
1-0	regular	mild activation; small hematopoiesis	regular	regular	mild focal emphysema	regular
1-0	regular	moderate activation; moderate hematopoiesis	regular	regular	mild focal emphysema	activated lymphoid tissue

*The liver damage index 1-0 means single cell necrosis and no fibrotic damage.

Table 23. Histological examination of organs isolated from animals administered the combination treatment of DE (0.35 µg/treatment) and SO1861 (30 µg/treatment).

Liver*	Kidney	Spleen	Heart	Pancreas	Lung	Intestine
1-0	regular	mild activation; small hematopoiesis	regular	regular	mild focal emphysema	regular
1-0	regular	mild activation; small hematopoiesis	regular	regular	mild focal emphysema	regular
1-0	regular	mild activation; strong hematopoiesis	regular	regular	mild focal emphysema	regular
1-0	regular	mild activation; moderate hematopoiesis	regular	regular	regular	regular
1-0	regular	moderate activation; moderate hematopoiesis	regular	regular	regular	regular

*The liver damage index 1-0 means single cell necrosis and no fibrotic damage.

3.7.3 Tumor EGFR expression level in different groups

Tumors isolated from the efficacy studies (DE, DE + SO1861 and placebo) accomplished in CD1 nu/nu xenografts were immunohistochemically analyzed for the expression of EGFR and the Ki67 proliferation marker. No specific OATP (1B1/1B3) antibody is present to dates in order to check in particular 1B1/1B3 expression level in tumor for immunohistochemistry isolated from the dianthin-dPGS based efficacy study.

Nevertheless, all isolated tumors from the placebo group expressed high levels of EGFR (Figure 28A) however, only a weak EGFR staining was examined in mice treated with the monotherapy (Figure 28B), indicating that the monotherapy is only suitable to kill tumor cells with high EGFR expression while tumor cells with lower EGFR expression escape from treatment and selectively proliferate.

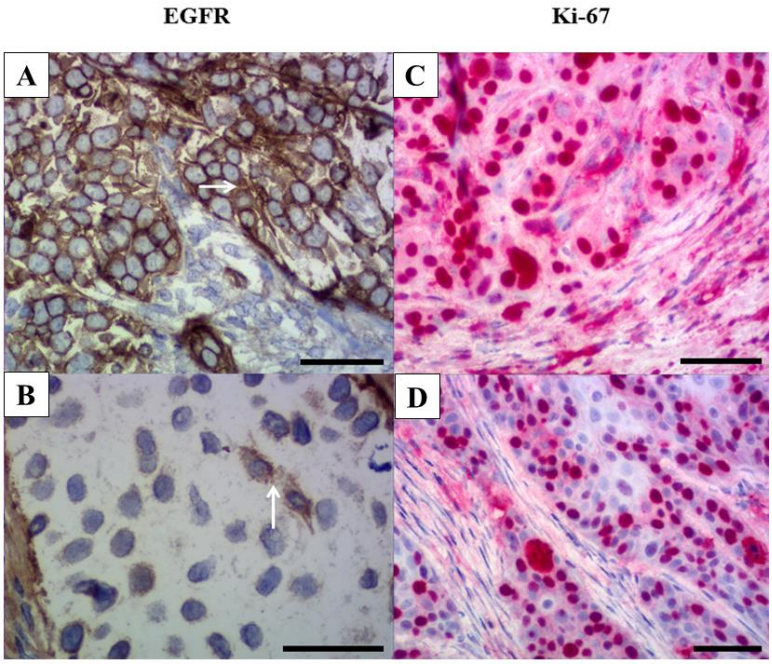

Figure 28. Immunohistochemical evaluation of (A–D) tumor tissue samples. (A) High EGFR expression level (arrow) was observed in untreated tumors whereas (B) a weak expression of EGFR (arrow) was observed in the treatment group depicting curative effect of therapy as compared to untreated. High Ki67 proliferation index (C) was observed in all tumors except the one obtained after combination therapy [50%; (D)].

A high Ki67 proliferation index (> 60%; figure 28C) was observed in all isolated tumors of the placebo and monotherapy group. This let us assume that the reduced tumor size in the monotherapy group can be attributed only to the killing of high EGFR expressing tumor cells but not to a lower proliferation rate of the tumor cells with lower EGFR

amount. In the combination therapy after six treatment cycles, only one out of five mice still had a tumor that could be investigated for the growth capacity. This tumor only had a 50% Ki67 proliferation index (Figure 28D).

3.8 Hematological repercussion of therapeutic regimen

In case of single and combination therapy of DE, the complete blood count was evaluated. In case of dianthin-dPGS based treatment, liver transaminases (ASAT and ALAT) were evaluated. This was done as the targeting moiety for dianthin-dPGS are liver specific OATPs.

No significant difference was seen in the non-platelet-derived parameters of blood as displayed in table 24. In contrast, the platelet-derived parameters showed statistically significant alterations as depicted in figure 29.

Table 24. Descriptive statistics of non-platelet derived hematological parameters. None of the differences are statistically significant. RBC, WBC, red and white blood cell counts; HGB, hemoglobin; RDW-SD, RDW-CV, red blood cell distribution width, standard deviation and coefficient of variation; HCT, hematocrit; MCV, mean corpuscular volume; MCH, mean corpuscular hemoglobin; MCHC, mean corpuscular hemoglobin concentration.

Parameters	Untreated	Placebo	DE	DE + SO1861
WBC	2.3 ± 0.5	3.2 ± 0.3	2.4 ± 0.8	3.0 ± 0.8
RBC	7.7 ± 1.0	7.7 ± 0.4	7.6 ± 0.6	7.1 ± 1.0
HGB	11.8 ± 1.4	11.6 ± 0.6	11.3 ± 0.8	10.9 ± 1.0
RDW-SD	26.5 ± 2.7	26.8 ± 1.8	26.8 ± 2.4	32.2 ± 6.0
RDW-CV	16.3 ± 2.0	16.3 ± 0.6	17.0 ± 0.2	18.0 ± 0.9
HCT	38.5 ± 1.0	39.0 ± 0.9	37.3 ± 1.2	37.8 ± 1.4
MCV	50.0 ± 0.9	50.7 ± 1.9	48.9 ± 2.3	53.5 ± 6.5
MCH	15.4 ± 0.3	15.1 ± 0.6	14.8 ± 0.3	15.3 ± 1.1
MCHC	30.8 ± 1.0	29.8 ± 0.9	30.3 ± 1.2	28.7 ± 1.4

A significant increase in platelet count was observed in case of the combination treatment ($p < 0.01$ versus healthy as well as placebo). Surprisingly, there was also a significant increase in platelet count observed for placebo when compared to healthy ($p < 0.05$), indicating that the puncture wound has some influence on the platelets. An increase in plateletcrit was also significant compared to placebo ($p < 0.05$ versus DE; $p < 0.0001$ versus DE + SO1861). A slight but significant difference in platelet distribution width was observed for monotherapy compared to the combination ($p < 0.05$) while the mean platelet volume showed no significant difference.

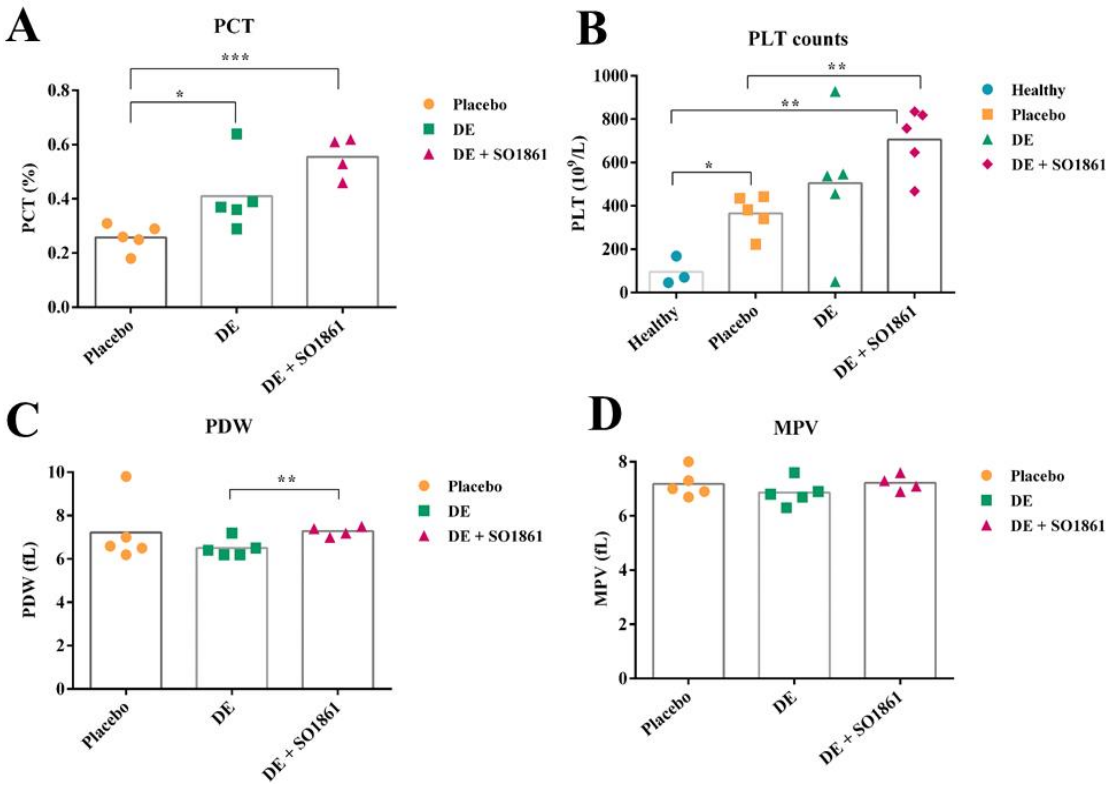

Figure 29. Platelet-derived parameters in different groups (healthy, placebo, DE and DE + SO1861 treated). Significance is indicated as * ($p < 0.05$), ** ($p < 0.01$) and *** ($p < 0.001$). PLT counts, platelet counts; PCT, plateletcrit; PDW, platelet distribution width; MPV, mean platelet volume.

Alanine transaminase (ALAT) and aspartate transaminase (ASAT) was elevated in dianthin-dPGS treated mice. Suprisingly, only one of the two enzymes was significantly elevated. No significant difference was seen in ASAT level (Figure 30A). In contrast, a significant increase in ALAT was observed in dianthin-dPGS treated animals compared to placebo (Figure 30B).

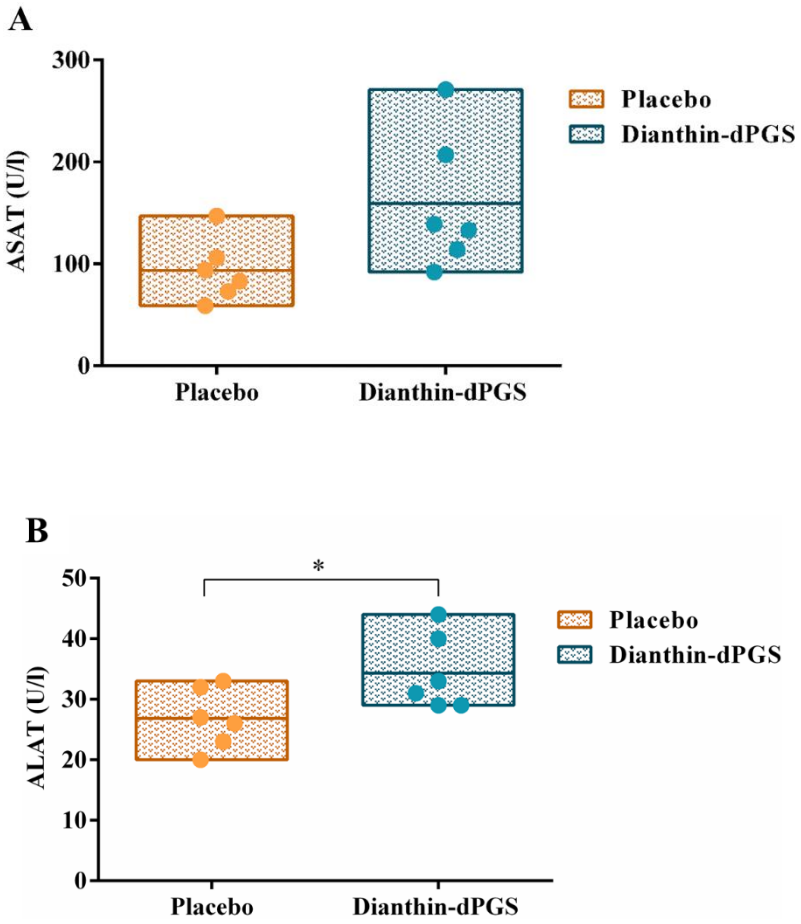

Figure 30. Liver enzymes elevation in different groups (dianthin-dPGS and placebo). Significance is indicated as * ($p < 0.05$). Each dot represents the (A) ASAT and (B) ALAT level of a single mouse. ASAT, aspartate transaminase; ALAT, alanine transaminase.

4. Discussion

4.1 Architecture of targeted toxins

The aim of engineering a targeted toxin was to flourish a novel technology platform for the intracellular transport of macromolecular antineoplastic therapeutics. The developments in biotechnology provide highly efficient tools to create and optimize new effective therapeutics based on protein structures. Today more than half of all new generation registrations already include drugs that are structurally based on peptides, proteins or antibodies [121-124]. The basic advantage of this class of drugs are high selectivity and specificity to the molecular processes involved in carcinogenesis or inflammation, which can be effectively blocked or inhibited. In contrast, the chemotherapeutic agents are not sufficiently selective for the cell to be controlled and are therefore distributed in the body leading to side effects throughout the organism. The small molecules of chemotherapeutic agents diffuse through cell membranes, however, the major limitation with high molecular weight protein-based therapeutics is that they are not absorbed by the cells [125, 126].

The general goal of the pharmaceutical research is therefore to find ways to modify protein-based drugs in such a way that they are selectively taken up by the tumor cells and produce their effect there. Various strategies for increasing the cellular uptake of active metabolites are being utilized. One strategy is to conjugate tumor-specific binding molecules to drugs [127]. Since the site of action for protein-based drugs is generally cytoplasm or nucleus, there is therefore a need of methods, which transport theses active substances effectively and undamaged into the cytoplasm of tumor cells. For this purpose, a novel class of synthetic molecules has been discovered, which allows the modification of protein-based active substances in such a way that the active substances are transported directly into the cytoplasm *via* intrinsic transport mechanisms of the cell (organic anion transporting polypeptide, OATPs). In the present research work, anionic dendrimers with a defined number (48) of negatively charged sulfated groups served as a substrate to OATPs exclusively thereby facilitating the cellular entry.

The outstanding feature of dendritic polyglycerols is their high biocompatibility [128]. In contrast to tiresome multistep synthetic pathways of perfectly branched dendrimers

[129], hyperbranched analogs can be prepared in various sizes by applying different synthetic strategies [130-132]. In the present research, a macromolecular targeted toxin was developed by conjugating hyperbranched dendritic-polyglycerol to the recombinantly expressed protein dianthin as a cytotoxic agent, however, dendrimer-based nanoparticles have also been developed to target cancer cells [133]. The unique advantages offered by a dendritic molecule over conventional macromolecules and polymers are the existence of multiple functional groups and their complaisance to further chemical modification, exceptionally low polydispersity, low solution viscosity, decreased molecular entanglement, the presence of nanocavities, and scalable size within the range of 1 – 10 nm [133]. Dendritic polyglycerol-based immunoconjugates with doxorubicin as cytostatic agent that specifically target EGFR expressing cancer cells and kills them have also shown therapeutic promise [134]. Nevertheless the synthesis, conjugation and purification steps of these dendritic polyglycerols-based protein therapeutics are highly challenging.

The multifunctional or multivalent property of dPGS facilitate its coupling to various chemotherapeutic agents by crosslinkers or near-infrared fluorescent dyes like indocyanine green [135, 136]. PEG-SPDP crosslinkers offer great advantage in protein conjugations *via* amine-to-amine or amine-to-sulfhydryl crosslinks. Polyethylene glycol (PEG) spacer arms confer greater solubility to the crosslinker and the linked proteins compared to crosslinkers having only hydrocarbon spacers. Herein sulfhydryl groups were created in dianthin by the application of 2-iminothiolane, also we conjugated dPGS to dianthin *via* NHS ester linkage, finally leading to amine-sulfhydryl crosslinks. Researchers have also conjugated antineoplastic tubulin-binding drug, paclitaxel to dPGS *via* a labile ester linkage [137] thus making macromolecular conjugates as ideal entities for drug delivery as they can be effectively optimized for drug uptake, binding, release and tolerability.

Automated chromatography techniques such as fast protein liquid chromatography (FPLC) represent an approach toward resolving or isolating the complex protein mixtures [138]. In our present study we found FPLC as a highly reproducible technique, which can be used for the analysis and purification of protein-based conjugate mixtures. In addition to proteins, the method is applicable to other kinds of biological samples including oligonucleotides and plasmids [139]. Several scientists have utilized this technique for diagnostic purposes as well.

A truly innovative method by Small, Stevens and Bauman at Dow Chemical Co. marked the origin of modern ion chromatography [140, 141]. As the existing research work comprises of polyanionic macromolecular protein conjugate (dianthin-dPGS), ion-exchange chromatography appeared to be a useful tool for the bioseparation of ionizable molecules on the basis of different charge properties. The aforementioned purification technique has been routinely employed to purify enzymes [142, 143], peptides [144], antibodies [145] and nucleic acids [146, 147]. However, the choice of a suitable ion-exchange matrix is probably the single most challenging criteria of this technique. The matrix can either be anion or cation-exchanger and each can be weak or strong. In the present study the novel targeted toxin is a highly anionic drug entity therefore, a weak anion-exchanger and positively charged diethylaminoethyl (DEAE) column was used. The weak anion exchanger was culled upon the requirement of mild elution conditions in order to obtain the purified conjugate without disturbing the stability, protein folding and enzymatic activity of the protein conjugate. In contrast, strong ion-exchangers often necessitates harsh elution conditions (up to 1 M NaCl) that may compromise sample stability [148].

Buffer condition is another important aspect in the purification of protein-conjugate mixture. A biocompatible CAPSO buffer, pH 9.5 was chosen as the pI of dianthin-30 is 8.65 [97] and as per the good rule of thumb for choosing buffer pH, the running buffer condition should be 0.5-1.5 pH units greater the pI of the protein of interest in case of anion exchange (DEAE) resin. Many researchers generally use TRIS buffer (pH range 7.6 – 8.6) for separation of protein samples on DEAE column. Nevertheless, the need of buffer condition greater than 8.65 was needed in present study, thereby CAPSO buffer (pH range 8.9 – 10.3) was adopted. Altogether, in a buffer with a pH greater than the pI of protein, the protein carries a net negative charge, therefore, positively charged DEAE resin was successful in capturing the polyanionic protein conjugate.

In the present study gradient elution comprising of 2 elution buffers were utilized. One devoid of salt and the second one with 2 M NaCl. During anion-exchange chromatography, the weakly adsorbed unconjugated protein resulted in early elution. However, as the salt concentration increased gradually in mobile phase, the negatively charged protein-conjugate was displaced by the addition of negatively charged chloride ions thus leading to successful purification of the desired targeted toxin as displayed in figure 12.

4.2 Ligand peculiarity to bind particular targets

The ligand specificity is of utmost importance to target particular targeting moieties in order to have cytocidal effect on neoplastic cells. The major limitation of cytotoxic chemotherapy or radiotherapy in cancer is severe side effects that arise from toxicities to sensitive normal cells due to their non-selective nature. So how can selectivity be enhanced or made better? The ligand present in antineoplastic drugs determines the overall fate of cancer cells both *in vitro* and *in vivo*. Thereby, it is a very important aspect that needs to be discussed in detail.

In the present study two dianthin-based targeted toxin containing disparate ligands are discussed. DE is a fusion protein containing EGF as ligand whereas dianthin-dPGS is a targeted toxin containing dPGS as ligand. Herein, the physiological effect is observed due to interaction between ligand and receptor/transporters. A selectively increased association occurs between molecules that bind to antigen or receptors that are either overexpressed or uniquely expressed on target cells as compared to normal cells. So what determines the choice of targeting ligand which are proving successful in clinic? The important factors are high density of target antigen/receptor on target cell surface, uniformity of antigen expression on target cells and non-shedding upregulated nature of receptor/antigen [149].

The epidermal growth factor receptor pathway is highly activated in pancreatic cancer, therefore it is a prudent target for new cancer treatments [150]. The differential EGFR expression level on cells thus have a peculiar pharmacological effect. The stumbling block in case of such ligand is its non-selective expression by binding to non-target tissues. Also, ligands that occur in the diet such as EGF, can be found in body fluids [151, 152] and the free ligand will compete for binding for targeted therapy.

Monoclonal antibodies or antibody fragments are also utilized in contrast to non-antibody ligands. Nowadays, antibodies possessing high degree of specificity and a wide range of binding affinities are built by antibody engineering and phase display technologies [153, 154]. There also occurs a possibility to synergize antibodies and chemotherapeutic agents as the cells will be targeted in two distinct ways [155, 156]. So why non-antibody ligands are chosen over antibody-based ligands? Despite new advances, they remain expensive, issues concerning stability and storage might arise

and the production is time-consuming. A major problem is immunogenicity and anti-idiotypic immune responses against humanized or fully human antibodies [157].

When whole monoclonal antibodies was used for the development of targeted toxins, the Fc domain turns out to be a mixed blessing. The Fc domain can lead to antibody-dependent cellular cytotoxicity (ADCC) and complement-dependent cytotoxicity (CDC), which might enhance cancer-cell kill. But it can also lead to binding to non-target normal tissues *via* Fc receptors, especially on macrophages, which leads to increased uptake of targeted toxin in liver and spleen thus increasing immunogenicity of molecule. Non-antibody ligands have certain advantages over antibody-based ligands. They are easily available, manufacturing is highly economical and easy to handle.

A fascinating unresolved question is the choice between high or low binding affinity of the ligand for its epitope. A decreased penetration of targeted drugs into the solid tumors is observed for high affinity ligands due to the binding-site barrier, as the drug binds to first targets encountered but fails to diffuse further into the tumor [158-160]. In order to produce a toxic effect, the toxin moiety of the RIP-based drug must be released into the cytosol without undergoing lysosomal degradation.

A transport-mediated tissue targeting strategy, where the structural features recognized by the transporters are incorporated into the therapeutic molecule design, is gaining heights as an effective approach in drug discovery. Similarly, dPGS consisting of polyanionic sulfates were coupled to dianthin in order to be recognized by the hypothesized membrane transporters (OATPs). The OATP-mediated pathway is hypothesized to present the active molecule directly into the cytosol without undergoing enzymatic degradation. Tissue-selective delivery of pharmacological agents is emerging as an effective approach to enhance the efficacy as well as to improve the therapeutic window in drug discovery.

A compelling question arises with respect to tumor targeting selectivity of dianthin-dPGS to OATPs as compared to normal tissues. The differential expression of transporters on neoplastic cells serve as a novel target to enhance drug delivery to tumor cells. An altered expression of OATPs, especially 1B1/1B3 is seen in some of pancreatic carcinomas [161]. However they are also expressed in normal hepatocytes

and called as ‘liver-specific’ [162]. In general, a dose optimization should be done so that the targeted drug does not cause hepatotoxicity.

4.3 Toxicity enhancement in presence of SO1861

In the present study, EGF and dPGS serves as ligands to target EGFR and OATP molecules. Toxicity analyses *in vitro* as well as *in vivo* is an important objective in order to determine the potency and selectivity of dianthin-based targeted toxins *via* differential signaling pathways. It is though noteworthy to observe the tremendous enhancement of cytotoxicity in presence of the triterpenoid saponin SO1861. A special focus was also given to the use of human cancer cell lines which can later be used to develop tumor models.

The most inquisitive question is whether cytotoxicity is enhanced in presence of SO1861 or not? *In vitro*, no significant difference between the cytotoxic effect on target and off-target cells when treated in the absence of SO1861 were observed (Figure 17). However, addition of SO1861 solely enhanced the cytotoxic effect on target cells, indicating that DE and dianthin-dPGS enters off-target cells *via* unspecific routes omitting late endosomes (explaining the absent enhancer effect of SO1861) while late endosomes are expectedly reached in target cells, but no increased cytotoxic effect compared to off-target cells is observed due to missing endosomal escape, which only occurs in the presence of SO1861 (Figure 17). Lately it was also found that genetic polymorphisms in drug transporters can also lead to impaired protein trafficking to the membrane and decreased bile acid transport *in vitro*. This in turn affects substrate specificity of the hepatocellular uptake transporter OATP1B3 [163].

Dianthin-based target toxin-induced growth inhibition in the presence of SO1861 varied between different panel of target cell lines. The difference in the cytotoxic effect between single and combination therapy proved to be more eminent in BxPC-3 cells (EGFR-overexpressing cell line, Figure 17A) and QGP-1 (OATP overexpressing cell line, Figure 17D), as portrayed by an IC_{50} of 100 nM in monotherapy and 0.17 nM in combination therapy (for BxPC-3 cells) and IC_{50} of 27 nM in monotherapy and an IC_{50} already reached below 0.01 pM in combination treatment (for QGP-1 cells) within 48 h.

Studies on saporin-based targeted toxins showed that the IC_{50} is strongly dependent on target receptor expression and can range from 2.5 nM to 206 nM in the absence of endosomal escape enhancers [164]. For DE, the IC_{50} was only 0.45 nM on transfected cells that highly overexpress EGFR [165] and greater than 10 nM for dianthin chemically conjugated to panitumumab, trastuzumab or cetuximab [119]. The effect by endosomal escape enhancers depends on the cell line, the targeting moiety, target receptor expression and the structure of the enhancer. Enhancement factors of more than one million were observed [165]. The IC_{50} for the above mentioned antibody-dianthin conjugates in the presence of SO1861 was 1.5 pM, 23 pM and 5.3 pM, respectively [119]. Real time cytotoxicity studies also revealed the combination treatment to be more superior compared to the monotherapy with only targeted toxin.

Can charge on the dendrimer surface modify cytotoxicity? Can size and molecular mass of the hyperbranched polyglycerols (HPG) affect cellular uptake? Yes, it has also been investigated that cationic dendrimers of generation 4 are proven to be highly toxic whereas anionic dendrimers are neither lytic nor cytotoxic over a broad concentration range [166]. A size-dependent cellular uptake of HPG occurs indicating an increase in endocytosis with increment in size. No endocytosis is expected for HPG below 20 kDa [167]. The choice of ICC as fluorescent probe has already proven valuable [128]. In general, HPG-ICC dye conjugates can be combined to targeted toxins for receptor mediated endocytosis to better understand the cellular uptake mechanism for future drug targeting applications. In acute toxicity experiments, 10.0 µg dianthin, 10.0 µg dianthin-dPGS and 0.4 µg DE per treatment *via* intraperitoneal administration resulted in no biological effect and no statistically significant weight loss except for dianthin-treated mice. Histology showed no organ toxicity at this dose. Increasing the dose to 30.0 µg (dianthin and dianthin-dPGS) and 4.0 µg (DE) caused significant weight loss but no adverse effects. Further increase to 100.0 µg (dianthin and dianthin-dPGS) and 40.0 µg (DE) caused moderate alterations in the liver by necrosis of groups of hepatocytes. The liver is the main organ that is effected when immunoconjugates are administered intraperitoneally [168]. Since we only observed moderate liver toxicity at 40.0 and 100.0 µg, it can be most likely assumed that the treatment dose of 0.35 µg DE, less than a hundredth of a moderately toxic dose, particularly when applied subcutaneously, is much below the highest NOAEL. Similarly the 15.0 µg dianthin-dPGS was assumed to be less than calculated NOAEL for dianthin (19.4 µg) and dianthin-dPGS (20.8 µg). Moreover, it can be assumed that multiple treatments will not

result in an accumulation effect since the endosomal escape enhancer is almost completely excreted after 4 hours [169].

4.4 Efficacy

As already mentioned the main objective of this study was to establish a treatment regimen for dianthin-based targeted toxins in a xenograft tumor model. In general, experimental animal cancer models provide a link between how cancer develops at cellular level and may be cured. Tumor models allows the collection of scientific and preclinical data that is unavailable from *in vitro* experiments. Furthermore it also brings to our knowledge various side effects arising from chemotherapeutic cycles. Thus a key focus of this thesis is to determine, which dianthin-based targeted toxin is more effective in the treatment of pancreatic carcinoma solid tumor in conjunction with least observed after-effects.

The combination of DE and SO1861 revealed a very strong synergistic effect when administered subcutaneously since SO1861 alone has no toxic effect at the applied concentration and the monotherapy with DE has a 13-fold weaker effect with respect to tumor reduction than the combination. Nevertheless, the monotherapy with dianthin-dPGS has only 5-fold weaker effect than the combination therapy. Earlier experiments showed that intraperitoneal injection of a targeted toxin did not cause a significant decrease in tumor size when the endosomal escape enhancer is applied at the same route [170]. The reason for this appears to be the high concentrations of targeted toxins and enhancer at the same site resulting in inflammation and possibly toxin degradation. To avoid inflammation, SO1861 was administered s.c. at the back of the neck and DE s.c. at the vicinity of the tumor. This strategy was already successful in the past [171, 172], however, required careful choice of the length of the time period between SO1861 and toxin application [169]. In contrast, dianthin-dPGS was injected intraperitoneally in order to stick to same route of administration as performed in acute toxicity study. With respect to clinical trials, the use of a deimmunized form of dianthin might facilitate systemic applications as shown for a deimmunized form of another ribosome-inactivating protein, bouganin, in an immunotoxin with trastuzumab [173]. Another possibility is to substantially decrease the systemic concentration of SO1861 by modifying the enhancer to a targeted molecule. Nevertheless, for the combination

treatment with dianthin-dPGS dose optimization for SO1861 concentration must be done.

Evaluation of the complete blood count revealed a significant change in the platelet-derived parameters (Figure 29) with DE treated animals. It was also observed that augmentation in the efficacy of treatment (combination therapy > monotherapy > placebo > untreated) led to an unexpectedly increased platelet count. This was also seen in more than a half of advanced non-small cell lung cancer patients at phase II clinical trials with a combination of gemcitabine and cisplatin [174], in studies performed with a combination of gemcitabine and vincristine [175] and in pancreatic cancer patients treated with gemcitabine alone [176]. Thus, an increase in platelet count appears to be not uncommon, but the molecular background behind this is yet to be explored.

OATPs are broad substrate carriers for organic anions, and other amphipathic organic solutes from portal blood including wide range of drugs as well as sodium-independent uptake of bile salts [177]. They are overexpressed in normal liver [178] so it is inevitable to test two reasonably sensitive indicators of liver damage. Subsequently, examination of two main liver enzymes: aspartate aminotransferase (ASAT) and alanine aminotransferase (ALAT) were quantified, which affirmed a significant change in ALAT levels in dianthin-dPGS treated mice compared to placebo. Studies by Steeg *et al.* revealed that another anticancer drug, methotrexate (MTX) is also uptaken by OATP 1B1/1B3 *in vivo* in transgenic mice [179]. This was further confirmed when the OATP inhibitor rifampicin inhibited MTX uptake even at low micromolar concentrations [180]. Hepatotoxic effects of MTX showing an increase in ALAT levels in contrast to ASAT were also seen clinically [181]. A slight activation of spleenocytes was observed, which is assumed to be due to uptake of dianthin-dPGS. Histological studies have disclosed the uptake of dPGS by spleen macrophages present in the red pulp [182]. Hence, there also occurs chances of drug-drug interactions in case of dianthin-dPGS administration in accordance with other drugs.

Over the decades, many bacterial- and plant-based targeted toxins have been developed with the goal of targeting cancers reliant upon EGFR overexpression [183]. The targeted toxin 425(scFv)-ETA, consisting of an anti-EGFR single chain Fv antibody fused to a truncated *Pseudomonas* exotoxin, was strongly cytotoxic towards metastatic pancreatic cancer cells (L3.6pl) with an IC_{50} of 0.1 nM [184]. In mice injected with L3.6pl cells, multiple applications of 425(scFv)-ETA reduced the number of lung

metastases from 56 per mouse to 0.28 per mouse [185] indicating the strong potential of this targeted toxin. Similar targeted toxins using single chain Fv antibodies derived from cetuximab and panitumumab resulted in IC_{50} values of 0.29 nM and 0.26 nM, respectively, on L3.6pl cells [186]. In contrast to dianthin, the truncated *Pseudomonas* exotoxin possesses its own natural translocation domain [187, 188], which makes it independent from endosomal escape enhancers, explaining the similar IC_{50} values observed for the exotoxin and dianthin in presence of SO1861.

On the one hand the weak expression after DE treatment can indicate that the tumor is now less aggressive after eradicating the part of tumor cells with high expression level. On the other hand, this let us assume that a monotherapy with DE is not sufficient to kill tumor cells with lower EGFR expression resulting in selective survival of these cells and continuous tumor growth (Figure 28). The reason for the missing potential of DE is most likely that only a small portion of the bound and internalized targeted toxin is able to escape from the endosomes before degradation or recycling. This can be overcome in general by the use of endosomal escape enhancers [189] and for ribosome-inactivating proteins in particular by certain glycosylated triterpenoids such as SO1861 [113, 190]. The present study indicates that, in the presence of SO1861, tumor cells with low EGFR expression are also eliminated, finally leading to complete remission in 4 of 5 cases without adverse events. Surprisingly, dianthin-dPGS treatment alone *via* intraperitoneal route caused marked reduction in tumor volume (81.4%, Table 14), the tumor size was however, ~5-fold more in comparison to combination therapy (96.3%, Figure 24).

In conclusion, combining a targeted toxin with SO1861 is proven to be a very promising approach for pancreatic cancer treatment. Long-term efficacy in mice for 60 days or more must still be investigated. Furthermore, the transporter-mediated tumor targeting *via* dPGS-targeting moeity is a valuable alternative to a classical ligand-receptor targeting. In future, the efficacy of dianthin-dPGS conjugate can be determined *in vivo* in combination with SO1861. In order to do so, a dose optimization of SO1861 must also be executed prior to the aforementioned study. Thus the dPGS-mediated transporter targeting suggests promising results in forthcoming *in vivo* studies. Furthermore, the present work also opens up the possibility of constructing new targeting toxins bearing dPGS as targeting moeity along with other RIPs. Also, the mutations in dianthin can be performed which can lead to the formation of highly

specific clickable dianthin molecule. Thus dianthin and dPGS both may serve as interesting candidates to achieve success in future cancer treatments.

5. Summary

Targeted tumor therapy provides the rationale for the arrest of tumor growth in aggressive pancreatic carcinoma, however, a number of protein-based targeted toxins lack efficacy due to insufficient endosomal escape after being endocytosed.

The main objective of this work was to test two disparate targeted toxins comprising the same ribosome-inactivating protein dianthin in both, however, targeting two different pathways. One contained human epidermal growth factor whereas the other contained dendritic polyglycerol sulfates. Both were tested in combination with a glycosylated triterpene (SO1861) that serves as an endosomal escape enhancer.

In vitro investigations with the epidermal growth factor receptor (BxPC-3) and organic anion transporting polypeptide overexpressing (QGP-1) pancreatic carcinoma cell lines revealed no significant differences to off-target cells in the half maximal inhibitory concentration (IC_{50}) for the dianthin-based targeted toxins. In contrast, combination with SO1861 decreased the IC_{50} for BxPC-3 cells from 100 nM to 0.17 nM in case of the fusion protein whereas control cells remained unaffected. However, a phenomenal augmentation of the cytotoxicity was observed from an IC_{50} of 1 nM to 10 fM when cells were treated with dianthin-dPGS in combination with enhancer.

Monotherapy of BxPC-3 xenografts with dianthin-EGF (DE) in CD-1 nude mice led to a 50.1% average reduction in tumor volume (40.8 mm^3) when compared to placebo, however, combined treatment with SO1861 resulted in a more than 13.6-fold better efficacy (3.0 mm^3 average tumor size) with complete regression in 80% of the cases. Moreover, monotherapy of dianthin-dPGS led to 81.4 % average reduction in tumor volume (15.2 mm^3) when compared to placebo. Nevertheless, dianthin-dPGS resulted in 2.6-fold better efficacy than DE, however, was 5-fold less efficacious than the combination treatment of DE with enhancer.

Immunohistochemical analyses showed that tumor cells with lower target receptor expression are, in contrast to the combination therapy, able to escape from the monotherapy, which finally results in tumor growth. At the effective concentration we did not observe liver toxicity and no other side effects with the exception of a reversible skin hardening at the SO1861 injection site. Increase in platelet counts, plateletcrit and platelet distribution width were observed in fusion protein targeted therapy whereas elevation in alanine transaminase in dianthin-dPGS targeted therapy. In conclusion,

combining a targeted toxin with SO1861 is proven to be a very promising approach for pancreatic cancer treatment.

I would also conclude that dPGS-targeting of a transporter is a valuable alternative to classical ligand-receptor targeting.

6. Zusammenfassung

Eine zielgerichtete Tumortherapie bietet sich als vielversprechende Methode zur Hemmung des Tumorwachstums und Reduktion bei aggressivem Pankreaskarzinom an. Jedoch zeigt eine Vielzahl proteinbasierter Toxine nur eine begrenzte Effektivität aufgrund einer unspezifischen endosomalen Freisetzung.

Das Hauptziel dieser Arbeit war es, zwei zielgerichtete Toxine zu untersuchen, welche zum einen aus dem Ribosomen-inaktivierenden Protein Dianthin, zum anderen aus zwei verschiedenen Zielmolekülen, bestehen. Zum einen wurde der menschliche epidermale Wachstumsfaktor (EGFR), zum anderen dendritische Polyglycerinsulfate mit dem Dianthin fusioniert und mit einem glykosylierten Triterpen (SO1861) kombinierend getestet. Dabei wirkt SO1861 verstärkend auf die endosomale Freisetzung.

In-vitro-Untersuchungen mit den EGFR (BxPC-3) und OATP-überexprimierenden (QGP-1) Pankreaskarzinom-Zelllinien zeigten keine signifikanten Unterschiede hinsichtlich der halbmaximalen inhibitorischen Konzentration (IC & sub5; & sub0;) zwischen nicht-zielgerichteten Zellen und Zellen mit Dianthin basierenden, zielgerichteten Toxinen. Im Gegensatz dazu verringerte sich in Kombination mit SO1861 die IC50 für BxPC-3-Zellen von 100 nM auf 0,17 nM, wogegen die Kontrollzellen keine Veränderungen zeigten. Des Weiteren konnte in Zellen mit Dianthin-dPGS und SO1861 eine große Erhöhung der Zytotoxizität von 1 nM bis 10 fM beobachtet werden.

Die Monotherapie von BxPC-3-Xenotransplantaten mit Dianthin-EGF (DE) in CD-1-Nacktmäusen führte im Vergleich zum Placebo zu einer durchschnittlichen Reduktion des Tumorvolumens um 50,1% (40,8 mm^3). In kombinierter Behandlung mit SO1861 konnte eine 13,6-fache Reduktion (3,0 mm^3, durchschnittliche Tumorgröße) mit vollständiger Regression in 80% der Fälle erzielt werden. Darüber hinaus führte die Monotherapie von Dianthin-dPGS zu einer durchschnittlichen Verringerung des Tumorvolumens um 81,4% (15,2 mm^3) im Vergleich zum Placebo. Zugegebenermaßen führte die Behandlung mit Dianthin-dPGS zu einer 2,6-fach höheren Wirksamkeit als DE, jedoch zeigte die Kombinationsbehandlung von Dianthin-dPGS mit SO1861 eine 5-fach geringere Wirksamkeit gegenüber DE mit SO1861.

Immunhistochemische Analysen zeigten, das Tumorzellen mit verringerter Expression des Zielrezeptors, sich verstärkt der Monotherapie entziehen können, was zum weiteren Tumorwachstum führt. Bei der wirksamen Konzentration beobachteten wir keine

Lebertoxizität und keine anderen Nebenwirkungen mit Ausnahme einer reversiblen Hautverhärtung an der Injektionsstelle von SO1861. Eine Zunahme der Plättchenzahl, des Plättchencharakters und der Plättchen-Verteilungsbreite wurde in der zielgerichteten Therapie mit dem Fusionsprotein beobachtet, wohingegen in der Dianthin-dPGS Zieltherapie eine Erhöhung der Alanintransaminase verzeichnet werden konnte. Zusammenfassend lässt sich sagen, dass die Kombination eines zielgerichteten Toxins mit SO1861 ein vielversprechender Ansatz für die Behandlung von Bauchspeicheldrüsenkrebs ist.

Würde ich auch schließen, dass dPGS-Targeting eines Transporters eine wertvolle Alternative zum klassischen Liganden-Rezeptor-Targeting ist.

7. References

1. Siegel, R.L., K.D. Miller, and A. Jemal, Cancer statistics, 2016. CA: A Cancer Journal for Clinicians, 2016. 66(1): p. 7-30.

2. Ferlay, J., I. Soerjomataram, R. Dikshit, S. Eser, C. Mathers, M. Rebelo, D.M. Parkin, D. Forman, and F. Bray, Cancer incidence and mortality worldwide: sources, methods and major patterns in GLOBOCAN 2012. Int J Cancer, 2015. 136(5): p. E359-86.

3. Bray, F., J.S. Ren, E. Masuyer, and J. Ferlay, Global estimates of cancer prevalence for 27 sites in the adult population in 2008. Int J Cancer, 2013. 132(5): p. 1133-45.

4. Bray, F., A. Jemal, N. Grey, J. Ferlay, and D. Forman, Global cancer transitions according to the Human Development Index (2008-2030): a population-based study. Lancet Oncol, 2012. 13(8): p. 790-801.

5. Feitelson, M.A., A. Arzumanyan, R.J. Kulathinal, S.W. Blain, R.F. Holcombe, J. Mahajna, M. Marino, M.L. Martinez-Chantar, R. Nawroth, I. Sanchez-Garcia, D. Sharma, N.K. Saxena, N. Singh, P.J. Vlachostergios, S. Guo, K. Honoki, H. Fujii, A.G. Georgakilas, A. Bilsland, A. Amedei, E. Niccolai, A. Amin, S.S. Ashraf, C.S. Boosani, G. Guha, M.R. Ciriolo, K. Aquilano, S. Chen, S.I. Mohammed, A.S. Azmi, D. Bhakta, D. Halicka, W.N. Keith, and S. Nowsheen, Sustained proliferation in cancer: Mechanisms and novel therapeutic targets. Seminars in Cancer Biology, 2015. 35, Supplement: p. S25-S54.

6. Miller, Jacques F.A.P. and M. Sadelain, The Journey from Discoveries in Fundamental Immunology to Cancer Immunotherapy. Cancer Cell, 2015. 27(4): p. 439-449.

7. Chen, Daniel S. and I. Mellman, Oncology Meets Immunology: The Cancer-Immunity Cycle. Immunity. 39(1): p. 1-10.

8. Chen, D.S. and I. Mellman, Oncology meets immunology: the cancer-immunity cycle. Immunity, 2013. 39(1): p. 1-10.

9. Motz, G.T. and G. Coukos, Deciphering and reversing tumor immune suppression. Immunity, 2013. 39(1): p. 61-73.

10. Lowenfels, A.B. and P. Maisonneuve, Epidemiology and risk factors for pancreatic cancer. Best Pract Res Clin Gastroenterol, 2006. 20(2): p. 197-209.

11. Hariharan, D., A. Saied, and H.M. Kocher, Analysis of mortality rates for pancreatic cancer across the world. HPB : The Official Journal of the International Hepato Pancreato Biliary Association, 2008. 10(1): p. 58-62.

12. Silverman, D.T., J.A. Dunn, R.N. Hoover, M. Schiffman, K.D. Lillemoe, J.B. Schoenberg, L.M. Brown, R.S. Greenberg, R.B. Hayes, G.M. Swanson, and et al., Cigarette smoking and pancreas cancer: a case-control study based on direct interviews. J Natl Cancer Inst, 1994. 86(20): p. 1510-6.

13. Calle , E.E., C. Rodriguez , K. Walker-Thurmond , and M.J. Thun Overweight, Obesity, and Mortality from Cancer in a Prospectively Studied Cohort of U.S. Adults. New England Journal of Medicine, 2003. 348(17): p. 1625-1638.

14. Ji, B.T., M.C. Hatch, W.H. Chow, J.K. McLaughlin, Q. Dai, G.R. Howe, Y.T. Gao, and J.F. Fraumeni, Jr., Anthropometric and reproductive factors and the risk of

pancreatic cancer: a case-control study in Shanghai, China. Int J Cancer, 1996. 66(4): p. 432-7.

15. Everhart, J. and D. Wright, Diabetes mellitus as a risk factor for pancreatic cancer. A meta-analysis. Jama, 1995. 273(20): p. 1605-9.

16. Conlon, K.C., D.S. Klimstra, and M.F. Brennan, Long-term survival after curative resection for pancreatic ductal adenocarcinoma. Clinicopathologic analysis of 5-year survivors. Ann Surg, 1996. 223(3): p. 273-9.

17. Wagner, M., C. Redaelli, M. Lietz, C.A. Seiler, H. Friess, and M.W. Buchler, Curative resection is the single most important factor determining outcome in patients with pancreatic adenocarcinoma. Br J Surg, 2004. 91(5): p. 586-94.

18. Carpelan-Holmstrom, M., S. Nordling, E. Pukkala, R. Sankila, J. Luttges, G. Kloppel, and C. Haglund, Does anyone survive pancreatic ductal adenocarcinoma? A nationwide study re-evaluating the data of the Finnish Cancer Registry. Gut, 2005. 54(3): p. 385-7.

19. Imamura, M., R. Doi, T. Imaizumi, A. Funakoshi, H. Wakasugi, M. Sunamura, Y. Ogata, S. Hishinuma, T. Asano, T. Aikou, R. Hosotani, and S. Maetani, A randomized multicenter trial comparing resection and radiochemotherapy for resectable locally invasive pancreatic cancer. Surgery, 2004. 136(5): p. 1003-11.

20. Kulemann, B., J. Hoeppner, U. Wittel, T. Glatz, T. Keck, U.F. Wellner, P. Bronsert, O. Sick, U.T. Hopt, F. Makowiec, and H. Riediger, Perioperative and long-term outcome after standard pancreaticoduodenectomy, additional portal vein and multivisceral resection for pancreatic head cancer. J Gastrointest Surg, 2015. 19(3): p. 438-44.

21. Moertel, C.G., S. Frytak, R.G. Hahn, M.J. O'Connell, R.J. Reitemeier, J. Rubin, A.J. Schutt, L.H. Weiland, D.S. Childs, M.A. Holbrook, P.T. Lavin, E. Livstone, H. Spiro, A. Knowlton, M. Kalser, J. Barkin, H. Lessner, R. Mann-Kaplan, K. Ramming, H.O. Douglas, Jr., P. Thomas, H. Nave, J. Bateman, J. Lokich, J. Brooks, J. Chaffey, J.M. Corson, N. Zamcheck, and J.W. Novak, Therapy of locally unresectable pancreatic carcinoma: a randomized comparison of high dose (6000 rads) radiation alone, moderate dose radiation (4000 rads + 5-fluorouracil), and high dose radiation + 5-fluorouracil: The Gastrointestinal Tumor Study Group. Cancer, 1981. 48(8): p. 1705-10.

22. Klaassen, D.J., J.M. MacIntyre, G.E. Catton, P.F. Engstrom, and C.G. Moertel, Treatment of locally unresectable cancer of the stomach and pancreas: a randomized comparison of 5-fluorouracil alone with radiation plus concurrent and maintenance 5-fluorouracil--an Eastern Cooperative Oncology Group study. J Clin Oncol, 1985. 3(3): p. 373-8.

23. Treatment of locally unresectable carcinoma of the pancreas: comparison of combined-modality therapy (chemotherapy plus radiotherapy) to chemotherapy alone. Gastrointestinal Tumor Study Group. J Natl Cancer Inst, 1988. 80(10): p. 751-5.

24. Chauffert, B., F. Mornex, F. Bonnetain, P. Rougier, C. Mariette, O. Bouche, J.F. Bosset, T. Aparicio, L. Mineur, A. Azzedine, P. Hammel, J. Butel, N. Stremsdoerfer, P. Maingon, and L. Bedenne, Phase III trial comparing intensive induction chemoradiotherapy (60 Gy, infusional 5-FU and intermittent cisplatin) followed by maintenance gemcitabine with gemcitabine alone for locally advanced unresectable pancreatic cancer. Definitive results of the 2000-01 FFCD/SFRO study. Ann Oncol, 2008. 19(9): p. 1592-9.

25. Shinoto, M., S. Yamada, K. Terashima, S. Yasuda, Y. Shioyama, H. Honda, T. Kamada, H. Tsujii, H. Saisho, T. Asano, T. Yamaguchi, H. Amano, T. Ishihara, M. Otsuka, M. Matsuda, O. Kainuma, A. Funakoshi, J. Furuse, T. Nakagori, T. Okusaka, H. Ishii, T. Nagakawa, S. Takahashi, S. Hishinuma, M. Nakamura, H. Saito, K. Ohara, S. Ohkawa, and M. Hiraoka, Carbon Ion Radiation Therapy With Concurrent Gemcitabine for Patients With Locally Advanced Pancreatic Cancer. International Journal of Radiation Oncology*Biology*Physics, 2016. 95(1): p. 498-504.

26. Shinoto, M., S. Yamada, S. Yasuda, H. Imada, Y. Shioyama, H. Honda, T. Kamada, H. Tsujii, and H. Saisho, Phase 1 trial of preoperative, short-course carbon-ion radiotherapy for patients with resectable pancreatic cancer. Cancer, 2013. 119(1): p. 45-51.

27. Shinoto, M., Y. Shioyama, A. Matsunobu, K. Okamoto, H. Suefuji, S. Toyama, H. Honda, and S. Kudo, Dosimetric analysis of upper gastrointestinal ulcer after carbon-ion radiotherapy for pancreatic cancer. Radiotherapy and Oncology, 2016. 120(1): p. 140-144.

28. Bramhall, S.R. and J.P. Neoptolemos, Adjuvant chemotherapy in pancreatic cancer. International Journal of Pancreatology, 1997. 21(1): p. 59-63.

29. Goldie, J.H., Scientific basis for adjuvant and primary (neoadjuvant) chemotherapy. Semin Oncol, 1987. 14(1): p. 1-7.

30. Bazrafshan, N. and M.M. Lotfi, A multi-objective multi-drug model for cancer chemotherapy treatment planning: A cost-effective approach to designing clinical trials. Computers & Chemical Engineering, 2016. 87: p. 226-233.

31. Neoptolemos, J.P., D.D. Stocken, H. Friess, C. Bassi, J.A. Dunn, H. Hickey, H. Beger, L. Fernandez-Cruz, C. Dervenis, F. Lacaine, M. Falconi, P. Pederzoli, A. Pap, D. Spooner, D.J. Kerr, and M.W. Buchler, A randomized trial of chemoradiotherapy and chemotherapy after resection of pancreatic cancer. N Engl J Med, 2004. 350(12): p. 1200-10.

32. Nitta, T., K. Fujii, J. Kataoka, T. Tominaga, H. Kawasaki, and T. Ishibashi, A case of long-term 24-month survival in pancreatic anaplastic carcinoma (giant cell type) after S1 postoperative adjuvant chemotherapy. International Journal of Surgery Case Reports, 2016. 23: p. 134-137.

33. Conroy, T., F. Desseigne, M. Ychou, O. Bouche, R. Guimbaud, Y. Becouarn, A. Adenis, J.L. Raoul, S. Gourgou-Bourgade, C. de la Fouchardiere, J. Bennouna, J.B. Bachet, F. Khemissa-Akouz, D. Pere-Verge, C. Delbaldo, E. Assenat, B. Chauffert, P. Michel, C. Montoto-Grillot, and M. Ducreux, FOLFIRINOX versus gemcitabine for metastatic pancreatic cancer. N Engl J Med, 2011. 364(19): p. 1817-25.

34. Heinemann, V., S. Boeck, A. Hinke, R. Labianca, and C. Louvet, Meta-analysis of randomized trials: evaluation of benefit from gemcitabine-based combination chemotherapy applied in advanced pancreatic cancer. BMC Cancer, 2008. 8: p. 82.

35. Sanchez-Castañón, M., T.-K. Er, L. Bujanda, and M. Herreros-Villanueva, Immunotherapy in colorectal cancer: What have we learned so far? Clinica Chimica Acta, 2016. 460: p. 78-87.

36. Kindler, H.L., G. Friberg, D.A. Singh, G. Locker, S. Nattam, M. Kozloff, D.A. Taber, T. Karrison, A. Dachman, W.M. Stadler, and E.E. Vokes, Phase II Trial of

Bevacizumab Plus Gemcitabine in Patients With Advanced Pancreatic Cancer. Journal of Clinical Oncology, 2005. 23(31): p. 8033-8040.

37. Xiong, H.Q., A. Rosenberg, A. LoBuglio, W. Schmidt, R.A. Wolff, J. Deutsch, M. Needle, and J.L. Abbruzzese, Cetuximab, a monoclonal antibody targeting the epidermal growth factor receptor, in combination with gemcitabine for advanced pancreatic cancer: a multicenter phase II Trial. J Clin Oncol, 2004. 22(13): p. 2610-6.

38. Slamon , D.J., B. Leyland-Jones , S. Shak , H. Fuchs , V. Paton , A. Bajamonde , T. Fleming , W. Eiermann , J. Wolter , M. Pegram , J. Baselga , and L. Norton Use of Chemotherapy plus a Monoclonal Antibody against HER2 for Metastatic Breast Cancer That Overexpresses HER2. New England Journal of Medicine, 2001. 344(11): p. 783-792.

39. Bennett, S.R.M., F.R. Carbone, F. Karamalis, R.A. Flavell, J.F.A.P. Miller, and W.R. Heath, Help for cytotoxic-T-cell responses is mediated by CD40 signalling. Nature, 1998. 393(6684): p. 478-480.

40. Goodsell, D.S., The Molecular Perspective: Targeted Toxins. The Oncologist, 2001. 6(1): p. 110-111.

41. Matsumura, Y. and H. Maeda, A new concept for macromolecular therapeutics in cancer chemotherapy: mechanism of tumoritropic accumulation of proteins and the antitumor agent smancs. Cancer Res, 1986. 46(12 Pt 1): p. 6387-92.

42. Maeda, H., The enhanced permeability and retention (EPR) effect in tumor vasculature: the key role of tumor-selective macromolecular drug targeting. Adv Enzyme Regul, 2001. 41: p. 189-207.

43. Torchilin, V.P., Targeted polymeric micelles for delivery of poorly soluble drugs. Cell Mol Life Sci, 2004. 61(19-20): p. 2549-59.

44. Lei, Y., Y. Hamada, J. Li, L. Cong, N. Wang, Y. Li, W. Zheng, and X. Jiang, Targeted tumor delivery and controlled release of neuronal drugs with ferritin nanoparticles to regulate pancreatic cancer progression. Journal of Controlled Release, 2016. 232: p. 131-142.

45. Khan, S., N. Chauhan, M.M. Yallapu, M.C. Ebeling, S. Balakrishna, R.T. Ellis, P.A. Thompson, P. Balabathula, S.W. Behrman, N. Zafar, M.M. Singh, F.T. Halaweish, M. Jaggi, and S.C. Chauhan, Nanoparticle formulation of ormeloxifene for pancreatic cancer. Biomaterials, 2015. 53: p. 731-743.

46. Maksimenko, A., J. Caron, J. Mougin, D. Desmaële, and P. Couvreur, Gemcitabine-based therapy for pancreatic cancer using the squalenoyl nucleoside monophosphate nanoassemblies. International Journal of Pharmaceutics, 2015. 482(1–2): p. 38-46.

47. Laheru, D., P. Shah, N.V. Rajeshkumar, F. McAllister, G. Taylor, H. Goldsweig, D.T. Le, R. Donehower, A. Jimeno, S. Linden, M. Zhao, D. Song, M.A. Rudek, and M. Hidalgo, Integrated preclinical and clinical development of S-trans, trans-farnesylthiosalicylic acid (FTS, Salirasib) in pancreatic cancer. Investigational New Drugs, 2012. 30(6): p. 2391-2399.

48. Melisi, D., S. Ishiyama, G.M. Sclabas, J.B. Fleming, Q. Xia, G. Tortora, J.L. Abbruzzese, and P.J. Chiao, LY2109761, a novel transforming growth factor β receptor type I and type II dual inhibitor, as a therapeutic approach to suppressing pancreatic cancer metastasis. Molecular cancer therapeutics, 2008. 7(4): p. 829-840.

49. Jones, S., X. Zhang, D.W. Parsons, J.C.-H. Lin, R.J. Leary, P. Angenendt, P. Mankoo, H. Carter, H. Kamiyama, A. Jimeno, S.-M. Hong, B. Fu, M.-T. Lin, E.S. Calhoun, M. Kamiyama, K. Walter, T. Nikolskaya, Y. Nikolsky, J. Hartigan, D.R. Smith, M. Hidalgo, S.D. Leach, A.P. Klein, E.M. Jaffee, M. Goggins, A. Maitra, C. Iacobuzio-Donahue, J.R. Eshleman, S.E. Kern, R.H. Hruban, R. Karchin, N. Papadopoulos, G. Parmigiani, B. Vogelstein, V.E. Velculescu, and K.W. Kinzler, Core Signaling Pathways in Human Pancreatic Cancers Revealed by Global Genomic Analyses. Science (New York, N.Y.), 2008. 321(5897): p. 1801-1806.

50. Olive, K.P., M.A. Jacobetz, C.J. Davidson, A. Gopinathan, D. McIntyre, D. Honess, B. Madhu, M.A. Goldgraben, M.E. Caldwell, D. Allard, K.K. Frese, G. DeNicola, C. Feig, C. Combs, S.P. Winter, H. Ireland, S. Reichelt, W.J. Howat, A. Chang, M. Dhara, L. Wang, F. Rückert, R. Grützmann, C. Pilarsky, K. Izeradjene, S.R. Hingorani, P. Huang, S.E. Davies, W. Plunkett, M. Egorin, R.H. Hruban, N. Whitebread, K. McGovern, J. Adams, C. Iacobuzio-Donahue, J. Griffiths, and D.A. Tuveson, Inhibition of Hedgehog Signaling Enhances Delivery of Chemotherapy in a Mouse Model of Pancreatic Cancer. Science (New York, N.Y.), 2009. 324(5933): p. 1457-1461.

51. Williams, T.M., D.B. Weiner, M.I. Greene, and H.C. Maguire, Jr., Expression of c-erbB-2 in human pancreatic adenocarcinomas. Pathobiology, 1991. 59(1): p. 46-52.

52. Moore, M.J., D. Goldstein, J. Hamm, A. Figer, J.R. Hecht, S. Gallinger, H.J. Au, P. Murawa, D. Walde, R.A. Wolff, D. Campos, R. Lim, K. Ding, G. Clark, T. Voskoglou-Nomikos, M. Ptasynski, and W. Parulekar, Erlotinib plus gemcitabine compared with gemcitabine alone in patients with advanced pancreatic cancer: a phase III trial of the National Cancer Institute of Canada Clinical Trials Group. J Clin Oncol, 2007. 25(15): p. 1960-6.

53. Ciechanover, A., A.L. Schwartz, A. Dautry-Varsat, and H.F. Lodish, Kinetics of internalization and recycling of transferrin and the transferrin receptor in a human hepatoma cell line. Effect of lysosomotropic agents. Journal of Biological Chemistry, 1983. 258(16): p. 9681-9.

54. Dautry-Varsat, A., Receptor-mediated endocytosis: the intracellular journey of transferrin and its receptor. Biochimie, 1986. 68(3): p. 375-81.

55. Sorkin, A. and L.K. Goh, Endocytosis and intracellular trafficking of ErbBs. Exp Cell Res, 2008. 314(17): p. 3093-106.

56. Rodman, J.S., R.W. Mercer, and P.D. Stahl, Endocytosis and transcytosis. Curr Opin Cell Biol, 1990. 2(4): p. 664-72.

57. Tycko, B. and F.R. Maxfield, Rapid acidification of endocytic vesicles containing alpha 2-macroglobulin. Cell, 1982. 28(3): p. 643-51.

58. Mellman, I., R. Fuchs, and A. Helenius, Acidification of the Endocytic and Exocytic Pathways. Annual Review of Biochemistry, 1986. 55(1): p. 663-700.

59. Yamashiro, D.J. and F.R. Maxfield, Regulation of endocytic processes by pH. Trends Pharmacol Sci, 1988. 9(6): p. 190-3.

60. Brinkmann, U., Recombinant antibody fragments and immunotoxin fusions for cancer therapy. In Vivo, 2000. 14(1): p. 21-7.

61. Onda, M., Q.C. Wang, H.F. Guo, N.K. Cheung, and I. Pastan, In vitro and in vivo cytotoxic activities of recombinant immunotoxin 8H9(Fv)-PE38 against breast cancer, osteosarcoma, and neuroblastoma. Cancer Res, 2004. 64(4): p. 1419-24.

62. Lemoine, N.R., C.M. Hughes, C.M. Barton, R. Poulsom, R.E. Jeffery, G. Kloppel, P.A. Hall, and W.J. Gullick, The epidermal growth factor receptor in human pancreatic cancer. J Pathol, 1992. 166(1): p. 7-12.

63. Korc, M., B. Chandrasekar, Y. Yamanaka, H. Friess, M. Buchier, and H.G. Beger, Overexpression of the epidermal growth factor receptor in human pancreatic cancer is associated with concomitant increases in the levels of epidermal growth factor and transforming growth factor alpha. J Clin Invest, 1992. 90(4): p. 1352-60.

64. Hassan, R., T. Bera, and I. Pastan, Mesothelin: a new target for immunotherapy. Clin Cancer Res, 2004. 10(12 Pt 1): p. 3937-42.

65. Chandler, L.A., B.A. Sosnowski, J.R. McDonald, J.E. Price, S.L. Aukerman, A. Baird, G.F. Pierce, and L.L. Houston, Targeting tumor cells via EGF receptors: selective toxicity of an HBEGF-toxin fusion protein. Int J Cancer, 1998. 78(1): p. 106-11.

66. de Virgilio, M., A. Lombardi, R. Caliandro, and M.S. Fabbrini, Ribosome-inactivating proteins: from plant defense to tumor attack. Toxins (Basel), 2010. 2(11): p. 2699-737.

67. Vago, R., R. Ippoliti, and M.S. Fabbrini, Current Status and Biomedical Applications of Ribosome-Inactivating Proteins, in Antitumor Potential and other Emerging Medicinal Properties of Natural Compounds, E.F. Fang and T.B. Ng, Editors. 2013, Springer Netherlands: Dordrecht. p. 145-179.

68. Olsen, E., M. Duvic, A. Frankel, Y. Kim, A. Martin, E. Vonderheid, B. Jegasothy, G. Wood, M. Gordon, P. Heald, A. Oseroff, L. Pinter-Brown, G. Bowen, T. Kuzel, D. Fivenson, F. Foss, M. Glode, A. Molina, E. Knobler, S. Stewart, K. Cooper, S. Stevens, F. Craig, J. Reuben, P. Bacha, and J. Nichols, Pivotal phase III trial of two dose levels of denileukin diftitox for the treatment of cutaneous T-cell lymphoma. J Clin Oncol, 2001. 19(2): p. 376-88.

69. Lindstrom, A.L., S.L. Erlandsen, J.H. Kersey, and C.A. Pennell, An in vitro model for toxin-mediated vascular leak syndrome: ricin toxin A chain increases the permeability of human endothelial cell monolayers. Blood, 1997. 90(6): p. 2323-34.

70. Soler-Rodríguez, A.-M.a., M.-A. Ghetie, N. Oppenheimer-Marks, J.W. Uhr, and E.S. Vitetta, Ricin A-Chain and Ricin A-Chain Immunotoxins Rapidly Damage Human Endothelial Cells: Implications for Vascular Leak Syndrome. Experimental Cell Research, 1993. 206(2): p. 227-234.

71. Frankel, A.E., D.R. Fleming, P.D. Hall, B.L. Powell, J.H. Black, C. Leftwich, and R. Gartenhaus, A Phase II Study of DT Fusion Protein Denileukin Diftitox in Patients with Fludarabine-refractory Chronic Lymphocytic Leukemia. Clinical Cancer Research, 2003. 9(10): p. 3555-3561.

72. Heisler, I., M. Sutherland, C. Bachran, P. Hebestreit, A. Schnitger, M.F. Melzig, and H. Fuchs, Combined application of saponin and chimeric toxins drastically enhances the targeted cytotoxicity on tumor cells. J Control Release, 2005. 106(1-2): p. 123-37.

73. Bachran, C., M. Sutherland, I. Heisler, P. Hebestreit, M.F. Melzig, and H. Fuchs, The saponin-mediated enhanced uptake of targeted saporin-based drugs is strongly dependent on the saponin structure. Exp Biol Med (Maywood), 2006. 231(4): p. 412-20.

74. Fuchs, H., D. Bachran, H. Panjideh, N. Schellmann, A. Weng, M.F. Melzig, M. Sutherland, and C. Bachran, Saponins as tool for improved targeted tumor therapies. Curr Drug Targets, 2009. 10(2): p. 140-51.

75. Bachran, C., H. Durkop, M. Sutherland, D. Bachran, C. Muller, A. Weng, M.F. Melzig, and H. Fuchs, Inhibition of tumor growth by targeted toxins in mice is dramatically improved by saponinum album in a synergistic way. J Immunother, 2009. 32(7): p. 713-25.

76. Bachran, C., S. Bachran, M. Sutherland, D. Bachran, and H. Fuchs, Saponins in tumor therapy. Mini Rev Med Chem, 2008. 8(6): p. 575-84.

77. Yamamoto, T., Y. Seino, H. Fukumoto, G. Koh, H. Yano, N. Inagaki, Y. Yamada, K. Inoue, T. Manabe, and H. Imura, Over-expression of facilitative glucose transporter genes in human cancer. Biochemical and Biophysical Research Communications, 1990. 170(1): p. 223-230.

78. Kounnis, V., E. Ioachim, M. Svoboda, A. Tzakos, I. Sainis, T. Thalhammer, G. Steiner, and E. Briasoulis, Expression of organic anion-transporting polypeptides 1B3, 1B1, and 1A2 in human pancreatic cancer reveals a new class of potential therapeutic targets. Onco Targets Ther, 2011. 4: p. 27-32.

79. Ahn, S.-Y. and S.K. Nigam, Toward a Systems Level Understanding of Organic Anion and Other Multispecific Drug Transporters: A Remote Sensing and Signaling Hypothesis. Molecular Pharmacology, 2009. 76(3): p. 481-490.

80. Koepsell, H., The SLC22 family with transporters of organic cations, anions and zwitterions. Mol Aspects Med, 2013. 34(2-3): p. 413-35.

81. Klaassen, C.D. and L.M. Aleksunes, Xenobiotic, Bile Acid, and Cholesterol Transporters: Function and Regulation. Pharmacological Reviews, 2010. 62(1): p. 1-96.

82. Wu, W., A.V. Dnyanmote, and S.K. Nigam, Remote Communication through Solute Carriers and ATP Binding Cassette Drug Transporter Pathways: An Update on the Remote Sensing and Signaling Hypothesis. Molecular Pharmacology, 2011. 79(5): p. 795-805.

83. Seeger, M.A. and H.W. van Veen, Molecular basis of multidrug transport by ABC transporters. Biochim Biophys Acta, 2009. 1794(5): p. 725-37.

84. Vlaming, M.L., A. van Esch, Z. Pala, E. Wagenaar, K. van de Wetering, O. van Tellingen, and A.H. Schinkel, Abcc2 (Mrp2), Abcc3 (Mrp3), and Abcg2 (Bcrp1) are the main determinants for rapid elimination of methotrexate and its toxic metabolite 7-hydroxymethotrexate in vivo. Mol Cancer Ther, 2009. 8(12): p. 3350-9.

85. Vlaming, M.L., S.F. Teunissen, E. van de Steeg, A. van Esch, E. Wagenaar, L. Brunsveld, T.F. de Greef, H. Rosing, J.H. Schellens, J.H. Beijnen, and A.H. Schinkel, Bcrp1;Mdr1a/b;Mrp2 combination knockout mice: altered disposition of the dietary carcinogen PhIP (2-amino-1-methyl-6-phenylimidazo[4,5-b]pyridine) and its genotoxic metabolites. Mol Pharmacol, 2014. 85(3): p. 520-30.

86. Eraly, S.A., V. Vallon, D.A. Vaughn, J.A. Gangoiti, K. Richter, M. Nagle, J.C. Monte, T. Rieg, D.M. Truong, J.M. Long, B.A. Barshop, G. Kaler, and S.K. Nigam, Decreased renal organic anion secretion and plasma accumulation of endogenous organic anions in OAT1 knock-out mice. J Biol Chem, 2006. 281(8): p. 5072-83.

87. Kounnis, V., E. Ioachim, M. Svoboda, A. Tzakos, I. Sainis, T. Thalhammer, G. Steiner, and E. Briasoulis, Expression of organic anion-transporting polypeptides 1B3, 1B1, and 1A2 in human pancreatic cancer reveals a new class of potential therapeutic targets. OncoTargets and therapy, 2011. 4: p. 27-32.

88. Sainis, I., D. Fokas, K. Vareli, A. Tzakos, V. Kounnis, and E. Briasoulis, Cyanobacterial Cyclopeptides as Lead Compounds to Novel Targeted Cancer Drugs. Marine Drugs, 2010. 8(3): p. 629.

89. Gui, C., Y. Miao, L. Thompson, B. Wahlgren, M. Mock, B. Stieger, and B. Hagenbuch, Effect of pregnane X receptor ligands on transport mediated by human OATP1B1 and OATP1B3. Eur J Pharmacol, 2008. 584(1): p. 57-65.

90. Hirano, M., K. Maeda, Y. Shitara, and Y. Sugiyama, Drug-drug interaction between pitavastatin and various drugs via OATP1B1. Drug Metab Dispos, 2006. 34(7): p. 1229-36.

91. Khurana, V., M. Minocha, D. Pal, and A.K. Mitra, Inhibition of OATP-1B1 and OATP-1B3 by tyrosine kinase inhibitors. Drug Metabol Drug Interact, 2014. 29(4): p. 249-59.

92. Peumans, W.J., Q. Hao, and E.J. Van Damme, Ribosome-inactivating proteins from plants: more than RNA N-glycosidases? Faseb j, 2001. 15(9): p. 1493-506.

93. Stirpe, F., Ribosome-inactivating proteins. Toxicon, 2004. 44(4): p. 371-383.

94. Dinota, A., L. Barbieri, M. Gobbi, P.L. Tazzari, S. Rizzi, A. Bontadini, A. Bolognesi, S. Tura, and F. Stirpe, An immunotoxin containing momordin suitable for bone marrow purging in multiple myeloma patients. British Journal of Cancer, 1989. 60(3): p. 315-319.

95. Bonardi, M.A., A. Bell, R.R. French, G. Gromo, T. Hamblin, D. Modena, A.L. Tutt, and M.J. Glennie, Initial experience in treating human lymphoma with a combination of bispecific antibody and saporin. International journal of cancer. Supplement = Journal international du cancer. Supplement, 1992. 7: p. 73-77.

96. Weng, A., C. Bachran, H. Fuchs, E. Krause, H. Stephanowitz, and M.F. Melzig, Enhancement of saporin cytotoxicity by Gypsophila saponins—More than stimulation of endocytosis. Chemico-Biological Interactions, 2009. 181(3): p. 424-429.

97. Falasca, A., A. Gasperi-Campani, A. Abbondanza, L. Barbieri, and F. Stirpe, Properties of the ribosome-inactivating proteins gelonin, Momordica charantia inhibitor, and dianthins. Biochem J, 1982. 207(3): p. 505-9.

98. Stirpe, F., D.G. Williams, L.J. Onyon, R.F. Legg, and W.A. Stevens, Dianthins, ribosome-damaging proteins with anti-viral properties from Dianthus caryophyllus L. (carnation). Biochem J, 1981. 195(2): p. 399-405.

99. Vitale, A. and J. Denecke, The Endoplasmic Reticulum—Gateway of the Secretory Pathway. The Plant Cell, 1999. 11(4): p. 615-628.

100. Fermani, S., G. Falini, A. Ripamonti, L. Polito, F. Stirpe, and A. Bolognesi, The 1.4 Å structure of dianthin 30 indicates a role of surface potential at the active site of type 1 ribosome inactivating proteins. Journal of Structural Biology, 2005. 149(2): p. 204-212.

101. Legname, G., G. Gromo, J.M. Lord, N. Monzini, and D. Modena, Expression and Activity of Pre-dianthin 30 and Dianthin 30. Biochemical and Biophysical Research Communications, 1993. 192(3): p. 1230-1237.

102. Stroochi, P., L. Barbieri, and F. Stirpe, Immunological properties of ribosome-inactivating proteins and a saporin immunotoxin. Journal of Immunological Methods, 1992. 155(1): p. 57-63.

103. Silverstein, A.M., The collected papers of Paul Ehrlich : why was volume 4 never published? Bull Hist Med, 2002. 76(2): p. 335-9.

104. Dernedde, J., A. Rausch, M. Weinhart, S. Enders, R. Tauber, K. Licha, M. Schirner, U. Zugel, A. von Bonin, and R. Haag, Dendritic polyglycerol sulfates as multivalent inhibitors of inflammation. Proc Natl Acad Sci U S A, 2010. 107(46): p. 19679-84.

105. Frey, H. and R. Haag, Dendritic polyglycerol: a new versatile biocompatible material. Reviews in Molecular Biotechnology, 2002. 90(3–4): p. 257-267.

106. Kainthan, R.K., J. Janzen, E. Levin, D.V. Devine, and D.E. Brooks, Biocompatibility testing of branched and linear polyglycidol. Biomacromolecules, 2006. 7(3): p. 703-9.

107. Kainthan, R.K., S.R. Hester, E. Levin, D.V. Devine, and D.E. Brooks, In vitro biological evaluation of high molecular weight hyperbranched polyglycerols. Biomaterials, 2007. 28(31): p. 4581-90.

108. Kainthan, R.K. and D.E. Brooks, In vivo biological evaluation of high molecular weight hyperbranched polyglycerols. Biomaterials, 2007. 28(32): p. 4779-87.

109. Kainthan, R.K., C. Mugabe, H.M. Burt, and D.E. Brooks, Unimolecular Micelles Based On Hydrophobically Derivatized Hyperbranched Polyglycerols: Ligand Binding Properties. Biomacromolecules, 2008. 9(3): p. 886-895.

110. Khandare, J., A. Mohr, M. Calderón, P. Welker, K. Licha, and R. Haag, Structure-biocompatibility relationship of dendritic polyglycerol derivatives. Biomaterials, 2010. 31(15): p. 4268-4277.

111. Yamanaka, Y., H. Friess, M.S. Kobrin, M. Buchler, H.G. Beger, and M. Korc, Coexpression of epidermal growth factor receptor and ligands in human pancreatic cancer is associated with enhanced tumor aggressiveness. Anticancer Res, 1993. 13(3): p. 565-9.

112. Fuchs, H. and C. Bachran, Targeted tumor therapies at a glance. Curr Drug Targets, 2009. 10(2): p. 89-93.

113. Weng, A., M. Thakur, F. Beceren-Braun, D. Bachran, C. Bachran, S.B. Riese, K. Jenett-Siems, R. Gilabert-Oriol, M.F. Melzig, and H. Fuchs, The toxin component of targeted anti-tumor toxins determines their efficacy increase by saponins. Molecular Oncology, 2012. 6(3): p. 323-332.

114. Gilabert-Oriol, R., M. Thakur, C. Weise, J. Dernedde, B. von Mallinckrodt, H. Fuchs, and A. Weng, Small structural differences of targeted anti-tumor toxins result in strong variation of protein expression. Protein Expression and Purification, 2013. 91(1): p. 54-60.

115. Oh, S., B.J. Stish, D. Sachdev, H. Chen, A.Z. Dudek, and D.A. Vallera, A novel "reduced immunogenicity" bispecific targeted toxin simultaneously recognizing

human EGF and IL-4 receptors in a mouse model of metastatic breast carcinoma. Clinical cancer research : an official journal of the American Association for Cancer Research, 2009. 15(19): p. 6137-6147.

116. Weng, A., C. Gorick, and M.F. Melzig, Enhancement of toxicity of saporin-based toxins by Gypsophila saponins--kinetic of the saponin. Exp Biol Med (Maywood), 2009. 234(8): p. 961-6.

117. Thakur, M., A. Weng, D. Bachran, S.B. Riese, S. Bottger, M.F. Melzig, and H. Fuchs, Electrophoretic isolation of saponin fractions from Saponinum album and their evaluation in synergistically enhancing the receptor-specific cytotoxicity of targeted toxins. Electrophoresis, 2011. 32(21): p. 3085-9.

118. Thakur, M., K. Mergel, A. Weng, B. von Mallinckrodt, R. Gilabert-Oriol, H. Durkop, M.F. Melzig, and H. Fuchs, Targeted tumor therapy by epidermal growth factor appended toxin and purified saponin: an evaluation of toxicity and therapeutic potential in syngeneic tumor bearing mice. Mol Oncol, 2013. 7(3): p. 475-83.

119. Gilabert-Oriol, R., A. Weng, A. Trautner, C. Weise, D. Schmid, C. Bhargava, N. Niesler, P.J. Wookey, H. Fuchs, and M. Thakur, Combinatorial approach to increase efficacy of Cetuximab, Panitumumab and Trastuzumab by dianthin conjugation and co-application of SO1861. Biochem Pharmacol, 2015. 97(3): p. 247-55.

120. Weng, A., M.D.I. Manunta, M. Thakur, R. Gilabert-Oriol, A.D. Tagalakis, A. Eddaoudi, M.M. Munye, C.A. Vink, B. Wiesner, J. Eichhorst, M.F. Melzig, and S.L. Hart, Improved intracellular delivery of peptide- and lipid-nanoplexes by natural glycosides. Journal of Controlled Release, 2015. 206: p. 75-90.

121. Bruno, B.J., G.D. Miller, and C.S. Lim, Basics and recent advances in peptide and protein drug delivery. Therapeutic delivery, 2013. 4(11): p. 1443-1467.

122. Fosgerau, K. and T. Hoffmann, Peptide therapeutics: current status and future directions. Drug Discovery Today, 2015. 20(1): p. 122-128.

123. Leader, B., Q.J. Baca, and D.E. Golan, Protein therapeutics: a summary and pharmacological classification. Nat Rev Drug Discov, 2008. 7(1): p. 21-39.

124. Beck, A., T. Wurch, C. Bailly, and N. Corvaia, Strategies and challenges for the next generation of therapeutic antibodies. Nat Rev Immunol, 2010. 10(5): p. 345-52.

125. Aungst, B.J., Absorption Enhancers: Applications and Advances. The AAPS Journal, 2012. 14(1): p. 10-18.

126. Schmidt, M.M. and K.D. Wittrup, A modeling analysis of the effects of molecular size and binding affinity on tumor targeting. Mol Cancer Ther, 2009. 8(10): p. 2861-71.

127. Peters, C. and S. Brown, Antibody–drug conjugates as novel anti-cancer chemotherapeutics. Bioscience Reports, 2015. 35(4): p. e00225.

128. Khandare, J., A. Mohr, M. Calderon, P. Welker, K. Licha, and R. Haag, Structure-biocompatibility relationship of dendritic polyglycerol derivatives. Biomaterials, 2010. 31(15): p. 4268-77.

129. Tomalia, D.A., Dendrimer research. Science, 1991. 252(5010): p. 1231.

130. Sunder, A., H. Frey, and R. Mülhaupt, Hyperbranched polyglycerols by ring-opening multibranching polymerization. Macromolecular Symposia, 2000. 153(1): p. 187-196.

131. Kainthan, R.K., E.B. Muliawan, S.G. Hatzikiriakos, and D.E. Brooks, Synthesis, Characterization, and Viscoelastic Properties of High Molecular Weight Hyperbranched Polyglycerols. Macromolecules, 2006. 39(22): p. 7708-7717.

132. Moore, E., A.T. Zill, C.A. Anderson, A.R. Jochem, S.C. Zimmerman, C.S. Bonder, T. Kraus, H. Thissen, and N.H. Voelcker, Synthesis and Conjugation of Alkyne-Functional Hyperbranched Polyglycerols. Macromolecular Chemistry and Physics, 2016. 217(20): p. 2252-2261.

133. Baker, J.R., Dendrimer-based nanoparticles for cancer therapy. ASH Education Program Book, 2009. 2009(1): p. 708-719.

134. Hussain, A.F., H.R. Krüger, F. Kampmeier, T. Weissbach, K. Licha, F. Kratz, R. Haag, M. Calderón, and S. Barth, Targeted Delivery of Dendritic Polyglycerol–Doxorubicin Conjugates by scFv-SNAP Fusion Protein Suppresses EGFR+ Cancer Cell Growth. Biomacromolecules, 2013. 14(8): p. 2510-2520.

135. Licha, K., P. Welker, M. Weinhart, N. Wegner, S. Kern, S. Reichert, I. Gemeinhardt, C. Weissbach, B. Ebert, R. Haag, and M. Schirner, Fluorescence Imaging with Multifunctional Polyglycerol Sulfates: Novel Polymeric near-IR Probes Targeting Inflammation. Bioconjugate Chemistry, 2011. 22(12): p. 2453-2460.

136. Biffi, S., S. Dal Monego, C. Dullin, C. Garrovo, B. Bosnjak, K. Licha, P. Welker, M.M. Epstein, and F. Alves, Dendritic polyglycerolsulfate near infrared fluorescent (NIRF) dye conjugate for non-invasively monitoring of inflammation in an allergic asthma mouse model. PLoS One, 2013. 8(2): p. e57150.

137. Sousa-Herves, A., P. Wurfel, N. Wegner, J. Khandare, K. Licha, R. Haag, P. Welker, and M. Calderon, Dendritic polyglycerol sulfate as a novel platform for paclitaxel delivery: pitfalls of ester linkage. Nanoscale, 2015. 7(9): p. 3923-3932.

138. Goke, B. and V. Keim, HPLC and FPLC. Recent progress in the use of automated chromatography systems for resolution of pancreatic secretory proteins. Int J Pancreatol, 1992. 11(2): p. 109-16.

139. Madadlou, A., S. O'Sullivan, and D. Sheehan, Fast protein liquid chromatography. Methods Mol Biol, 2011. 681: p. 439-47.

140. Fritz, J.S., Early milestones in the development of ion-exchange chromatography: a personal account. J Chromatogr A, 2004. 1039(1-2): p. 3-12.

141. Lucy, C.A., Evolution of ion-exchange: from Moses to the Manhattan Project to modern times. J Chromatogr A, 2003. 1000(1-2): p. 711-24.

142. Levison, P.R., Large-scale ion-exchange column chromatography of proteins. Comparison of different formats. J Chromatogr B Analyt Technol Biomed Life Sci, 2003. 790(1-2): p. 17-33.

143. Cummins, P.M. and B. O'Connor, Bovine brain pyroglutamyl aminopeptidase (type-1): purification and characterisation of a neuropeptide-inactivating peptidase. Int J Biochem Cell Biol, 1996. 28(8): p. 883-93.

144. Mant, C.T. and R.S. Hodges, Mixed-mode hydrophilic interaction/cation-exchange chromatography: separation of complex mixtures of peptides of varying charge and hydrophobicity. J Sep Sci, 2008. 31(9): p. 1573-84.

145. Kent, U.M., Purification of antibodies using ion-exchange chromatography. Methods Mol Biol, 1999. 115: p. 19-22.

146. Fekkes, D., A. Voskuilen-Kooyman, R. Jankie, and J. Huijmans, Precise analysis of primary amino acids in urine by an automated high-performance liquid chromatography method: comparison with ion-exchange chromatography. J Chromatogr B Biomed Sci Appl, 2000. 744(1): p. 183-8.

147. Yang, Y., H.R. Hebron, and J. Hang, High performance DNA purification using a novel ion exchange matrix. J Biomol Tech, 2008. 19(3): p. 205-10.

148. Cummins, P.M., O. Dowling, and B.F. O'Connor, Ion-exchange chromatography: basic principles and application to the partial purification of soluble mammalian prolyl oligopeptidase. Methods Mol Biol, 2011. 681: p. 215-28.

149. Allen, T.M., Ligand-targeted therapeutics in anticancer therapy. Nat Rev Cancer, 2002. 2(10): p. 750-63.

150. Philip, P.A. and M.P. Lutz, Targeting Epidermal Growth Factor Receptor–Related Signaling Pathways in Pancreatic Cancer. Pancreas, 2015. 44(7): p. 1046-1052.

151. Hirata, Y., M. Uchihashi, M. Nakajima, T. Fujita, and S. Matsukura, Immunoreactive human epidermal growth factor in human pancreatic juice. J Clin Endocrinol Metab, 1982. 54(6): p. 1242-5.

152. Pesonen, K., L. Viinikka, A.L. Mattila, A. Koskimies, and J. Perheentupa, Epidermal growth factor (EGF) in human body fluids. Pediatr Res, 1986. 20(11): p. 1184-1184.

153. Carter, P., Improving the efficacy of antibody-based cancer therapies. Nat Rev Cancer, 2001. 1(2): p. 118-129.

154. Maynard, J. and G. Georgiou, Antibody engineering. Annu Rev Biomed Eng, 2000. 2: p. 339-76.

155. Vose, J.M., B.K. Link, M.L. Grossbard, M. Czuczman, A. Grillo-Lopez, P. Gilman, A. Lowe, L.A. Kunkel, and R.I. Fisher, Phase II study of rituximab in combination with chop chemotherapy in patients with previously untreated, aggressive non-Hodgkin's lymphoma. J Clin Oncol, 2001. 19(2): p. 389-97.

156. Baselga, J., Herceptin alone or in combination with chemotherapy in the treatment of HER2-positive metastatic breast cancer: pivotal trials. Oncology, 2001. 61 Suppl 2: p. 14-21.

157. Dillman, R.O., Monoclonal antibodies in the treatment of malignancy: basic concepts and recent developments. Cancer Invest, 2001. 19(8): p. 833-41.

158. Juweid, M., R. Neumann, C. Paik, M.J. Perez-Bacete, J. Sato, W. van Osdol, and J.N. Weinstein, Micropharmacology of monoclonal antibodies in solid tumors: direct experimental evidence for a binding site barrier. Cancer Res, 1992. 52(19): p. 5144-53.

159. Banerjee, R.K., W.W. van Osdol, P.M. Bungay, C. Sung, and R.L. Dedrick, Finite element model of antibody penetration in a prevascular tumor nodule embedded in normal tissue. J Control Release, 2001. 74(1-3): p. 193-202.

160. Adams, G.P., R. Schier, A.M. McCall, H.H. Simmons, E.M. Horak, R.K. Alpaugh, J.D. Marks, and L.M. Weiner, High affinity restricts the localization and tumor penetration of single-chain fv antibody molecules. Cancer Res, 2001. 61(12): p. 4750-5.

161. Thakkar, N., K. Kim, E.R. Jang, S. Han, K. Kim, D. Kim, N. Merchant, A.C. Lockhart, and W. Lee, A Cancer-Specific Variant of the SLCO1B3 Gene Encodes a Novel Human Organic Anion Transporting Polypeptide 1B3 (OATP1B3) Localized Mainly in the Cytoplasm of Colon and Pancreatic Cancer Cells. Molecular Pharmaceutics, 2013. 10(1): p. 406-416.

162. Obaidat, A., M. Roth, and B. Hagenbuch, The Expression and Function of Organic Anion Transporting Polypeptides in Normal Tissues and in Cancer. Annual Review of Pharmacology and Toxicology, 2012. 52: p. 135-151.

163. Letschert, K., D. Keppler, and J. Konig, Mutations in the SLCO1B3 gene affecting the substrate specificity of the hepatocellular uptake transporter OATP1B3 (OATP8). Pharmacogenetics, 2004. 14(7): p. 441-52.

164. Bachran, D., S. Schneider, C. Bachran, R. Urban, A. Weng, M.F. Melzig, C. Hoffmann, A.M. Kaufmann, and H. Fuchs, Epidermal growth factor receptor expression affects the efficacy of the combined application of saponin and a targeted toxin on human cervical carcinoma cells. Int J Cancer, 2010. 127(6): p. 1453-61.

165. Weng, A., M. Thakur, F. Beceren-Braun, D. Bachran, C. Bachran, S.B. Riese, K. Jenett-Siems, R. Gilabert-Oriol, M.F. Melzig, and H. Fuchs, The toxin component of targeted anti-tumor toxins determines their efficacy increase by saponins. Mol Oncol, 2012. 6(3): p. 323-32.

166. Malik, N., R. Wiwattanapatapee, R. Klopsch, K. Lorenz, H. Frey, J.W. Weener, E.W. Meijer, W. Paulus, and R. Duncan, Dendrimers:: Relationship between structure and biocompatibility in vitro, and preliminary studies on the biodistribution of 125I-labelled polyamidoamine dendrimers in vivo. Journal of Controlled Release, 2000. 65(1–2): p. 133-148.

167. Reichert, S., P. Welker, M. Calderón, J. Khandare, D. Mangoldt, K. Licha, R.K. Kainthan, D.E. Brooks, and R. Haag, Size-Dependant Cellular Uptake of Dendritic Polyglycerol. Small, 2011. 7(6): p. 820-829.

168. Ito, T., H. Qiu, J.A. Collins, A.B. Brill, D.K. Johnson, and T.W. Griffin, Preclinical Assessments of ⁹⁰Y-labeled C110 Anti-Carcinoembryonic Antigen Immunotoxin: A Therapeutic Immunoconjugate for Human Colon Cancer. Cancer Research, 1991. 51(1): p. 255.

169. Bachran, C., A. Weng, D. Bachran, S.B. Riese, N. Schellmann, M.F. Melzig, and H. Fuchs, The distribution of saponins in vivo affects their synergy with chimeric toxins against tumours expressing human epidermal growth factor receptors in mice. British Journal of Pharmacology, 2010. 159(2): p. 345-352.

170. Bachran, C., H. Dürkop, M. Sutherland, D. Bachran, C. Müller, A. Weng, M.F. Melzig, and H. Fuchs, Inhibition of Tumor Growth by Targeted Toxins in Mice is Dramatically Improved by Saponinum Album in a Synergistic Way. Journal of Immunotherapy, 2009. 32(7): p. 713-725.

171. Gilabert-Oriol, R., M. Thakur, C. Weise, J. Dernedde, B. von Mallinckrodt, H. Fuchs, and A. Weng, Small structural differences of targeted anti-tumor toxins result in strong variation of protein expression. Protein Expr Purif, 2013. 91(1): p. 54-60.

172. von Mallinckrodt, B., M. Thakur, A. Weng, R. Gilabert-Oriol, H. Durkop, W. Brenner, M. Lukas, N. Beindorff, M.F. Melzig, and H. Fuchs, Dianthin-EGF is an effective tumor targeted toxin in combination with saponins in a xenograft model for colon carcinoma. Future Oncol, 2014. 10(14): p. 2161-75.

173. Dillon, R.L., S. Chooniedass, A. Premsukh, G.P. Adams, J. Entwistle, G.C. MacDonald, and J. Cizeau, Trastuzumab-deBouganin Conjugate Overcomes Multiple Mechanisms of T-DM1 Drug Resistance. J Immunother, 2016. 39(3): p. 117-26.

174. Zwitter, M., V. Kovac, U. Smrdel, I. Kocijancic, B. Segedin, and M. Vrankar, Phase I–II trial of low-dose gemcitabine in prolonged infusion and cisplatin for advanced non-small cell lung cancer. Anti-Cancer Drugs, 2005. 16(10): p. 1129-1134.

175. Zwitter, M., T. Cufer, and W. Wein, Gemcitabine and vincristine: an effective outpatient regimen with low myelotoxicity for stage IV non-small cell lung cancer. Neoplasma, 2001. 48(3): p. 200-2.

176. Świeboda-Sadlej, A., L. Kraj, J. Krawczyk, E. Nita, and J. Dwilewicz-Trojaczek, Thrombocytosis in patients with pancreatic cancer treated with gemcitabine – does it have clinical significance? Description of 6 cases. Contemporary Oncology, 2012. 16(4): p. 353-355.

177. Padda, M.S., M. Sanchez, A.J. Akhtar, and J.L. Boyer, Drug induced cholestasis. Hepatology (Baltimore, Md.), 2011. 53(4): p. 1377-1387.

178. Konig, J., Y. Cui, A.T. Nies, and D. Keppler, Localization and genomic organization of a new hepatocellular organic anion transporting polypeptide. J Biol Chem, 2000. 275(30): p. 23161-8.

179. van de Steeg, E., A. van Esch, E. Wagenaar, K.E. Kenworthy, and A.H. Schinkel, Influence of Human OATP1B1, OATP1B3, and OATP1A2 on the Pharmacokinetics of Methotrexate and Paclitaxel in Humanized Transgenic Mice. Clinical Cancer Research, 2013. 19(4): p. 821.

180. Durmus, S., G. Lozano-Mena, A. van Esch, E. Wagenaar, O. van Tellingen, and A.H. Schinkel, Preclinical Mouse Models To Study Human OATP1B1- and OATP1B3-Mediated Drug–Drug Interactions in Vivo. Molecular Pharmaceutics, 2015. 12(12): p. 4259-4269.

181. Hersh, E.M., V.G. Wong, E.S. Henderson, and E.J. Freireich, Hepatotoxic effects of methotrexate. Cancer, 1966. 19(4): p. 600-606.

182. Schneider, T., P. Welker, K. Licha, R. Haag, and G. Schulze-Tanzil, Influence of dendritic polyglycerol sulfates on knee osteoarthritis: an experimental study in the rat osteoarthritis model. BMC Musculoskeletal Disorders, 2015. 16(1): p. 387.

183. Simon, N. and D. FitzGerald, Immunotoxin Therapies for the Treatment of Epidermal Growth Factor Receptor-Dependent Cancers. Toxins, 2016. 8(5): p. 137.

184. Bruell, D., M. Stocker, M. Huhn, N. Redding, M. Kupper, P. Schumacher, A. Paetz, C.J. Bruns, H.J. Haisma, R. Fischer, R. Finnern, and S. Barth, The recombinant anti-EGF receptor immunotoxin 425(scFv)-ETA' suppresses growth of a highly metastatic pancreatic carcinoma cell line. Int J Oncol, 2003. 23(4): p. 1179-86.

185. Bruell, Bruns, Yezhelyev, Huhn, Müller, Ischenko, Fischer, Finnern, Jauch, and Barth, Recombinant anti-EGFR immunotoxin 425(scFv)-ETA' demonstrates anti-tumor

activity against disseminated human pancreatic cancer in nude mice. International Journal of Molecular Medicine, 2005. 15(2): p. 305-313.

186. Niesen, J., C. Stein, H. Brehm, G. Hehmann-Titt, R. Fendel, G. Melmer, R. Fischer, and S. Barth, Novel EGFR-specific immunotoxins based on panitumumab and cetuximab show in vitro and ex vivo activity against different tumor entities. J Cancer Res Clin Oncol, 2015. 141(12): p. 2079-95.

187. Hwang, J., D.J. Fitzgerald, S. Adhya, and I. Pastan, Functional domains of Pseudomonas exotoxin identified by deletion analysis of the gene expressed in E. coli. Cell, 1987. 48(1): p. 129-36.

188. Allured, V.S., R.J. Collier, S.F. Carroll, and D.B. McKay, Structure of exotoxin A of Pseudomonas aeruginosa at 3.0-Angstrom resolution. Proc Natl Acad Sci U S A, 1986. 83(5): p. 1320-4.

189. Fuchs, H., A. Weng, and R. Gilabert-Oriol, Augmenting the Efficacy of Immunotoxins and Other Targeted Protein Toxins by Endosomal Escape Enhancers. Toxins, 2016. 8(7): p. 200.

190. Bachran, D., S. Schneider, C. Bachran, A. Weng, M.F. Melzig, and H. Fuchs, The Endocytic Uptake Pathways of Targeted Toxins Are Influenced by Synergistically Acting Gypsophila Saponins. Molecular Pharmaceutics, 2011. 8(6): p. 2262-2272.

8. List of publications

8.1 Original research articles in peer reviewed journal

1. Gilabert-Oriol R, Thakur M, Haussmann K, Niesler N, **Bhargava C**, Gorick C, Fuchs H, Weng A; Saponins from *Saponaria officinalis* L. Augment the Efficacy of a Rituximab-Immunotoxin. Planta Med 2016. **[Impact Factor: 1.99]**
2. Gilabert-Oriol R, Weng A, Trautner A, Weise C, Schmid D, **Bhargava C**, Niesler N, Wookey PJ, Fuchs, Mayank T; Combinatorial approach to increase efficacy of Cetuximab, Panitumumab and Trastuzumab by dianthin conjugation and co-application of SO1861. Biochem Pharmacol 2015; 97:247-55. **[Impact Factor: 5.091]**
3. Gilabert-Oriol R, Thakur M, von Mallinckrodt B, **Bhargava C**, Wiesner B, Eichhorst J, Melzig MF, Fuchs H, Weng A; Reporter Assay for Endo/Lysosomal Escape of Toxin-Based Therapeutics. Toxins 2014; 6:1644-66. **[Impact Factor: 3.571]**

8.2 Original research article after major and under second review process

"Targeted dianthin is a powerful toxin to treat pancreatic carcinoma when applied in combination with the glycosylated triterpene SO1861"

First Author: Cheenu Bhargava

Co-authors: Horst Dürkop, Xiang Li, Alexander Weng, Matthias F. Melzig, Hendrik Fuchs

Manuscript ID: MOLONC-2016-09-0051.R1 **[Impact Factor: 5.33]**

8.3 Review article in peer reviewed journal

1. Thakur M, Bhargava C. S., **Bhargava C**, Bhargava S, Patil U. K., Dixit V. K.; Ayurvedic Rasayan: The ideology of healthy ageing and performance, Light of Ayurveda Journal, 8 (4), (Ayurveda Education Series), 2010; 31-37.

8.4 Published poster abstract

1. Abstracts of the 82nd Annual Meeting of the German Society for Experimental and Clinical Pharmacology and Toxicology (DGPT) and the 18th Annual Meeting of the Network Clinical Pharmacology Germany (VKliPha) in cooperation with the Arbeitsgemeinschaft für Angewandte Humanpharmakologie e.V. (AGAH). Naunyn-Schmiedeberg's Archives of Pharmacology 2016; 389:1-104. **[Impact Factor: 2.376; Abstract ID - 405]**

8.5 Posters in academic conferences

1. **C. Bhargava**, B. von Mallinckrodt, H. Dürkop, M. Thakur, R. Gilabert-Oriol, A. Weng, M. F. Melzig, H. Fuchs; Combination therapy of Targeted toxin with SO1861: A shooting star in the world of Pancreatic carcinoma. German Pharm-Tox Summit. Berlin, Germany: February 29 – March 3, 2016
2. **C. Bhargava**, M. Thakur, K. Licha, B. von Mallinckrodt, R. Gilabert-Oriol, P. Welker, A. Weng, M. Schirner, H. Fuchs; Conjugates of polysulfated dendrimers and toxins as an effective measure for intracellular delivery and targeted tumor therapy. Cancer Diagnosis and Therapy Congress. London, UK: September 3 – 4, 2015
3. R. Gilabert-Oriol, M. Thakur, B. von Mallinckrodt, **C. Bhargava**, B. Wiesner, J. Eichhorst, M. F. Melzig, H. Fuchs, A. Weng; Monitoring of the endo/lysosomal escape of targeted toxin-based therapeutics: development of a reporter assay. International Conference on From Omics to Novel Therapies in Cancer. Berlin, Germany: May 23 – 24, 2014
4. **C. Bhargava**, C. S. Bhargava, M. Thakur, S. Bhargava, A. Mishra; Role of Antioxidants in human diseases. U.G.C. Sponsored National Conference on Current Status & Challenges in Pharmacy Healthcare. Kanpur, India: March 28, 2010

9. Curriculum Vitae

For reasons of data protection,

the curriculum vitae is not published in the electronic version

For reasons of data protection,

the curriculum vitae is not published in the electronic version

For reasons of data protection,

the curriculum vitae is not published in the electronic version

For reasons of data protection,

the curriculum vitae is not published in the electronic version

10. Acknowledgement

A journey into an unknown territory this is how I felt at the onset of this PhD project. Today, when the journey seems to be a fruitful one, I look back and feel cherished at my success. It is apt for me that it was the blessings of Ganesh Ji that cradles me out safely through the perplexing path and made indelible contribution in shaping my career and personality.

As the present project has acquired this final form, I dedicate my project to my dearest parents (Dr. C.S. Bhargava and Mrs. Abha Bhargava), my elder sister and brother (Dr. Shilpi Bhargava and Sachin) who not only led by to the completion of the project but have always been alongside me in my faults and flounders. It is because of their blessings and endeavor, I have been able to walk straight on the tortuous path.

The pages that follow contain typed words, tables & graph but also the suggestions, blessings, co-operation & criticism of many people. All these efforts have gone in to materializing my work into thesis cannot be thanked in this limited space. However the following deserve a special mention.

It is beyond the reach of words and phrases to express my gratitude to my esteemed supervisor, Prof. Dr. Hendrik Fuchs. I am quiet cognizant about the mere fact that my words will flutter in expressing the true magnanimity of his greatness and scientific horizons, still I would like to express my deepest sense of gratitude for his complete dedication towards cancer research. A mentor to every student and the epitome of pharmaceutical education it was his intellect vision, research skills, peering criticism and continuous interaction that served as the soul of the embodied work.

I would also like to express my heartfelt acknowledgement to my first supervisor Prof. Dr. Matthias F. Melzig for his critical assessment, affectionate words and ever available patience always. His motivation kept me charged and motivated to give my best shot even in a letdown situation. I am beyond the reachability of words to express my thankfulness towards his support and guidance.

I also owe my sincere thanks to Dr. Alexander Weng and Dr. Mayank Thakur, who have helped me tremendously all throughout my project work. The kind of knowledge, affection and cognizance showered upon me has left a long lasting impression on my

scientific soul. They were always kind, patient and ready to share new ideas that has made my stay in Berlin worthwhile.

I express my warm thanks to Dr. Roger Gilabert Oriol and Dr. Benedicta von Ingelheim for introducing me to a lot of experimental techniques. I am thankful for their friendly advice, constant help and encouragement during the research. I am sincerely grateful to them for sharing their truthful and illuminating views on a number of issues related to the project.

I am extremely thankful to Dr. Heiko Funke-Kaiser, Dr. Jens Dernedde, Dr. Dilyara Lauer and Dr. Kai F. Albring, for helping me in one way or other to achieve the goal. I am highly obliged to Dr. Michael Schirner, Dr. Kai Licha and Dr. Pia Welker from Epiios Therapeutics GmbH i.L. They are the ocean of knowledge and have had a tremendous role in providing me with various support in synthesis of ligands.

I offer my warmest acknowledgement to the non-teaching staff for helping me in need. It is their support and help that allowed the project to shape in proper way.

I would also like to thank Dr. Katharina Achazi and Dr. Stephanie Wedepohl from Freie Universität Berlin for their support in performing cell culture experiments. I am highly obliged to Prof. Dr. Horst Dürkop for helping me carrying out various histopathological studies at Pathodiagnostik Berlin, Berlin. Sincere thanks are due to Labor 28 GmbH, Berlin for their support in hematological analyses.

It would be unforgiving if I fail to thank my colleagues Dr. Hossein Panjideh, Marriane Boxberger, Nicole Neisler, Serena Rossi, Xiangli Zhao and Alexandra Trautner without whose support the journey would not have been possible.

I would like to thank all my friends Mehak, Ketaki, Arobendo, Prateek and Sneha and all others for always being with me and supporting me throughout a well.

Words are not sufficient to express my regards to Mummy, Papa, for their patience, care, affection, support and understanding; they are thanked for the sacrifices they cheerfully underwent. At every step of this venture, they shared with me all the moments of different colors with immense love. My respect and profound affection for them is beyond the range of inscription of words. It would be matter of great pleasure for me if I can do something for them.

I am cordially thankful to all my relatives and friends for their love, constant inspiration and affection from the core of my heart.

I accord my thanks to Zentrales Innovationsprogramm Mittelstand (ZIM) for providing the funding. I am well cognizant that this is not the personal success but is the victory of the crew who kept the ship sailing diligently and splendidly ahead over the tempest.

11. Declaration

I, Cheenu Bhargava, declare that the doctoral thesis entitled *"Efficacy of dianthin-based targeted toxins in a pancreatic carcinoma xenograft model"* contains no material that has been submitted previously, in whole or in part, for the award of any other academic degree or diploma. This dissertation is not being concurrently submitted in candidature for any degree. I would hereby like to confirm that there is no conflict of interest in the present study of any kind. I state that this dissertation is the result of my own independent work/investigation, except otherwise indicated. Where I have quoted from the work of others, I have included the source in the references.

Cheenu Bhargava

Berlin, 2017